NTNU
Norwegian University of
Science and Technology

Implementation of the Cracked Membrane Model for Crack Width Predictions in Reinforced Concrete Shell Structures

Simen Kvam

Civil and Environmental Engineering
Submission date: June 2018
Supervisor: Max Hendriks, KT
Co-supervisor: Reignard Tan, KT

Norwegian University of Science and Technology
Department of Structural Engineering

Department of Structural Engineering
Faculty of Engineering
NTNU - Norwegian University of Science and Technology

ACCESSIBILITY

OPEN

MASTER THESIS 2018

SUBJECT AREA:	DATE:	NUMBER OF PAGES:
Concrete Structures	10.06.2018	16 + 109

TITLE:

Implementation of the Cracked Membrane Model for Crack Width Predictions in Reinforced Concrete Shell Structures

Implementering av cracked membrane model for beregning av rissvidder i skallkonstruksjoner av armert betong

BY:

Simen Kvam

SUMMARY:

Crack control is an important part of design of reinforced concrete shell structures in the serviceability limit state. Crack width calculations are performed in accordance with design codes, which are based on beams and columns, and thus, challenging subjective interpretations are necessary for application to shell sections. In addition, inherent physical inconsistencies in the formulas available in the present building codes, complicate the crack width expressions.

This thesis has aimed at contributing to an improved description of the crack width development in concrete shell structures. A new method was thus proposed, with purpose of providing more accurate response predictions where the physical nature of the problem is better reflected in the formulas. In that context, the cracked membrane model (Kaufmann & Marti 1998) combined with a layered approach was employed for crack width calculation of shell structures. The iteration method (Øverli & Sørensen 2012) gives the distribution of forces across the shell cross section, while the cracked membrane model estimates the response at the cracked surface.

The investigations performed in this thesis indicate that the cracked membrane model formulation contributes to an enhanced physical description of the crack development, both for one-dimensional beams and two-dimensional shells with orthogonal reinforcement. Experimental verification also showed that the cracked membrane model and the new approach for shell structures proposed in this thesis provide considerable improvements in crack width estimates compared to the current design codes. Also a simplified version of the cracked membrane model showed to provide accurate response predictions for loading in the serviceability limit state.

Based on the findings of this thesis it is recommended that the cracked membrane model formulation is used as basis for new crack width formulas in design codes. Although more research and verification of the new proposed method is necessary, it can potentially be implemented in post-processing analysis of concrete shell structures.

RESPONSIBLE TEACHER: Prof. Max Hendriks, NTNU & Delft University of Technology

SUPERVISOR: PhD-Candidate Reignard Tan, NTNU & Multiconsult

CARRIED OUT AT: The Department of Structural Engineering, NTNU

Abstract

Crack control is an important part of design of reinforced concrete shell structures in the serviceability limit state. Crack width calculations are performed in accordance with design codes, which are based on beams and columns, and thus, challenging subjective interpretations are necessary for application to shell sections. In addition, inherent physical inconsistencies in the formulas available in the present building codes, complicate the crack width expressions.

This thesis has aimed at contributing to an improved description of the crack width development in concrete shell structures. A new method was thus proposed, with purpose of providing more accurate response predictions where the physical nature of the problem is better reflected in the formulas. In that context, the cracked membrane model (Kaufmann & Marti 1998) combined with a layered approach was employed for crack width calculations of shell structures. The iteration method (Øverli & Sørensen 2012) gives the distribution of forces across the shell cross section, while the cracked membrane model estimates the response at the cracked surface.

The investigations performed in this thesis indicate that the cracked membrane model formulation contributes to an enhanced physical description of the crack development, both for one-dimensional beams and two-dimensional shells with orthogonal reinforcement. Experimental verification also showed that the cracked membrane model and the new approach for shell structures proposed in this thesis provide considerable improvements in crack width estimates compared to the current design codes. Also a simplified version of the cracked membrane model showed to provide accurate response predictions for loading in the serviceability limit state.

Based on the findings of this thesis it is recommended that the cracked membrane model formulation is used as basis for new crack width formulas in design codes. Although more research and verification of the new proposed method is necessary, it can potentially be implemented in post-processing analysis of concrete shell structures.

Sammendrag

Begrensning av rissvidde utgjør en viktig del av prosjekteringen av skallkonstruksjoner av armert betong i bruksgrensetilstanden. Rissviddeberegninger utføres i henhold til prosjekteringsstandarder som er basert på bjelker og søyler, og det kreves dermed utfordrende, subjektive tilpasninger for å kunne anvende formlene for skallkonstruksjoner. I tillegg inneholder formlene i prosjekteringsstandardene fysiske inkonsistenser, som gjør beregningene av rissvidde mindre intuitive.

Denne avhandlingen har hatt som mål å bidra til en forbedret beskrivelse av rissviddeutviklingen i skallkonstruksjoner. En ny metode har blitt foreslått, der formålet er å gi mer presise responspredikskjoner, i tillegg til at formlene bedre reflekterer den fysiske oppførselen de forsøker å beskrive. Det har blitt foreslått å benytte "cracked membrane model" (Kaufmann & Marti 1998) i kombinasjon med en lagdelt tilnærming for å estimere rissvidder. Iterasjonsmetoden (Øverli & Sørensen 2012) gir fordelingen av krefter over skalltverrsnittet, og "cracked membrane model" gir responsen ved den rissede overflaten.

Undersøkelsene utført i denne oppgaven har vist at uttrykkene i "cracked membrane model" bidrar til en forbedret fysisk beskrivelse av rissutviklingen, både for endimensjonale bjelker og for todimensjonale ortogonalt armerte betongskall. Verifikasjon mot eksperimentelle resultater har vist at "cracked membrane model" og den nye metoden for skallkonstruksjoner som er foreslått i denne oppgaven, gir en betydelig forbedring av rissviddeestimatene sammenlignet med de gjeldende prosjekteringsstandardene. En forenklet versjon av "cracked membrane model" har også gitt nøyaktige responspredikasjoner for last i bruksgrensetilstanden.

Basert på funnene i oppgaven anbefales det at uttrykkene i "cracked membrane model" benyttes som et grunnlag i arbeidet med å utvikle nye beregningsregler for rissviddebegrensning i prosjekteringsstandarder. Selv om det er behov for mer forskning på og verifisering av den nye foreslåtte metoden, har den potensiale til å kunne bli implementert i etterprosesseringsanalyser av skallkonstruksjoner i betong.

Preface

This thesis concludes my Master of Science education in Civil and Environmental Engineering at The Norwegian University of Science and Technology (NTNU) in Trondheim. The thesis was performed throughout my 10 th semester, spring 2018, at the Department of Structural Engineering.

A special thanks is given to PhD candidate Reignard Tan at NTNU for his guidance and enthusiastic support in connection with the work of this thesis. He has always been available for discussions, and his knowledge has been of great help.

I would also like to thank professor Max Hendriks from NTNU and Delft University of Technology for his guidance throughout the period.

Trondheim, June 2018

Simen Kvam

Table of Contents

List of Tables

List of Figures

Notation and Abbreviations

Roman letters

A	area
$\boldsymbol{C}$	material matrix
D	diameter
E	Young's modulus
G	shear modulus
$\boldsymbol{K}$	stiffness matrix
M	bending moment
N	axial force
S	crack spacing
b	width
c	concrete cover
d	effective height
f	material strength
h	height
k	coefficient
l	debonding length
w	crack width
x	compressive height

Greek letters

α	ratio
β	convergence tolerance
γ	shear strain
δ	relative displacement
ε	axial strain
η	ratio
θ	angle
κ	curvature
λ	crack coefficient
ν	Poisson's ratio
ρ	geometrical reinforcement ratio
σ	axial stress
τ	shear stress
ϕ	diameter

Subscripts

b	bond
c	concrete, compression
d	design value
h	hardening
i	counter
k	characteristic
m	mean
p	principal
r	crack
s	reinforcement steel
t	tension
u	ultimate
x,y,z	coordinates
1,3	principal direction
ext	external

Abbreviations

CMM	Cracked Membrane Model
EC2	Eurocode 2
MCFT	Modified Compression Field Theory
MC10	Model Code 2010
SLS	Serviceability Limit State

1 Introduction

1.1 Defining the Problem

Serviceability design is an important part of the design process for concrete structures. Contrary to other types of structures, concrete structures will crack because of concrete's inherent properties. It is generally accepted that some cracking will occur, and trying to avoid it would lead to improper design and excessive use of materials. However, crack control is important in the design process. Excessive cracking may lead to drawbacks in service, and must be kept within reasonable limits. As a part of the serviceability design, the crack width is therefore a significant parameter to keep track of.

In design of large concrete shell structures the serviceability limit state (SLS) often becomes governing in determining of required proportions, dimensions and detailing of reinforcement and concrete. However, the methods used for design in SLS today seem to be overly conservative (Karagiannis & Kaufmann 2016). Many of them are based on improper assumptions and involve an inconsistent physical formulation, which limits their general applicability (Tan et al. 2017). Obtaining a more suitable method for design of shell structures might significantly reduce the necessary amounts of material used in such structures.

The design process should be conducted in accordance with regulations provided by design codes. The design codes, however, are mostly based on beams, columns and one-way plates. The one-directional beam formulas must therefore be translated in order to fit two-directional elements, such as plates and shells. Calculation of crack widths and the corresponding code checks in orthogonally reinforced shell structures thus demand subjective interpretations and choices, which cause higher risk of erroneous calculations. Furthermore, different interpretations will lead to various results for the same problem.

1.2 Scope

This thesis aims at contributing to a new and improved method for estimation of crack widths in reinforced concrete shell structures. Current design regulations (CEN (2004), *fib* (2013)) are incomplete when it comes to crack width assessment for shell and membrane elements, and it is desirable to develop a better methodology to handle the problem. Therefore, the goal of this thesis is to provide a realistic model that is able to determine the response of a reinforced concrete shell section on whose basis current design provision can be critically reviewed and supplemented.

The cracked membrane model is proposed as a tool to solve the problems associated with SLS design of concrete shell structures. The cracked membrane model is capable of fulfilling compatibility and equilibrium requirements, and gives a realistic physical estimate of the behaviour of a cracked concrete panel. The model has proven to give good response predictions compared to experimental results (Kaufmann 1998).

However, the cracked membrane model is developed for cases of plane stress, while shell structures generally are subjected to a combination of moments, membrane forces and transverse shear forces. Adapting a shell model with a layered approach, the basic concepts of the cracked membrane model could be extended to shell structures. If the shell is divided into different layers, each layer can be considered to be in a state of plane stress. That way, the cracked membrane model can be implemented for calculation of shell structures.

Although the cracked membrane method could be used for design both in ultimate limit state and serviceability limit state, this thesis will be limited to serviceability considerations only. Furthermore, cracks are assumed to occur as a result of external loading, and the effects of creep, shrinkage and restrained deformations are neglected. Only the effect of normal reinforcement is considered throughout the thesis.

1.3 Objectives

The main objectives of this thesis are:

- Review current crack width formulas relevant for shell design in Eurocode 2 (CEN 2004) and Model Code 2010 (*fib* 2013).

- Present and derive contents of the cracked membrane model (Kaufmann & Marti 1998).
- Present and derive contents of the iteration method (Øverli & Sørensen 2012).
- Propose a new method for crack width estimation of shell sections, based on the cracked membrane model and the iteration method.
- Verify the methods presented in this thesis with experimental results, and compare with results obtained with the design codes.

1.4 Overview

In the first part of this thesis, chapter 2, previous work on plane stress problems will be briefly reviewed. Most attention is given to the modified compression field theory, which is the main precursor of the cracked membrane model. In addition, crack calculations according to current design methods will be reviewed and their shortcomings when it comes to membrane and shell structures are mentioned. The post-processing program MultiCon is briefly described, to exemplify how design of concrete shell structures is conducted in the industry today.

The second part covers the methods of the thesis. First, in chapter 3, the cracked membrane model is presented. Assumptions, derivations and obtained equations are all included. Furthermore, an algorithm is proposed for calculation with the model. Some modifications that have been suggested after the model was introduced in 1998 are included. Secondly, in chapter 4, the iteration method is described. The iteration method is employed to shell sections to determine the strain state that ensures equilibrium between external and internal forces. All necessary equations are presented, and the algorithm is explained. Based on the cracked membrane model and the iteration method, a new procedure is proposed in chapter 5 for response predictions of reinforced concrete shell structures.

In the third part, chapter 6, the models described in the second part of this thesis are employed at different examples. The results are compared with experimental observations. Results are also obtained with the building codes described in the first part, and compared with the results of the presented methods.

In the fourth and last part, the observations and results of the first three parts of this thesis are summarized and discussed, along with a set of recommendations for future work.

2 — Literature Review

2.1 Work on Plane Stress Problems: Compression Field Approaches

2.1.1 General

Membrane elements are structural elements subjected to in-plane stresses only, i.e. in-plane shear and normal stresses, also denoted membrane stresses. Figure 2.1 shows examples of some concrete structures that carry load primarily through the action of in-plane stresses, which make membrane elements suitable for modelling.

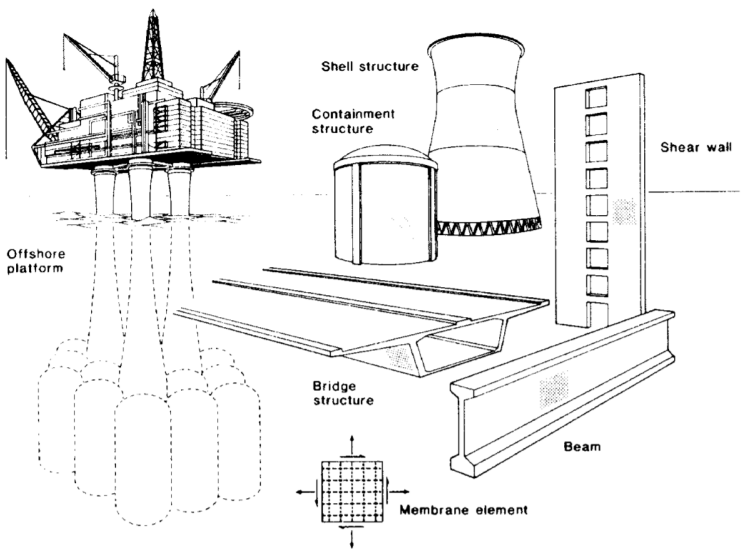

Figure 2.1: Structures with load primarily carried as in-plane stresses (Vecchio & Collins 1986)

Analysis of reinforced concrete membrane elements have been a topic of research for a long time. Diverse approaches have been proposed to determine their response when subjected to 2D-plane stress. However, it has proven to be difficult to develop a model that takes into account all the factors that affect the response of such elements (Collins et al. 1985). The main difficulty is that the behaviour of a cracked panel is completely different from an uncracked one (Vecchio & Collins 1986). For an increasing load, new cracks will form and old cracks may both propagate and close. External forces are resisted by the combined action of reinforcement and concrete. At the cracks concrete may transfer compressive and lateral stresses due to aggregate interlocking. Concrete may carry some tensile stresses in between cracks, but at the crack all tensile stresses must be transferred by the reinforcement.

In an international competition, where 43 leading researchers within the field of reinforced concrete structures attended, it was attempted to predict the response of four reinforced concrete panels tested by Collins et al. (1985). The different approaches proposed by the researchers resulted in a wide scatter of response predictions, and it was made clear that non of them could accurately predict the response of the four panels tested.

The international competition showed that a better method was needed to solve the problem. As a result, the modified compression field model was developed (Vecchio & Collins 1986). The model made an important contribution both when it was presented and the following years, and is a natural model to compare the cracked membrane model with. The most basic parts of the modified compression field theory are addressed in a qualitative fashion.

2.1.2 Modified Compression Field Theory

The modified compression field theory (Vecchio & Collins 1986) was considered to be revolutionary within the field of concrete technology when it was presented. Unlike earlier models, the modified compression field theory was able to accurately predict both the strength and the load-deformation response of a reinforced concrete element exposed to in-plane stresses. The model is used in multiple post-processing programs of concrete structures in the industry today, e.g. ShellDesign (Nyhus 2014) developed by Dr.techn. Olav Olsen.

In the modified compression field theory, cracked concrete is treated as a new material with its own stress-strain relationship. Equilibrium, compatibility and material laws are formulated in terms of average strains and average stresses (Vecchio &

Collins 1986). Based on the relations established, a set of equations is formulated, that must be solved with a suitable algorithm.

In order to determine the material laws for cracked concrete, an experimental program was initiated (Vecchio & Collins 1986). Based on the results, empirical expressions for the principal tensile and compressive concrete stresses were proposed. For the reinforcement, a bilinear uniaxial stress-strain relation is assumed, and the contribution from the reinforcement to the shear resistance is neglected. In reality, the average stress-average strain relationships for concrete and reinforcement are not completely independent. However, this is assumed in the model for simplicity.

The modified compression field theory is based on the original compression field theory. The difference between the two models is that the contribution of tensile stresses in the cracked concrete is neglected in the original compression field theory. Hence, deformations are overestimated and capacity underestimated. By including this effect (tension stiffening) in the modified compression field theory, a more physical and accurate estimate is obtained (Vecchio & Collins 1986).

Locally at cracks, the stresses will be different from the average values calculated. This is due to the fact that concrete stresses vary in between cracks. Therefore, local stresses at cracks are handled separately, and an equilibrium formulation at the crack is established. The ability of the crack to transfer shear forces is included, with an empirical relation developed based on the work of Walraven (1981).

2.1.3 Previous Work with the Cracked Membrane Model

The cracked membrane model (Kaufmann & Marti 1998) has a number of good features, which makes it relevant for several implementations. For cracked concrete panels subjected to a state of plane stress, it obtains excellent response predictions and is capable of predicting the correct failure mode (Kaufmann 1998). Furthermore, the model is based on simple, physical relations. The model will be described in more detail in chapter 3, while this section is devoted to previous work and implementations of the model.

Since the model was presented, multiple researchers have suggested adjustments in order to eliminate inconsistencies of the original version. Seelhofer (2009) introduced an additional steel stress-strain relation in order to take into account the crack formation stage where slip is not occurring over the entire crack. Dabbagh & Foster (2006) presented expressions to solve crack spacing analytically on closed form. Furthermore, they derived new equations and boundaries for situations where

the crack angle direction is approaching the direction of one of the reinforcement directions.

The cracked membrane model is suitable for implementation in finite element modelling of orthogonally reinforced structural elements in-plane stress. Foster & Marti (2003) developed the CMM into a finite element formulation, where the contribution of tension stiffening is added to the material elasticity matrix that gives

$$\boldsymbol{D}_{xy} = \boldsymbol{D}_{cxy} + \boldsymbol{D}_{cts} + \boldsymbol{D}_{s} \tag{2.1}$$

where $\boldsymbol{D}_{cxy}$ is the concrete component, $\boldsymbol{D}_{cts}$ is the concrete tension stiffening component and $\boldsymbol{D}_{s}$ is the reinforcing steel component. Dabbagh & Foster (2006) and Pimentel et al. (2010) have proposed more complex finite element formulations where CMM is extended to account for fixed cracks and incorporate aggregate interlock effects.

In this thesis the idea is to extend the applicability of the cracked membrane model into problems related to plate structures, which are generally subjected to combined moments, membrane forces and transverse shear forces. This idea was proposed by Kaufmann (1998) as recommendation for future research. Seelhofer (2009) examined this in a general way in his dissertation. Recently, Karagiannis & Kaufmann (2016, 2018) have considered the approach for a more specific problem. They have looked into the shear strength of hollow-box bridge girder webs, which are subjected to transverse bending moments in addition to in-plane shear. In relation with the research, a series of large-scale experiments will be performed in the Large Universal Shell Element Tester (Kaufmann et al. 2018), which is a new testing facility. The new testing facility will enable the application of well controlled arbitrary load combinations that produce 8 independent stress resultants, and thus contribute to an improved basis for the development of current shell response formulations.

2.2 Crack Width Calculations

2.2.1 Cracking Theory

The basic cracking behaviour of reinforced concrete can be illustrated by consideration of a prismatic reinforced concrete bar, subjected to axial tension as shown in Figure 2.2. Cracks develop in concrete when the tensile strength of the concrete is exceeded. Once cracking initiates, the structure will not fail because of the reinforcement that transfers the forces across the crack. At the cracks, all of the load will therefore be carried by the reinforcement. Due to bond between the concrete and the reinforcement, parts of the load are transferred to the concrete between cracks. The tensile stresses in the concrete are increasing with the distance from the crack until full compatibility between concrete and reinforcement is re-established. This distance is called the transfer length, and is indicated by the shaded grey area denoted "discontinuity area" in Figure 2.2.

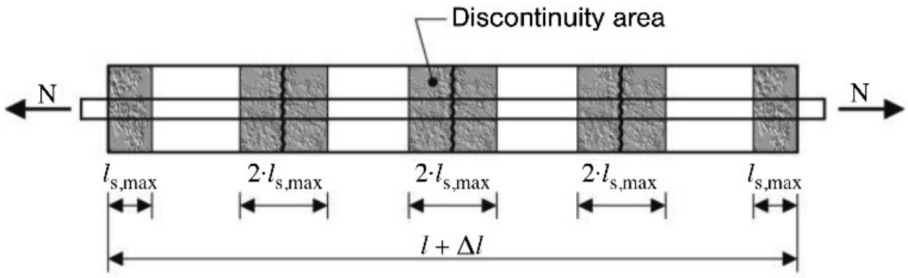

Figure 2.2: Basic cracking behaviour of a reinforced prismatic bar subjected to axial tension (*fib* 2013)

When the cause of cracking is external loading, the structure will in principle experience two different stages, a crack formation stage and a stabilized cracking stage. If the crack spacing and bond properties are adequate, the concrete stress will reach the tensile strength of concrete, and a new crack will form. When new cracks keep on forming, the structure is said to be in the crack formation stage. This process continues until the spacing between adjacent cracks is so small that no new cracks may form, and the stabilized cracking stage is reached. In this stage the crack spacing is not sufficient to transfer stresses equal to the tensile strength of concrete to the concrete. If the loading is further increased, existing cracks will widen. The loading can be increased until the steel starts to yield.

Four stages of a reinforced concrete bar subjected to axial tension are though distinguished. The different stages are illustrated in a simplified manner with the load - deformation relation in Figure 2.3. Note that the dotted line illustrates the behaviour of naked steel. Since the tensile stresses in concrete between cracks are accounted for, a stiffer response is observed. This effect is called tension stiffening.

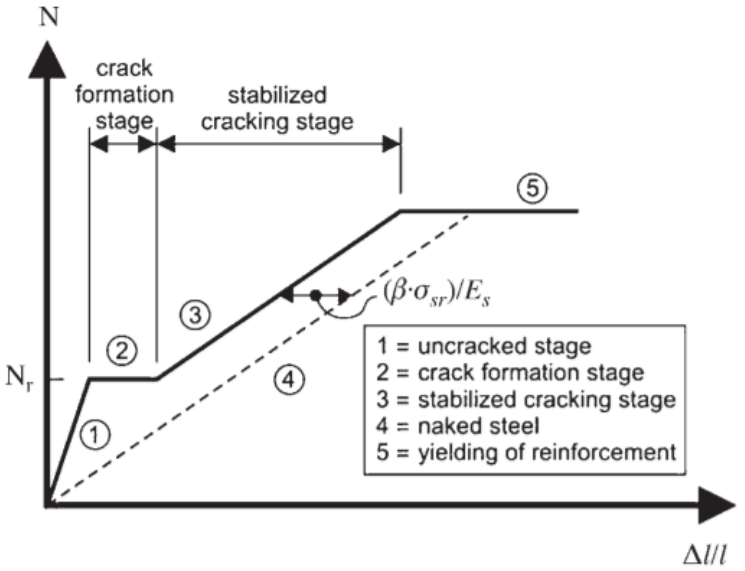

Figure 2.3: Simplified load - strain relation for a centrically reinforced member subjected to tension (*fib* 2013)

2.2.2 Code Regulations

Crack control is an important part of design of reinforced concrete structures. The purpose is to ensure that functionality, durability and appearance of the structure are maintained. Wide cracks are aesthetically undesirable and may cause the public to believe that there are structural problems. In addition, problems related to durability are a major concern when cracks form. Cracking causes the concrete cover to open that cause easier penetration of harmful substances. This may lead to corrosion of rebars and thus structural deterioration. Loss of functionality may occur, for instance, in containment structures where wide cracks lead to leakage problems. In order to meet the serviceability requirements mentioned above, the crack width should be limited.

As a designer you have to act in accordance with given laws and regulations when

you are designing a structure. The guidelines considered in this thesis are

- EN 1992-1-1:2004, Eurocode 2: Design of concrete structures, Part 1-1: General rules and rules for buildings (CEN 2004)
- *fib* Model Code for Concrete Structures 2010 (*fib* 2013)

For countries within the European Union the Eurocodes provide the technical rules on how structural design should be conducted. In Norway, Eurocode 2 (EC2) (CEN 2004) is used as standard for design of concrete structures. The International Federation for Structural Concrete, *fib*, is a worldwide association with purpose of advancing the performance of concrete structures. As a result of their work the *fib* Model Code 2010 (MC10) was released (*fib* 2013), with objective to serve as basis for future guidelines within the field of concrete structures.

In the following, the formulas for crack width calculation from these two references will be briefly presented. For a more thorough investigation and for more details, the design codes themselves should be examined.

Calculation of Crack Width in Eurocode 2

Chapter 7.3 in Eurocode 2 (CEN 2004) deals with crack control of concrete structures. The expression for crack width is given as

$$w_k = S_{r,max}(\varepsilon_{sm} - \varepsilon_{cm}) \tag{2.2}$$

where $S_{r,max}$ is the maximum crack spacing equal to twice the maximum transfer length to each side of the crack, ε_{sm} is the mean strain in the reinforcement, and ε_{cm} is the mean strain in the concrete between cracks. The mean strain in the reinforcement should take into account the effect of tension stiffening (CEN 2004).

The relative strain $(\varepsilon_{sm} - \varepsilon_{cm})$ may be calculated from the expression

$$\varepsilon_{sm} - \varepsilon_{cm} = \frac{\sigma_s - k_t \frac{f_{ct,eff}}{\rho_{s,eff}}(1 + \alpha_e \rho_{s,eff})}{E_s} \geq 0.6\frac{\sigma_s}{E_s} \tag{2.3}$$

where σ_s is the stress in the tensile reinforcement, $\alpha_e = E_s/E_{cm}$, $\rho_{s,eff}$ is the effective reinforcement ratio and k_t is a factor dependent on the duration of the load. The effective reinforcement ratio is dependent of the effective height given by Eq. (2.4), where x is the height of the compressive zone

$$h_{c,eff} = min\left\{2.5(h-d); \quad \frac{h-x}{3}; \quad h/2\right\} \tag{2.4}$$

The maximum crack spacing in the uniaxial case is calculated as in Eq. (2.5). This expression is semi-empirical, with constants k_1, k_2, k_3 and k_4 adjusted to match experimental results. k_1 and k_2 are determined based on the bond properties of the reinforcement and the strain distribution, respectively. Furthermore, c is the concrete cover, ϕ is the bar diameter and $\rho_{s,eff}$ is the reinforcement ratio.

$$S_{r,max} = k_3 c + k_1 k_2 k_4 \frac{\phi}{\rho_{s,eff}} \tag{2.5}$$

In an orthogonally reinforced shell structure, cracks will generally not form perpendicular to the reinforcement direction. In such cases, where the angle between the axes of principal stress and the direction of the reinforcement, θ, is significant ($> 15°$), the crack spacing can be determined by Eq. (2.6). $S_{r,max,x}$ and $S_{r,max,z}$ are the uniaxial crack spacings calculated in the x and z directions respectively.

$$S_{r,max} = \frac{1}{\frac{\cos\theta}{S_{r,max,x}} + \frac{\sin\theta}{S_{r,max,z}}} \tag{2.6}$$

As shown above, Eurocode 2 provide Eq. (2.3) for determination of the mean strain difference between reinforcement and concrete. However, this expression is derived based on beams and bars. No formulas or recommendations describes how the relative strain in Eq. (2.2) should be determined for a two-directional plate problem. Hence, the formula is difficult to employ when it comes to crack width design for orthogonally reinforced membrane and shell structures, at which the direction of the maximum principle strain no longer is aligned with reinforcement.

Calculation of Crack Width in Model Code 2010

Chapter 7.6.4.4 in *fib* Model Code 2010 (*fib* 2013) considers the calculation of crack width in reinforced concrete members. The expression for crack width may be calculated by Eq. (2.7).

$$w_d = 2 l_{s,max} (\varepsilon_{sm} - \varepsilon_{cm}) \tag{2.7}$$

The relative mean strain term is given in Eq. (2.8). The expression is equal to

Eq. (2.3) from EC2, only differing in the way they are presented. Note also that a lower limit is not included here.

$$\varepsilon_{sm} - \varepsilon_{cm} = \frac{\sigma_s - \beta\sigma_{sr}}{E_s} \tag{2.8}$$

In Eq. (2.8) β is a coefficient depending on the type of loading and σ_{sr} is the maximum steel stress in a crack in the crack formation stage. For pure tension this is equal to

$$\sigma_{sr} = \frac{f_{ctm}}{\rho_{s,eff}}(1 + \alpha_e\rho_{s,eff}) \tag{2.9}$$

The factor $l_{s,max}$ denotes the distance where slip between concrete and steel occurs, and twice this length is equal to the maximum crack spacing. The slip length is determined with Eq. (2.10), which consists of two parts. The first part takes the influence of the concrete cover into consideration. The other part describes the transfer of shear bond stresses between steel and concrete. k and τ_{bms} are empirically adjusted factors.

$$l_{s,max} = kc + \frac{1}{4}\frac{f_{ctm}}{\tau_{bms}}\frac{\phi_s}{\rho_{s,eff}} \tag{2.10}$$

In the case of cracking of members reinforced in two orthogonal directions, where the crack angle is expected to differ substantially ($> 15°$) from the reinforcement directions, the transfer length of bond forces is adjusted by Eq. (2.11). This equation looks similar to Eq. 2.6, but with slippage lengths $l_{sx,k}$ and $l_{sy,k}$ instead of crack spacings in the reinforcement directions. Furthermore, the crack spacing perpendicular to the crack S_{rm} is replaced by the length $l_{s,max,\theta}$. While the crack spacing perpendicular to the crack indeed has a physical interpretation, the length $l_{s,max,\theta}$ may be regarded as the slippage length for an imaginary reinforcement in the direction perpendicular to the crack.

$$l_{s,max,\theta} = \left(\frac{\cos\theta}{l_{sx,k}} + \frac{\sin\theta}{l_{sy,k}}\right)^{-1} \tag{2.11}$$

While Eurocode 2 provides no proposal on how the relative mean strain term of the crack width equation should be obtained in case of an crack angle that differs from the reinforcement direction, MC10 gives Eq. (2.12). The expression is quite similar to Eq. (2.7) for the uniaxial case, however it is adjusted to account for skew

cracks with regard to the reinforcement. $\varepsilon_{\perp}$ and $\varepsilon_{c,\perp}$ represent the mean strain and the mean concrete strain evaluated in the direction orthogonal to the crack, as indicated in Figure 2.4.

$$w_d = 2l_{s,max,\theta}(\varepsilon_{\perp} - \varepsilon_{c,\perp}) \tag{2.12}$$

Eq. (2.11) and (2.12) are both formulated for the case of reinforced concrete members with orthogonal reinforcement. However, the provision provides no proposed procedure to determine the strains perpendicular to the crack.

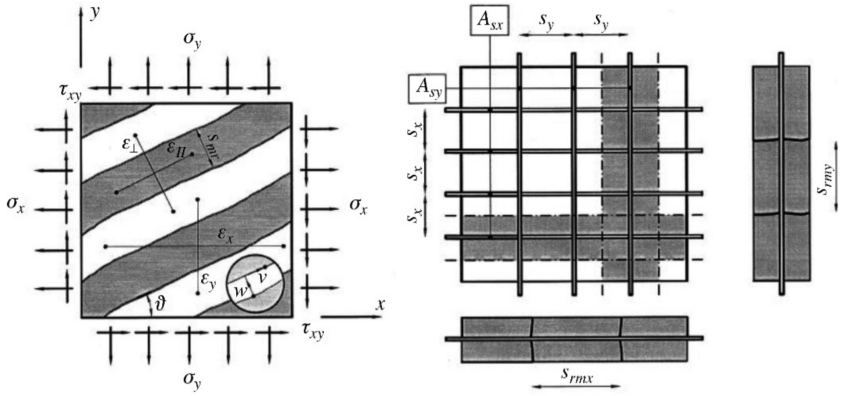

Figure 2.4: Basis for calculation of crack width for orthogonally reinforced membranes (*fib* 2013)

2.2.3 MultiCon

MultiCon is a design and post-processing program for analysis and design of complex concrete structures (Multiconsult 2016). Although the program is applicable for all kinds of concrete structures, it is particularly suitable for marine concrete structures. The program has been the market leading design program for concrete platforms for the last 30 years. In the beginning of the 1990s MultiCon was, for instance, used in the design of the Troll A platform, which is the biggest gravity based concrete platform ever installed.

MultiCon includes state of the art design for concrete shell sections based on a number of international codes, including codes for offshore concrete structures. Over the last 30 years the program has continuously been updated and improved, for example with the implementation of new standards and regulations. As mentioned

in subsection 2.2.2, the equations given for crack control are not easy to interprete in the case of shell structures. However, in MultiCon an approach is proposed to deal with the problem. In the following, this approach will be presented.

MultiCon Approach

Crack width estimation in MultiCon is based on the regulations of Eurocode 2 (CEN 2004) and guidelines of Model Code 2010 (*fib* 2013). However, to make the equations suitable for shell sections with orthogonal reinforcement layout, subjective assumptions and choices are required. Below it is shown how MultiCon transformes the crack width formulas of EC2 and MC10, Eq. (2.2) and (2.7), into a more suitable expression for cracking in shell structures.

$$w_k = S_{r,max,\theta}(\varepsilon_{sm} - \varepsilon_{cm}) \tag{2.13a}$$

$$= S_{r,max,\theta}\left(\frac{\sigma_s - \beta\sigma_{sr}}{E_s}\right) \tag{2.13b}$$

$$= S_{r,max,\theta}\frac{\sigma_s}{E_s}\left(1 - \beta\frac{\sigma_{sr}}{\sigma_s}\right) \tag{2.13c}$$

$$= S_{r,max,\theta}\varepsilon_s(1 - \beta k) \tag{2.13d}$$

Here $S_{r,max,\theta}$ is calculated in the same way as in Eq. (2.6) and (2.5) in EC2, or with Eq. (2.11) and (2.10) in MC10 where $S_{r,max,\theta} = 2l_{s,max,\theta}$. The crack angle is determined at the outermost face and kept constant throughout the thickness.

The fraction σ_s/E_s is equal to the steel strain. However, in a shell section with orthogonal reinforcement, the maximum principal stress direction is generally not aligned with the reinforcement directions. In the MultiCon approach, this is handled by considering the maximum principal strain as the strain of a fictive reinforcement perpendicular to the crack direction. The maximum principal strain is determined at the reinforcement level.

When it comes to the determination of the k factor it is assumed that the section is uncracked (stadium I) with linear elastic stiffness. This implies that the stress distribution is linear over the cross-sectional height. With this assumption, the ratio σ_{sr}/σ_s is equal to the ratio f_{ct}/σ_{cI} since the neutral axis will not move. Figure 2.5 shows the situations. f_{ct} is the tensile strength of concrete that is just reached for the steel stress σ_{sr}. Similarly, σ_{cI} is the maximum principal concrete stress at

the outermost point of the cross section corresponding to the steel stress σ_s. Note that this concrete stress is calculated as if the section is uncracked regardless of whether $\sigma_{cI} > f_{ct}$ or not.

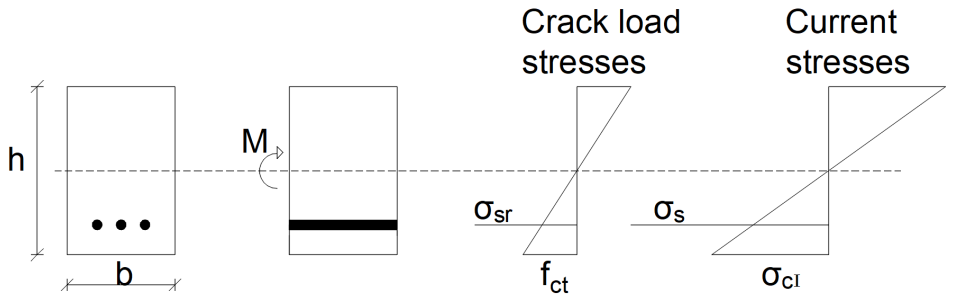

Figure 2.5: Basis for determination of k-factor in MultiCon approach

With these considerations and assumptions, the crack width can be determined for situations where the crack angle differs from the direction of the reinforcement. The result is summarized below.

$$\begin{aligned} w_k &= S_{r,max,\theta}\varepsilon_{II}(1-\beta k) \\ \text{where} \quad k &= \frac{f_{ct}}{\sigma_{cI}} \end{aligned} \tag{2.14}$$

To determine the crack width with Eq. (2.14), the values of the maximum principal strain at level of the reinforcement ε_{II} and the maximum principal stress direction θ, need to be determined in stadium II, i.e. for a cracked cross section. The values are obtained from a layered approach where, in general, a few iterations are necessary. The maximum principal concrete stress at the outermost point of the uncracked face σ_{cI} is determined in stadium I. The internal response of a shell section is determined by a layered approach also in this case, but due to the assumption of uncracked concrete with linear elastic material properties no iterations are necessary in order to reach equilibrium with the external loads.

3 — Response of a Cracked Membrane

In this thesis the cracked membrane model (Kaufmann & Marti 1998) is proposed as tool to estimate the response of reinforced concrete panels in a state of plane stress, and its applicability will be extended to analysis of shell sections. The model has been chosen as it has proven to give good response predictions (Kaufmann 1998) for plane stress panels, and as it has been proposed for shell section applications before (Kaufmann 1998, Seelhofer 2009, Karagiannis & Kaufmann 2018), see subsection 2.1.3.

In the following the basis for the model is presented, section 3.1, before the cracked membrane model is introduced, section 3.2.

3.1 Basis for the Cracked Membrane Model

3.1.1 Material Properties for Steel

Steel has a relatively high tension capacity compared to concrete. In a reinforced concrete structure this is taken advantage of by letting the steel carry tension and concrete carry compression. In design it is common practice to choose steel amounts that governs a failure mode by yielding of the reinforcement rather than crushing of concrete. This gives the structure improved ductility, which permits forces to be redistributed.

Steel can be processed both as hot or cold rolled at the mill. In Figure 3.1 (a) and (b) the stress-strain curves for both types are schematically illustrated. Both have an almost linear elastic behaviour up to yield stress, f_{sy}, and strain, ε_{sy}. Then

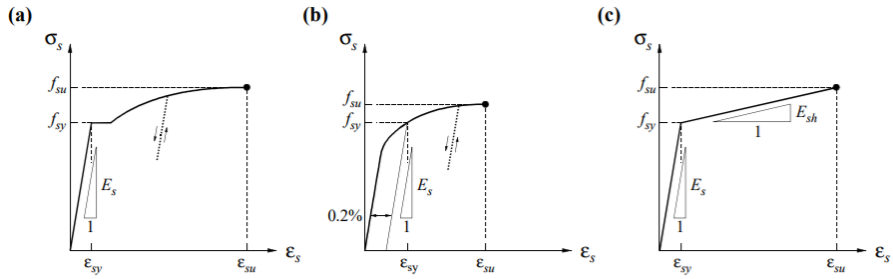

Figure 3.1: Stress-strain curves for reinforcement: (a) hot-rolled, (b) cold-worked, (c) bilinear idealization (Kaufmann 1998)

they exhibit a nonlinear behaviour up to the ultimate load, f_{su}, with corresponding strain, ε_{su}. These characteristics can be approximated by a bilinear idealization of the stress-strain response as shown in Figure 3.1 (c). The modulus of elasticity, E_s, is used for the linear elastic part, while the strain hardening modulus, E_{sh}, is used for the yield part. The strain hardening modulus is given as

$$E_{sh} = \frac{f_{su} - f_{sy}}{\varepsilon_{su} - \varepsilon_{sy}} \tag{3.1}$$

The effect of unbonded prestressed reinforcement can easily be included in the cracked membrane method. Prestressing steel exhibits a similar behaviour as ordinary reinforcement, and the same bilinear idealization shown in Figure 3.1 (c) can be used.

3.1.2 Material Properties for Concrete

Concrete is one of the most popular construction materials, due to its high strength relative to price and formability. The behaviour of concrete is very dependent on the loading, concrete exhibits significantly different properties in tension and compression.

The tension capacity, f_{ct}, of concrete is relatively low. Hence, when assessing the strength of a concrete section, tension capacity is often neglected without remarkable impact on the results. On the other hand, tension stresses provide an important contribution to the performance of a member in serviceability calculations, such as for crack spacings, crack widths and deformations. In this thesis the serviceability calculations are the scope of interest, and the tension capacity of the concrete is therefore included. The value of f_{ct} is based on the concrete mixture

used, and can be found in Eurocode 2 (CEN 2004). The stress-strain curve for concrete in tension can be assumed to be linear up to the limit f_{ct}.

The main advantage of concrete is the high compressive strength. When a concrete structure is designed, we make sure that most of the concrete is in compression. By doing this, the compressive properties of the concrete are exploited, while the disadvantages related to the tension properties are avoided.

The values for compressive strength are found in Eurocode 2 (CEN 2004). Most properties of a specific concrete mix are determined by means of the compressive cylinder strength, denoted f'_c. This value is obtained from tests of uniaxial compression applied to a concrete cylinder.

However, in a cracked concrete element exposed to a biaxial stress state, the compressive strength will be influenced. The reason is the deviation of lateral tensile strains, ε_1, in the two cases. In the uniaxial case, only small amounts of tensile strains occur as a result of Poisson's effect. Between cracks in a cracked member on the other hand, considerable tensile stresses perpendicular to the compressive direction will develop and cause bigger tensile strains. As a result, the concrete strut in a cracked concrete membrane will exhibit a weaker response than a uniaxially compressed cylinder.

The lateral influence of cracking on the compressive strength has been studied by different researchers. Based on the results of many of the tests, the following relation for the concrete compressive strength of a cracked concrete member is proposed (Kaufmann & Marti 1998)

$$f_c = \frac{(f'_c)^{2/3}}{0.4 + 30\varepsilon_1} \leq f'_c \tag{3.2}$$

The compressive stress-strain response for the pre-peak behaviour can be approximated by a parabolic curve given as

$$\sigma_{c3} = f_c \frac{\varepsilon_3^2 + 2\varepsilon_3\varepsilon_{co}}{\varepsilon_{co}^2} \tag{3.3}$$

where σ_{c3} = the concrete stress, ε_3 = the concrete strain, f_c = the peak compressive stress from Eq. (3.2), and ε_{co} = the concrete strain at peak compressive stress.

3.1.3 Bond

In a reinforced concrete structure there is interaction between concrete and steel. This interaction is called bond and allows stresses to be transferred from one material to the other. When relative displacements between concrete and steel occur, bond stresses will develop at the concrete-steel interface. Some of the bond stresses are a result of pure friction, but most of them originates from the interlocking between the ribs of the steel and the concrete (Kaufmann 1998). Hence, the magnitude of the bond stresses depend on the size and shape of the reinforcement, but also other factors such as relative displacement, concrete strength, cover, boundary conditions and state of load.

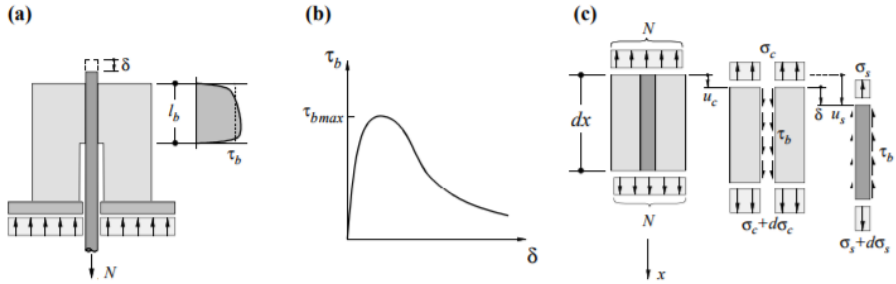

Figure 3.2: Shear bond stress: (a) pull out, (b) shear bond stress-slip relationship, (c) differential element (Kaufmann 1998)

Figure 3.2 (a) shows a reinforcement bar that is pulled out of a concrete section with a force N. In order for the average shear bond stresses, τ_b, to be in equilibrium with the applied force over an embedment length, l_b, the following expression has to be fulfilled

$$\tau_b = \frac{N}{D\pi l_b} \tag{3.4}$$

Here it is assumed that the shear bond stresses are evenly distributed over the nominal steel diameter, D. Furthermore, knowing that the total force in each section must equal the total force applied, we get the following relations

$$N = A_s\sigma_s + \hat{A}_c\sigma_c \tag{3.5a}$$

$$\frac{N}{A_s} = \sigma_s + \frac{(1-\rho)}{\rho}\sigma_c \tag{3.5b}$$

where $\hat{A}_c = A_c$ - A_s, A_s = cross sectional area of steel, A_c = gross cross section of concrete, and $\rho = A_s/A_c$ = geometrical reinforcement ratio.

By consideration of the differential element in Figure 3.2 (c) and Eq. (3.4), we find the change of steel stresses over the differential length dx

$$d\sigma_s A_s = dN = \tau_b D\pi dx, \quad A_s = \frac{\pi}{4}D^2$$

giving

$$\frac{d\sigma_s}{dx} = \frac{4\tau_b}{D} \tag{3.6}$$

Similarly, the change of concrete stresses over the differential length becomes

$$\frac{d\sigma_c}{dx} = -\frac{4\tau_b}{D}\frac{\rho}{(1-\rho)} \tag{3.7}$$

The relative displacement, δ, can be expressed in terms of the displacement of the steel, u_s, and concrete, u_c, which gives $\delta = u_s$ - u_c. Differentiation over the relative displacements gives

$$\frac{d\delta}{dx} = \frac{d}{dx}\big[u_s - u_c\big] = \varepsilon_s - \varepsilon_c \tag{3.8}$$

where ε_s = steel strain and ε_c = concrete strain. By differentiation of this expression once more, a second order differential equation for slip is obtained, which generally has to be solved in an iterative manner. Assuming linear elastic behaviour, $\sigma_s = E_s\varepsilon_s$ and $\sigma_c = E_c\varepsilon_c$, we get

$$\frac{d^2\delta}{dx^2} = \frac{1}{E_s}\frac{d\sigma_s}{dx} - \frac{1}{E_c}\frac{d\sigma_c}{dx} \tag{3.9}$$

which by insertion of Eq. (3.6) and (3.7) gives

$$\frac{d^2\delta}{dx^2} = \frac{4\tau_b}{DE_s}\big(1 - \frac{n\rho}{1-\rho}\big) \tag{3.10}$$

where $n = E_s/E_c$ = modular ratio. This expression can be solved analytically for certain bond shear stress-slip relations. This is the case for the tension chord model (Sigrist et al. 1998) which is addressed in the next section.

3.1.4 Tension Stiffening

The term "tension stiffening" refers to the tension carrying contribution of concrete between cracks, as described in subsection 2.2.1. As a result of the concrete contribution, the response of a member in a reinforced concrete structure is stiffer than naked reinforcement. However, tension stiffening will not influence the strength of the member directly, since the strength still is bounded by the steel stress at the crack.

By assuming that concrete carries tension between the cracks only, the entire axial load at the crack must be carried by the reinforcement. Between cracks, a part of the load is transferred to the concrete through bond shear stresses, so that the tension is carried both by concrete and steel. If sufficient amount of stresses are transferred so that the concrete tensile strength is exceeded, a new crack will form.

Figure 3.3 illustrates the distribution of concrete and steel stresses between two cracks for a symmetric case of uniaxial tension. The figure illustrates the remarks above. Steel stresses are at their maximum at cracks and decrease to their minimum in the centre between cracks. In contrary, concrete tensile stresses reach their maximum in the centre between cracks and vanish at cracks. The figure also includes the bond shear stresses, which typically have a distribution like the one sketched.

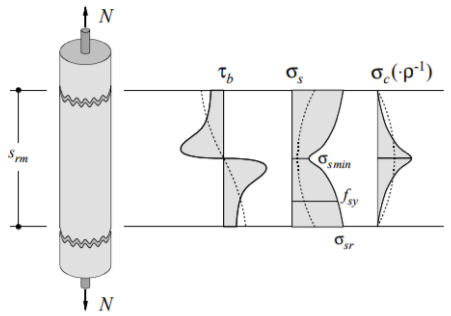

Figure 3.3: Stresses of a chord element between two cracks (Kaufmann 1998)

By assessment of the Figure 3.3 and Eq. (3.7), an expression for the maximum concrete stresses can be established. Since the tensile concrete stress cannot exceed its tensile capacity, the following limit must be fulfilled

$$\sigma_{c1} = \int d\sigma_c = \int_{x=0}^{S_{rm0}/2} \frac{4\tau_b}{D} \frac{\rho}{(1-\rho)} dx \leq f_{ct}$$

Here, all parameters in the integral are constant except for the bond shear stresses. This gives

$$\frac{4}{D}\frac{\rho}{(1-\rho)}\int_{x=0}^{S_{rm0}/2}\tau_b dx \leq f_{ct} \tag{3.11}$$

where S_{rm0} is maximum crack spacing for the fully developed crack pattern. The minimum crack spacing, $S_{rm0}/2$, is the necessary length for tensile stresses equal the capacity of concrete to be transferred to the concrete (Sigrist et al. 1998). Through the considerations of the crack pattern, the crack spacing will be constrained by the following boundary

$$S_{rm0}/2 \leq S_{rm} \leq S_{rm0}$$

often expressed on the form

$$0.5 \leq \lambda \leq 1 \tag{3.12a}$$

$$\lambda = \frac{S_{rm}}{S_{rm0}} \tag{3.12b}$$

The real distribution of bond shear stresses is nonlinear, and is complicated to solve analytically. However, Sigrist et al. (1998) has proposed a simplified approximation of the shear stress-slip relation, which match the overall real behaviour satisfyingly. The simplified idealization is the stepped, rigid-perfectly plastic bond shear stress-slip relation. Here a constant bond shear stress of $\tau_{b0} = 2f_{ct}$ and $\tau_{b1} = f_{ct}$ is assumed before and after yielding of the reinforcement respectively. This idealization of bond shear stress combined with bilinear stress-strain relationship for reinforcement, forms the basis of the tension chord model (TCM) (Sigrist et al. (1998), Kaufmann (1998)).

With this shear bond stress model established, the maximum crack spacing in uniaxial tension can be determined from Eq. (3.11)

$$\frac{4}{D}\frac{\rho}{(1-\rho)}\int_{x=0}^{S_{rm0}/2}\tau_b dx = \frac{4}{D}\frac{\rho}{(1-\rho)}\frac{\tau_b S_{rm0}}{2} = f_{ct}$$

With some rearranging this can be written as

$$S_{rm0} = \frac{f_{ct}D}{2\tau_{b0}}\frac{(1-\rho)}{\rho} \tag{3.13}$$

The assumption of constant bond shear stresses also yields that steel and concrete stresses between cracks vary linearly. This result can be seen by consideration of Eq. (3.6) and (3.7). If the maximum steel stresses at the crack are known, the distribution of bond shear, steel and concrete stresses can be determined. This situation is illustrated in Figure 3.4 (a).

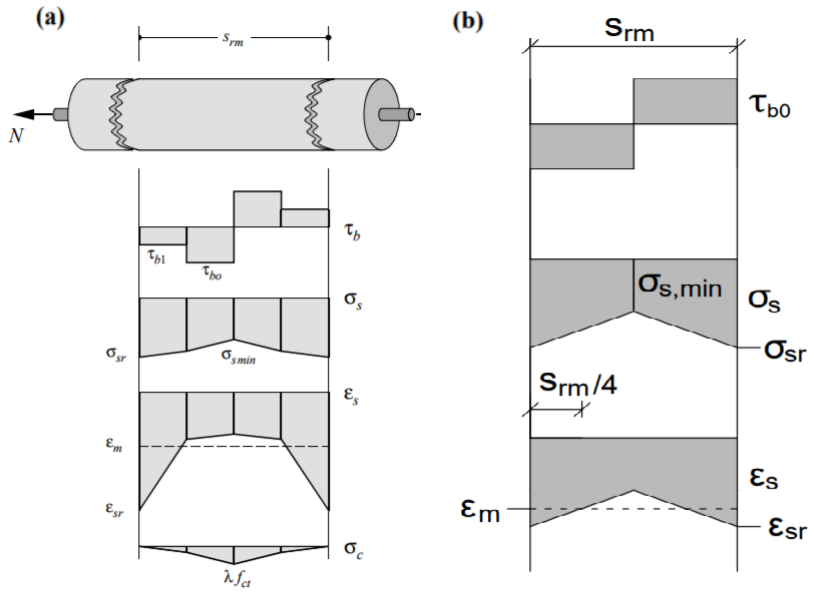

Figure 3.4: Tension chord model: (a) General distribution of stresses and strains (Kaufmann 1998), (b) distribution of stresses and strains for steel stresses lower than yield stress

The average strain, ε_m, which describes the overall behaviour in the direction of the reinforcement, can be used to determine the maximum steel stresses at the crack (Sigrist et al. 1998). The expression depends on whether the steel stresses are higher, lower or both higher and lower than the yield strength between cracks.

For steel stresses below yield stress over the whole element, $\sigma_{sr} \leq f_{sy}$, the shear bond stress, steel stress and steel strain distributions are given in Figure 3.4 (b). Since the stresses are below yield stress over the whole element we use the modulus of elasticity, E_s, and the constant shear bond stress, τ_{b0}, to describe the elastic behaviour. The steel stress at crack is now easily obtained from the average stress and the change of steel stress over the embedment length $S_{rm}/4$

$$\begin{aligned}\sigma_{sr} &= \sigma_m + \int_{x=0}^{S_{rm}/4} d\sigma_s \\ &= E_s\varepsilon_m + \int_{x=0}^{S_{rm}/4} \frac{4\tau_{b0}}{D} dx \\ &= E_s\varepsilon_m + \frac{\tau_{b0}S_{rm}}{D}\end{aligned} \tag{3.14}$$

When steel stresses are higher than yield stress over the whole element, $f_{sy} < \sigma_{s,min}$, the distribution of stresses is similar to Figure 3.4 (b). However, we now use the constant shear bond stress τ_{b1}. Furthermore, the average steel stress is determined from a combination of elastic and plastic behaviour. The expression is given as

$$\begin{aligned}\sigma_{sr} &= \sigma_m + \int_{x=0}^{S_{rm}/4} d\sigma_s \\ &= f_{sy} + (\varepsilon_m - \frac{f_{sy}}{E_s})E_{sh} + \int_{x=0}^{S_{rm}/4} \frac{4\tau_{b1}}{D} dx \\ &= f_{sy} + (\varepsilon_m - \frac{f_{sy}}{E_s})E_{sh} + \frac{\tau_{b1}S_{rm}}{D}\end{aligned} \tag{3.15}$$

Similar considerations can be performed for the case of steel stresses partially above and below yield stress, $\sigma_{s,min} \leq f_{sy} \leq \sigma_{sr}$. The expression becomes

$$\begin{aligned}\sigma_{sr} =& f_{sy} \\ &+ 2\frac{\frac{\tau_{b0}S_{rm}}{D} - \sqrt{(f_{sy} - E_s\varepsilon_m)\frac{\tau_{b1}S_{rm}}{D}(\frac{\tau_{b0}}{\tau_{b1}} - \frac{E_s}{E_{sh}}) + \frac{E_s}{E_{sh}}\tau_{b0}\tau_{b1}\frac{S_{rm}^2}{D^2}}}{\frac{\tau_{b0}}{\tau_{b1}} - \frac{E_s}{E_{sh}}}\end{aligned} \tag{3.16}$$

Noting that the average stresses between cracks must be in equilibrium with the stresses at crack, the following relation can be established

$$\sigma_{sm} + (\frac{1-\rho}{\rho})\sigma_{cm} = \sigma_{sr} \tag{3.17}$$

where σ_{sm} = the average steel stresses, and σ_{cm} = the average concrete stresses.

The maximum concrete tensile stress in the middle between two cracks becomes

λf_{ct}. Since the concrete stresses are zero at cracks, the mean concrete tensile stress between cracks becomes

$$\sigma_{cm} = \frac{\lambda f_{ct}}{2} \tag{3.18}$$

It should be noted that all relations presented here are based on the assumption of stabilized cracking stage. To take into account situations of low loading values where slip is not occurring over the entire element, Seelhofer (2009) adjusted the steel stress formulas Eq. (3.14), (3.15) and (3.16).

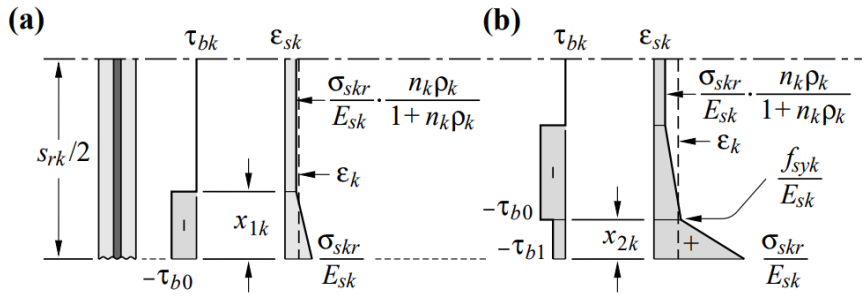

Figure 3.5: General distribution of bond stress and and steel strain in crack formation stage. (a) Steel stresses below yield stress, (b) steel stresses partially below and above yield stress (Seelhofer 2009). Note: subscript k indicate coordinate x or z.

Figure 3.5 (a) shows the situation where slip is occurring only over the length x_1. This length is smaller than half the crack spacing S_{rm}, and thus compatibility between steel and concrete is re-established at the distance x_1 from the crack. Since the steel stresses are below yield over the entire crack length in Figure 3.5 (a), the following relations can be established

$$\sigma_{c,max} = x_1 \frac{4\tau_{b0}}{D} \rho$$

$$\sigma_{s,min} = n\sigma_{c,max}$$

where Eq. (3.7) is used to determine the change of concrete stresses over the distance x_1 (assume $1 - \rho \simeq 1$) and $n = E_s/E_c$. With Eq. (3.6), the steel stress at crack is easily obtained

$$\begin{aligned}\sigma_{sr} &= \sigma_{s,min} + \int d\sigma_s \\ &= x_1 \frac{4\tau_{b0}}{D} n\rho + \int_{x=0}^{x_1} \frac{4\tau_{b0}}{D} dx \\ &= x_1 \frac{4\tau_{b0}}{D}(1+n\rho)\end{aligned}$$

The transfer length x_1 is determined based on the average strain ε_m, with the following relation

$$\begin{aligned}\varepsilon_m E_s \frac{S_{rm}}{2} &= \frac{\sigma_{sr}+\sigma_{s,min}}{2} x_1 + \sigma_{s,min}\left(\frac{S_{rm}}{2} - x_1\right) \\ \varepsilon_s E_s S_{rm} &= x_1^2 \frac{4\tau_{b0}}{D}(1+n\rho) + x_1 \frac{4\tau_{b0}}{D} n\rho (S_{rm} - x_1)\end{aligned}$$

Solving with respect to x_1 produce a quadratic equation, with solution

$$x_1 = \frac{S_{rm}}{2}\left(\sqrt{n^2\rho^2 + \frac{E_s\varepsilon_m}{\tau_{b0}}\frac{D}{S_{rm}}} - n\rho\right) \qquad \text{for } 0 \le x_1 \le S_{rm}/2 \tag{3.19}$$

Below the modifying expressions are given as they are presented in Seelhofer (2009). For steel stresses below the yield stress over the entire element, Eq. (3.20) is applied as derived above.

$$\begin{aligned}&\sigma_{sr} = x_1 \frac{4\tau_{b0}}{D}(1+n\rho) && \textit{where} \\ &x_1 = \frac{S_{rm}}{2}\left(\sqrt{n^2\rho^2 + \frac{E_s\varepsilon_m}{\tau_{b0}}\frac{D}{S_{rm}}} - n\rho\right) && [0 \le x_1 \le S_{rm}/2]\end{aligned} \tag{3.20}$$

For steel stresses exceeding the yield stress, Eq. (3.21) is applied. This expression is derived with similar consideration as for Eq. (3.20), based on Figure 3.5 (b).

$$\begin{aligned}&\sigma_{sr} = f_{sy} + x_2 \frac{4\tau_{b1}}{D} \qquad \text{where} \\ &x_2 = \frac{D f_{sy} E_{sh}}{4\tau_{b1}\alpha E_s}\left[\sqrt{1 + 4\alpha\frac{E_s}{E_{sh}}\left[\frac{S_{rm}\tau_{b1}}{D f_{sy}}\left(\frac{\alpha E_s \varepsilon_m}{f_{sy}} - n\rho\right) - \frac{\tau_{b1}}{4\alpha\tau_{b0}}\right]} - 1\right] \\ &\text{where } \alpha = 1 + n\rho \qquad [0 \le x_2 \le S_{rm}/2]\end{aligned} \tag{3.21}$$

3.1.5 Compatibility

Compatibility relations in a cracked orthogonally reinforced concrete membrane can simplified be derived based on the average total strains. From Mohr's circle of strains, Figure 3.6, the necessary relations are easily obtained by simple, geometrical considerations.

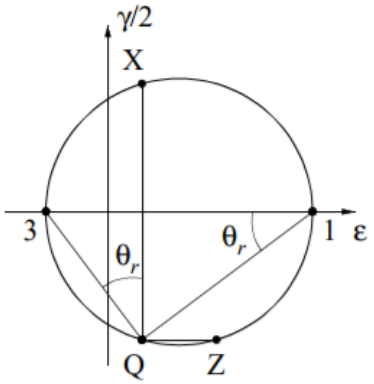

Figure 3.6: Mohr's circle of strains (Kaufmann 1998)

First, we see that

$$\varepsilon_1 + \varepsilon_3 = \varepsilon_x + \varepsilon_z \tag{3.22}$$

for the average total strains in the principal, x- and z-directions respectively. Furthermore, the relation between the crack angle and the average strains is (Kaufmann & Marti 1998)

$$cot^2\theta_r = \frac{\varepsilon_z - \varepsilon_3}{\varepsilon_x - \varepsilon_3} \tag{3.23}$$

where the crack angle is given by the angle between the crack direction and the x-axis. Rearranging Eq. (3.23) we get an equation solved with respect to the crack angle

$$\theta_r = \arctan\left(\sqrt{\frac{\varepsilon_x - \varepsilon_3}{\varepsilon_z - \varepsilon_3}}\right) \tag{3.24}$$

However, these equations are not completely general. Due to the squared term on

the left side of Eq. (3.23) information is lost. For a given combination of strains ε_x, ε_z and ε_3 the equations are not capable of determining in which quadrant the crack angle will appear. It is in this thesis suggested to make an initial estimate, to determine the correct quadrant for the crack angle. The procedure is presented in a proposed algorithm in Appendix A.

3.2 The Cracked Membrane Model

3.2.1 General

The cracked membrane model was developed by Kaufmann & Marti (1998) for analysis of reinforced concrete panels. The model combines the basic concepts of the compression field theory (Vecchio & Collins 1986) with a two-dimensional representation of the tension chord model (Sigrist et al. 1998).

In the cracked membrane model we consider a set of parallel, uniformly distributed cracks in an orthogonally reinforced concrete panel. The panel is subjected to a set of membrane forces, which are axial stresses in the x- and z-direction and shear stress. The situation is illustrated in Figure 3.7 (a). Equilibrium is satisfied at the crack and tension stiffening effects are accounted for by the tension chord model.

For a given state of external loading on a predefined membrane section, the model will predict the internal steel and concrete stresses. Or, more generally, the model can determine the complete load-deformation response. The designer can check the capacity of a given section, and the associated deformations. In addition, the model obtains the necessary information to estimate crack widths and crack spacing.

The underlying assumptions of the cracked membrane model are that cracks are stress free and able to rotate, and the concrete principal stress and principal strain directions are coincident. Furthermore, it is assumed that the section is cracked.

Note that a XZ-axis system is chosen for the derivation of the model to be consistent with the the way it was presented by Kaufmann & Marti (1998). Also note that the sign convention used for shear stress is opposite of most other models.

3.2.2 Equilibrium

In the cracked membrane model equilibrium is obtained at the cracks. Figure 3.7 (b) shows the stress situations at the crack. By consideration of the elements in Figure 3.7 (b), we can relate the external stresses σ_x, σ_z and $\tau_{xz} = \tau_{zx}$ to the internal reinforcement and concrete stresses at the crack σ_{sxr}, σ_{szr} and σ_{c3r}. Since the cracks are assumed to be stress free, $\sigma_{cnr} = 0$ and $\tau_{ctnr} = \tau_{cntr} = 0$. It is assumed that the reinforcement bars are well distributed, allowing us to model their effect by equivalent stresses over the element face. Concrete stress in the strut at a crack use the notation $\sigma_{ctr} = \sigma_{c3r}$. Now, equilibrium at the cracks yields (Kaufmann & Marti 1998)

$$\sigma_x = \rho_x \sigma_{sxr} + \sigma_{c3r} cos^2\theta_r \tag{3.25a}$$

$$\sigma_z = \rho_z \sigma_{szr} + \sigma_{c3r} sin^2\theta_r \tag{3.25b}$$

$$\tau_{xz} = -\sigma_{c3r} sin\theta_r cos\theta_r \tag{3.25c}$$

Rearranging, we get the following equations for reinforcement and concrete stresses at the crack

$$\sigma_{sxr} = (\sigma_x + \tau_{xz} cot\theta_r)/\rho_x \tag{3.26a}$$

$$\sigma_{szr} = (\sigma_z + \tau_{xz} tan\theta_r)/\rho_z \tag{3.26b}$$

$$\sigma_{c3r} = -\tau_{xz}(cot\theta_r + tan\theta_r) \tag{3.26c}$$

In the cracked membrane model the concepts of the tension chord model are extended to the two-dimensional case of cracked panels. This allows us to use Eq. (3.14)-(3.16) to determine the steel stresses at the crack for known average strains in the in the x- and z-directions, ε_x and ε_z. Furthermore, Eq. (3.2) and (3.3) are used to determine the concrete stress at the cracks for a given set of maximum and minimum principal strains, ε_1 and ε_3. The crack angle θ_r is given by the angle between the crack direction and the x-axis (in the range $-\pi/2$ and $\pi/2$), and is determined by Eq. (3.24).

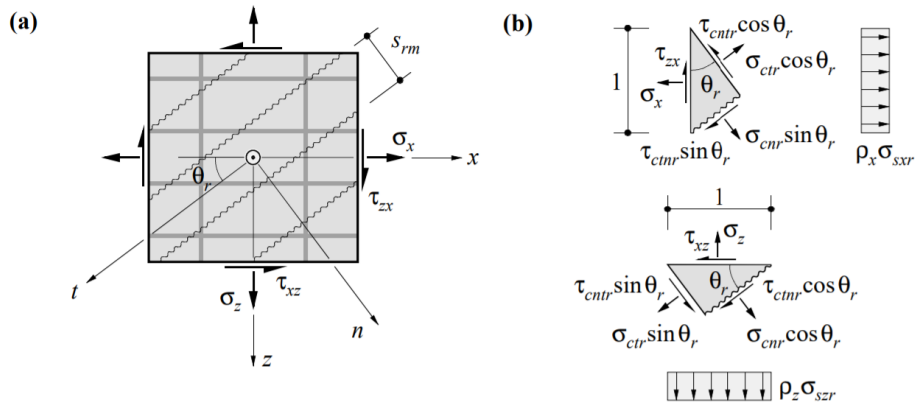

Figure 3.7: Cracked membrane model: (a) cracked membrane section, (b) stress equilibrium at crack (Kaufmann 1998)

3.2.3 Crack Spacings

Figure 3.8 shows crack spacing in the directions of the reinforcement, S_{rmx} and S_{rmz}, in addition to the diagonal crack spacing S_{rm}. For a given crack inclination, θ_r, the following relations are easily obtained

$$S_{rm} = S_{rmx} sin\theta_r = S_{rmz} cos\theta_r \tag{3.27}$$

In subsection 3.1.4, an expression for the maximum crack spacing in the uniaxial case was derived, Eq. (3.13). By extending the tension chord model to the present biaxial case, the maximum crack spacing in the x- and z-direction is obtained (Kaufmann & Marti 1998)

$$S_{rmx0} = \frac{f_{ct} D_x}{2\tau_{b0}} \frac{1-\rho_x}{\rho_x} \tag{3.28a}$$

$$S_{rmz0} = \frac{f_{ct} D_z}{2\tau_{b0}} \frac{1-\rho_z}{\rho_z} \tag{3.28b}$$

And, similarly as we did in subsection 3.1.4, we introduce

$$\lambda_x = \frac{S_{rmx}}{S_{rmx0}} \tag{3.29a}$$

$$\lambda_z = \frac{S_{rmz}}{S_{rmz0}} \tag{3.29b}$$

If $\lambda_x = 1$, the crack spacing in the x-direction is equal to the maximum crack spacing. In this case the stress transferred to the concrete at the centre between two cracks will be equal to the tensile strength of the concrete. For a smaller crack spacing however, the maximum concrete stress will not reach the tensile capacity. The same reasoning applies for the z-direction. This can be expressed as $\Delta\sigma_x = \lambda_x f_{ct}$ and $\Delta\sigma_z = \lambda_z f_{ct}$, where $\Delta\sigma_x$ and $\Delta\sigma_z$ denote the change of concrete stresses between cracks, see Figure 3.8. Combining these relations with Eq. (3.27) and (3.29), gives

$$\lambda_x = \frac{\Delta\sigma_x}{f_{ct}} = \frac{S_{rm}}{S_{rmx0} sin\theta_r} \tag{3.30a}$$

$$\lambda_z = \frac{\Delta\sigma_z}{f_{ct}} = \frac{S_{rm}}{S_{rmz0} cos\theta_r} \tag{3.30b}$$

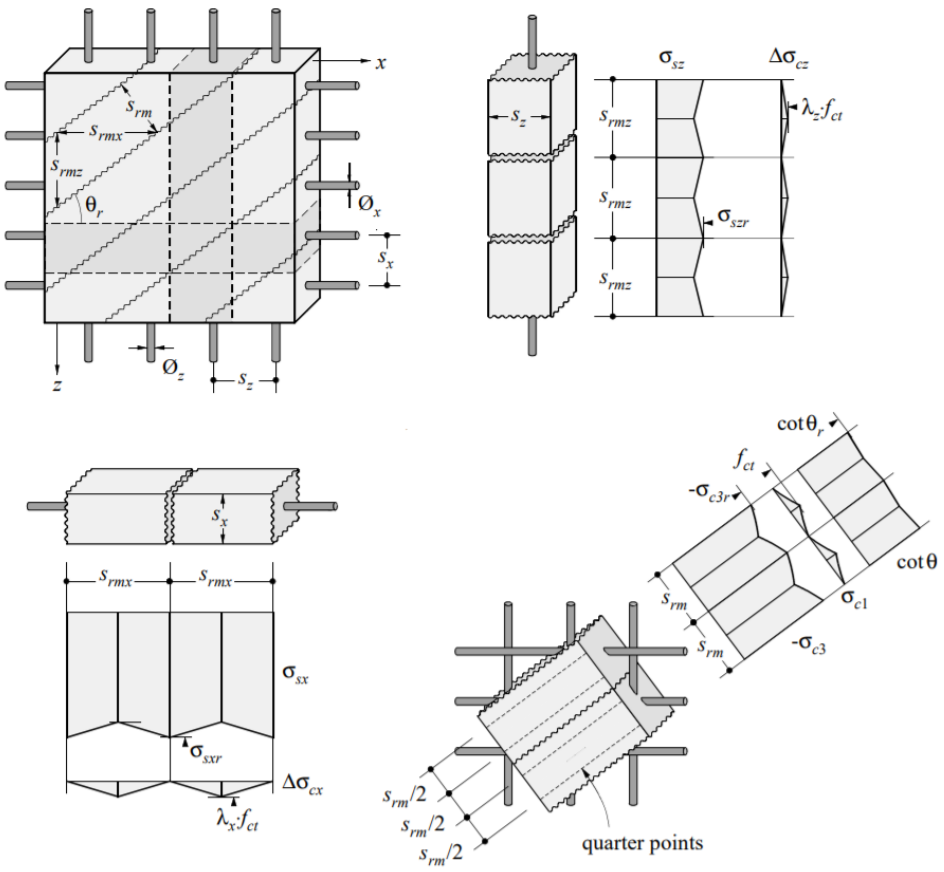

Figure 3.8: Crack spacings and concrete stresses (Kaufmann 1998)

Now, we want to determine the maximum diagonal crack spacing, S_{rm0}. First we consider Figure 3.9, which sketches Mohr's circle for stresses at cracks and at the centre between cracks. From simple geometrical considerations of the situation at crack we find the following relations

$$\sigma_{c3r} = \tau_{xz}(cot\theta_r + tan\theta_r)$$

$$\frac{\sigma_x + \sigma_z}{2} = -\frac{\sigma_{c3r}}{2} = -\frac{\tau_{xz}}{2}(cot\theta_r + tan\theta_r)$$

$$\sigma_z - \sigma_x = \frac{2\tau_{xz}}{tan2\theta_r} = \tau_{xz}(cot\theta_r - tan\theta_r)$$

In the last relation, the identity $tan2\theta_r = \frac{2tan\theta_r}{1-tan^2\theta_r}$ is used. With these relations

in mind, the centre and radius of Mohr's circle of the situation at centre between cracks become

$$C = \frac{(\sigma_x + \lambda_x f_{ct}) + (\sigma_z + \lambda_z f_{ct})}{2} = \frac{\sigma_x + \sigma_z}{2} + \frac{f_{ct}}{2}(\lambda_x + \lambda_z)$$

$$R = \sqrt{\left[\frac{(\sigma_z + \lambda_z f_{ct}) - (\sigma_x + \lambda_x f_{ct})}{2}\right]^2 + \tau_{xz}^2}$$
$$= \sqrt{\left[\frac{\sigma_z - \sigma_x}{2} - \frac{f_{ct}}{2}(\lambda_x - \lambda_z)\right]^2 + \tau_{xz}}$$

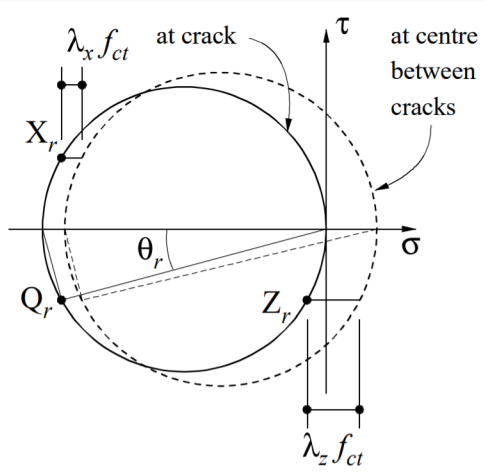

Figure 3.9: Mohr's circle of concrete stresses: total stresses at crack and at centre between cracks (Kaufmann 1998)

We want to find the maximum principle stress σ_1 at centre between cracks. σ_1 is located at the rightmost point of the dashed circle in Figure 3.9. This stress cannot exceed the tensile capacity of concrete. With the observations above we obtain the following equation

$$C + R = \sigma_1 \leq f_{ct}$$

$$\frac{f_{ct}}{2}(\lambda_x + \lambda_z) - \frac{\tau_{xz}}{2}(cot\theta_r + tan\theta_r) + \sqrt{\left[\frac{\tau_{xz}}{2}(cot\theta_r - tan\theta_r) - \frac{f_{ct}}{2}(\lambda_x - \lambda_z)\right]^2 + \tau_{xz}^2} \leq f_{ct} \quad (3.31)$$

which is how the formula is presented in Kaufmann & Marti (1998). This equation may be used to find the maximum crack spacing. Solving Eq. (3.31) at the limit, a solution for the maximum crack spacing S_{rm0} is obtained on closed form (Dabbagh & Foster 2006)

$$S_{rm0} = \frac{a + \eta b - \sqrt{\eta c + d + S_{rmz0}^2 + \eta^2(S_{rmx0}^2 - d)}}{2} \quad (3.32)$$

where $\eta = |\tau_{xz}|/f_{ct}$ and the parameters a, b, c and d given by

$$\begin{aligned} a =& S_{rmx0}\sin|\theta_r| + S_{rmz0}\cos|\theta_r| \\ b =& S_{rmx0}\cos|\theta_r| + S_{rmz0}\sin|\theta_r| \\ c =& 2(S_{rmx0}^2 + S_{rmz0}^2)\sin|\theta_r|\cos|\theta_r| - 2S_{rmx0}S_{rmz0} \\ d =& (S_{rmx0}^2 - S_{rmz0}^2)\sin^2|\theta_r| - 2S_{rmx0}S_{rmz0}\sin|\theta_r|\cos|\theta_r| \end{aligned}$$

The derivation of Eq. (3.32) is given in Appendix C. Note however that stabilized cracking stage is assumed for both Eq. (3.31) and (3.32).

The minimum crack spacing is determined in the same way as for uniaxial tension. Tensile stresses equal to the concrete tensile strength have to be transferred to the concrete in order to form a new crack. Therefore, the minimum crack spacing equals $S_{rm0}/2$, and the crack spacing is limited by $0.5 \leq \lambda \leq 1$ for the fully developed crack pattern, where $\lambda = S_{rm}/S_{rm0}$.

Calculations based on Eq. (3.32) have been implemented in a Matlab-script. The output from the program is a plot of the maximum crack spacing for different crack inclinations. The result is shown in Figure 3.10. As seen from the plot, the maximum crack spacing follow a curly shape for small ratios of $|\tau_{xz}|/f_{ct}$. For higher ratios, a linear upper bound is approached.

However, Eq. (3.31) and Eq. (3.32) are not valid for small values of applied shear stress (crack angle close to 0 or $\pm\pi$). Considering Eq. (3.30a) it is clear

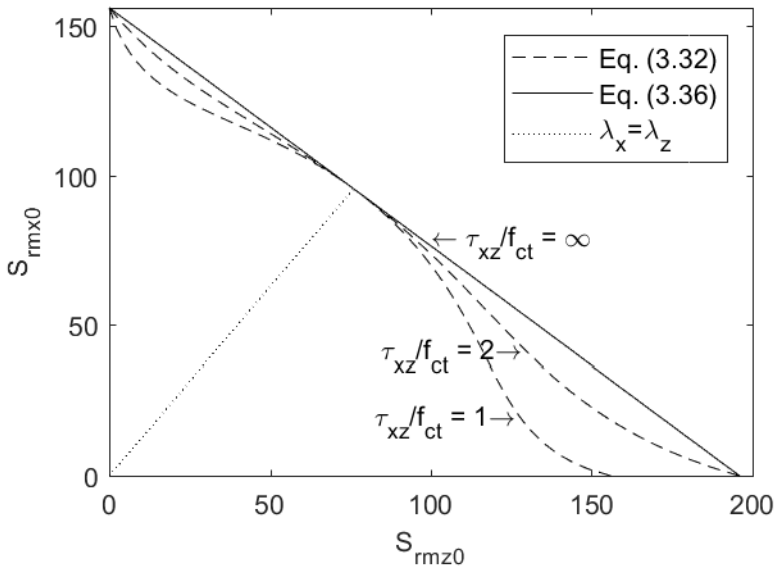

Figure 3.10: Plot of maximum crack spacing S_{rm0}. Upper bound calculated with Eq. (3.36).

that difficulties arise for the special case of $\theta_r = 0$. In that case, the solution should reduce to the known solution of uniaxial tension in the z-direction, where $\lambda_x = 0$, $\lambda_z = 1$ and $S_{rm} = S_{rmz0}$. However, as elaborated by Dabbagh & Foster (2006), the problem occures due to an over-calculation of the bond stress in the x-reinforcement. The tension chord model assumes that the limiting bond stress is $\tau_b = \tau_{b0}$, while for the special case of $\theta_r = 0$ the force in the x-reinforcement is zero, and thus the shear bond stress should also be zero in the x-direction. The same reasoning applies for the limit case of $|\theta_r| = \pm\pi/2$.

If Eq. (3.32) is solved for η with $S_{rm} = S_{rmz0}$ for the limit case $\theta_r = 0$, one obtains the result $\eta = S_{rmz0}/S_{rmx0}$. Similarly, with $S_{rm} = S_{rmx0}$ for $|\theta_r| = \pm\pi/2$ gives $\eta = S_{rmx0}/S_{rmz0}$. Generally, in order for the solutions of Eq. (3.31) and (3.32) to satisfy the boundary limits, Dabbagh & Foster (2006) present the following limiting condition

$$\text{for} \theta_r < \theta_{\lambda_x=\lambda_z} \qquad \eta \geq S_{rmz0}/S_{rmx0} \tag{3.33a}$$

$$\text{for} \theta_r > \theta_{\lambda_x=\lambda_z} \qquad \eta \geq S_{rmx0}/S_{rmz0} \tag{3.33b}$$

For values of η that are not fulfilling the conditions of Eq. (3.33), the shear bond

stress in either the x- or z-direction is smaller than τ_{b0}. Or in other words, the stabilized cracking stage is not reached in one of the directions.

To deal with situations where the conditions of Eq. (3.33) are not met, Dabbagh & Foster (2006) have proposed a solution procedure that handles all cases. For more details about this procedure, see the article of Dabbagh & Foster (2006).

Simplified Expression for Max. Crack Spacing

In the modified compression field theory (Vecchio & Collins 1986) a simple expression was proposed for the maximum crack spacing. This is similar to the expressions given in Eurocode 2 (CEN 2004) and Model Code 2010 (*fib* 2013):

$$S_{rm0} = \left(\frac{sin|\theta_r|}{S_{rmx0}} + \frac{cos|\theta_r|}{S_{rmz0}} \right)^{-1} \tag{3.34}$$

Eq. (3.34) may be used as a simple, approximate solution, and in the following the derivation of the expression is shown.

Once again, the Mohr circle shown in Figure 3.9 is considered. The stresses transferred to the concrete are divided into two parts, one symmetric and one antisymmetric part. The concrete stresses at cracks are now expressed with two new Mohr circles, as illustrated in Figure 3.11 (a) and (b).

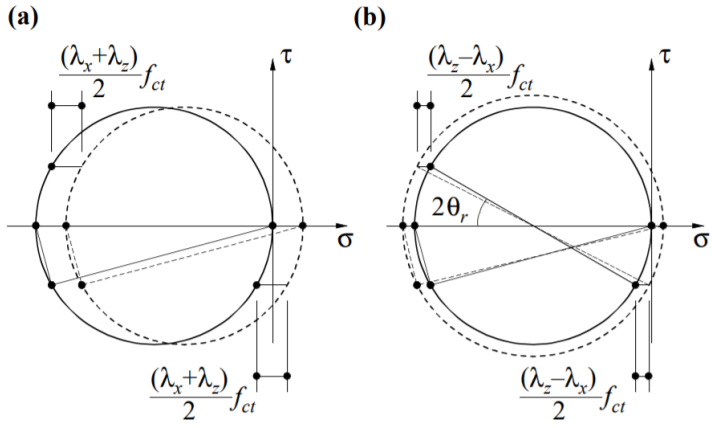

Figure 3.11: Mohr's circle of concrete stresses divided into (a) symmetric and (b) antisymmetric parts (Kaufmann 1998)

The symmetric part moves the circle of stresses at crack to the right by $\frac{f_{ct}}{2}(\lambda_x+\lambda_z)$, while the anti-symmetric part expands its radius by $\frac{f_{ct}}{2}(\lambda_z-\lambda_x)cos(2\theta_r)$. Now the maximum principle stresses at centre between cracks become

$$\sigma_{c1} = \frac{f_{ct}}{2}(\lambda_x+\lambda_z) - \frac{f_{ct}}{2}(\lambda_x-\lambda_z)cos(2\theta_r) \tag{3.35}$$

Noting the identity $cos2\theta_r = 2cos^2\theta_r - 1 = 1 - 2sin^2\theta_r$, the relation becomes

$$\frac{f_{ct}}{2}\big[\lambda_x - \lambda_x(1-2sin^2\theta_r)\big] + \frac{f_{ct}}{2}\big[\lambda_z + \lambda_z(2cos^2\theta_r - 1)\big]$$

or

$$f_{ct}\big[\lambda_x sin^2\theta_r + \lambda_z cos^2\theta_r\big]$$

Setting this expression equal to $f_{ct}\lambda$, we get the relation

$$\lambda = \lambda_x sin^2\theta_r + \lambda_z cos^2\theta_r$$

Recalling Eq. (3.12) and (3.27), the approximate solution of the maximum crack spacing simplifies to

$$S_{rm0} = \left(\frac{sin|\theta_r|}{S_{rmx0}} + \frac{cos|\theta_r|}{S_{rmz0}}\right)^{-1} \tag{3.36}$$

This expression is not dependent on loading. Comparing it with Eq. (3.31) we see that the factor $|\tau_{xz}|$ is omitted. Therefore this method only gives an approximate solution. However, it coincides with Eq. (3.31)/(3.32) for large ratios of $|\tau_{xz}|/f_{ct}$, and for $\lambda_x = \lambda_z$. The upper boundary obtained from Eq. (3.36) is included in Figure 3.10. Furthermore, the problems related to low values of $|\tau_{xz}|$ disappears.

3.2.4 Solution Methods

With all derivations and relations presented so far, a solution can be obtained. The material, compatibility and equilibrium equations provide the tools to find the solution where the internal forces are in equilibrium with the applied external forces.

In the general solution, the average strains ε_x, ε_z and ε_3 are considered as the primary unknowns. All necessary relations can be determined as functions of these

three unknowns. For a given set of applied loads, equilibrium between external and internal forces is determined through iterations.

If complete load-deformation response is to be determined, Kaufmann & Marti (1998) advice to increment ε_3 instead of τ_{xz}. The response curve is deformation controlled in order to avoid difficulties related to the post peak behaviour of concrete (post-peak behaviour not included in this thesis). For each increment of ε_3, the values of ε_x and ε_z are determined in an iterative manner for the corresponding external loads.

In Appendix A an algorithm is proposed to find the internal response corresponding to a given set of applied loads σ_x, σ_z and τ_{xz}, based on the cracked membrane model. If instead we are interested in the complete load-deformation response or the response corresponding to a given set of known steel and shear stresses (σ_{sxr}, σ_{szr} and τ_{xz}), the algorithm is easily adjusted.

In the algorithm, Newton-Raphson iterations are performed in order to solve the system of non linear equations. This leads to a robust procedure, where convergence in general is obtain after few iterations. Since all the equations of the model are on closed form, analytical expressions of the derivatives are obtained. The derivatives are given in Appendix B. Below, Step 12-15 of the algorithm are repeated. These steps shows how Newton-Raphson iterations are implemented in the solution procedure.

Step 12 - Calculate the function value for current estimates of ε_x, ε_z and ε_3

$$f_1 = \sigma_x - \sigma_{x,ext}$$
$$f_2 = \sigma_z - \sigma_{z,ext}$$
$$f_3 = \tau_{xz} - \tau_{xz,ext}$$

$$\boldsymbol{f} = \begin{bmatrix} f1 \\ f2 \\ f3 \end{bmatrix}$$

Step 13 - Check convergence according to chosen tolerance β

- If max($\boldsymbol{f}$) $\leq$ beta, convergence obtained and calculation can be terminated.
- If max($\boldsymbol{f}$) $>$ beta, no convergence obtained and calculation must proceed

Step 14 - Calculate the Jacobian matrix. The derivatives of function f_1, f_2 andf_3 must be calculated with respect to ε_x, ε_z and ε_3.

$$\boldsymbol{J} = \begin{bmatrix} \frac{\partial f_1}{\partial \varepsilon_x} & \frac{\partial f_1}{\partial \varepsilon_z} & \frac{\partial f_1}{\partial \varepsilon_3} \\ \frac{\partial f_2}{\partial \varepsilon_x} & \frac{\partial f_2}{\partial \varepsilon_z} & \frac{\partial f_2}{\partial \varepsilon_3} \\ \frac{\partial f_3}{\partial \varepsilon_x} & \frac{\partial f_3}{\partial \varepsilon_z} & \frac{\partial f_3}{\partial \varepsilon_3} \end{bmatrix}$$

The elements of the matrix, and details of the derivations are given in Appendix B.

Step 15 - Calculate new estimations of ε_x, ε_z and ε_3 (Newton-Raphson step).

$$\boldsymbol{\varepsilon}_{i+1} = \boldsymbol{\varepsilon}_i - \boldsymbol{J}(\boldsymbol{\varepsilon}_i)^{-1}\boldsymbol{f}(\boldsymbol{\varepsilon}_i)$$

$$\begin{bmatrix} \varepsilon_x \\ \varepsilon_z \\ \varepsilon_3 \end{bmatrix}_{i+1} = \begin{bmatrix} \varepsilon_x \\ \varepsilon_z \\ \varepsilon_3 \end{bmatrix}_i - \begin{bmatrix} \frac{\partial f_1}{\partial \varepsilon_x} & \frac{\partial f_1}{\partial \varepsilon_z} & \frac{\partial f_1}{\partial \varepsilon_3} \\ \frac{\partial f_2}{\partial \varepsilon_x} & \frac{\partial f_2}{\partial \varepsilon_z} & \frac{\partial f_2}{\partial \varepsilon_3} \\ \frac{\partial f_3}{\partial \varepsilon_x} & \frac{\partial f_3}{\partial \varepsilon_z} & \frac{\partial f_3}{\partial \varepsilon_3} \end{bmatrix}_i^{-1} \begin{bmatrix} f_1 \\ f_2 \\ f_3 \end{bmatrix}_i$$

3.3 Approximate Analytical Solution

A simplified, approximate solution has also been proposed by Kaufmann (1998). Here it is assumed that the stresses and strains at the quarter points between cracks are representative for the total response of the element.

Now we combine Eq. (3.26a) and (3.26b) for the relation between steel stresses at cracks and external loading, Eq. (3.30a) and (3.30b) for the change of concrete stresses between cracks, and Eq. (3.17) and (3.18) for the relation between stresses at crack and average stresses. This gives steel stresses at the quarter points between cracks expressed as

$$\rho_x \sigma_{sx} = \sigma_x + \tau_{xz} cot\theta_r - \frac{f_{ct}}{2}\lambda_x(1-\rho_x) \tag{3.37a}$$

$$\rho_z \sigma_{sz} = \sigma_z + \tau_{xz} tan\theta_r - \frac{f_{ct}}{2}\lambda_z(1-\rho_z) \tag{3.37b}$$

Assuming, as we did in subsection 3.2.3, that the tensile stresses transferred to the concrete are divided into one symmetric and one anti-symmetric part, the minimal

principal stress of the concrete at the centre between cracks is

$$-\tau_{xz}(tan\theta_r + cot\theta_r) + \frac{f_{ct}}{2}(\lambda_x + \lambda_z) + \frac{f_{ct}}{2}(\lambda_x - \lambda_z)cos2\theta_r$$

This can be seen from Figure 3.11 and with the same considerations as in subsection 3.2.3. The minimum and maximum principal stresses are assumed to vary linearly between the cracks, and Eq. (3.35) gives the maximum principal concrete stress at the centre between cracks. Using these equations, the minimum principal stress at the quarter points is derived as

$$\sigma_{c3} = -\tau_{xz}(tan\theta_r + cot\theta_r) + \frac{f_{ct}}{2}(\lambda_x + \lambda_z - \lambda) \tag{3.38}$$

If linear elastic response is assumed and Poisson's ratio is set to zero, the strains ε_x, ε_z and ε_3 are determined with Eq. (3.37) and (3.38) as

$$\varepsilon_x = \frac{\sigma_{sx}}{E_s} = \frac{\sigma_x + \tau_{xz}cot\theta_r - \frac{f_{ct}}{2}\lambda_x(1-\rho_x)}{\rho_x E_s} \tag{3.39a}$$

$$\varepsilon_z = \frac{\sigma_{sz}}{E_s} = \frac{\sigma_z + \tau_{xz}tan\theta_r - \frac{f_{ct}}{2}\lambda_z(1-\rho_z)}{\rho_z E_s} \tag{3.39b}$$

$$\varepsilon_3 = \frac{\sigma_{c3}}{E_c} = -\frac{\tau_{xz}(tan\theta_r + cot\theta_r) - \frac{f_{ct}}{2}(\lambda_x + \lambda_z - \lambda)}{E_c} \tag{3.39c}$$

If the results of Eq. (3.39) are substituted into the relation $\cot^2\theta_r = \frac{\varepsilon_z - \varepsilon_3}{\varepsilon_x - \varepsilon_3}$ we obtain the following equation

$$\begin{aligned} &tan^2\theta_r\rho_x(1+n\rho_z) + tan\theta_r\rho_x\left\{\frac{\sigma_z}{\tau_{xz}} - \frac{f_{ct}}{2\tau_{xz}}\Big[\lambda_z + n\rho_z(\lambda_x + \frac{n-1}{n}\lambda_z - \lambda)\Big]\right\} \\ &= cot^2\theta_r\rho_z(1+n\rho_x) + cot\theta_r\rho_z\left\{\frac{\sigma_x}{\tau_{xz}} - \frac{f_{ct}}{2\tau_{xz}}\Big[\lambda_x + n\rho_x(\lambda_z + \frac{n-1}{n}\lambda_x - \lambda)\Big]\right\} \end{aligned} \tag{3.40}$$

This result can be used to find the crack angle θ_r. However, the solution is obtained through iterations since λ_x and λ_z depend on θ_r.

A way to avoid iterations is to neglect the tensile capacity of concrete. Then, the equation simplifies to

$$tan^2\theta_r\rho_x(1+n\rho_z) + tan\theta_r\rho_x\frac{\sigma_z}{\tau_{xz}} = cot^2\theta_r\rho_z(1+n\rho_x) + cot\theta_r\rho_z\frac{\sigma_x}{\tau_{xz}} \tag{3.41}$$

Another solution is obtained if the maximum principal direction is assumed constant between the cracks and maximum principal stresses varying linearly with direction perpendicular to the cracks. Noting that this causes λ_x=λ_z=λ, gives

$$\begin{aligned} tan^2\theta_r\rho_x(1+n\rho_z) + tan\theta_r\rho_x\left\{\frac{\sigma_z}{\tau_{xz}} - \frac{f_{ct}}{2\tau_{xz}}\lambda\Big[1+(n-1)\rho_z\Big]\right\} \\ = cot^2\theta_r\rho_z(1+n\rho_x) + cot\theta_r\rho_z\left\{\frac{\sigma_x}{\tau_{xz}} - \frac{f_{ct}}{2\tau_{xz}}\lambda\Big[1+(n-1)\rho_x\Big]\right\} \end{aligned} \tag{3.42}$$

Figure 3.12 shows a plot of the crack angle $\cot\theta_r$ for varying reinforcement ratios, obtained from a Matlab-script with a given set of geometrical and material inputs. Here the three equations above are included, in addition to the general solution. The different methods give the same result for equal reinforcement amounts in both x- and z-direction. However, for increasing difference of the ρ_x/ρ_z ratio the results deviate more. According to Kaufmann (1998) both Eq. (3.40) and Eq. (3.41) seem to provide a good estimation of the crack angle, as they follow the behaviour of the general method closely. Eq. (3.42) on the other hand deviate more from the general solution.

With known crack angle from one of the equations above, steel and concrete stresses at cracks can easily be determined from Eq. (3.26). These stresses can be controlled for failure criteria of reinforcement and concrete.

3.4 Crack Width

Based on the response predictions obtained with either the general or the approximate method, we can get an estimate of the crack widths of a cracked concrete panel. The crack width, w_r, is determined by the tensile strain at crack, denoted $\varepsilon_1^{(r)}$, and the crack spacing, S_{rm}. The expression is (Kaufmann 1998)

$$w_r = S_{rm}\varepsilon_1^{(r)} \tag{3.43}$$

The overall maximum principal strain, ε_1, consists of two parts, the tensile strain at crack, $\varepsilon_1^{(r)}$, and the tensile concrete strains, $\varepsilon_1^{(c)}$. If linear elastic behaviour is

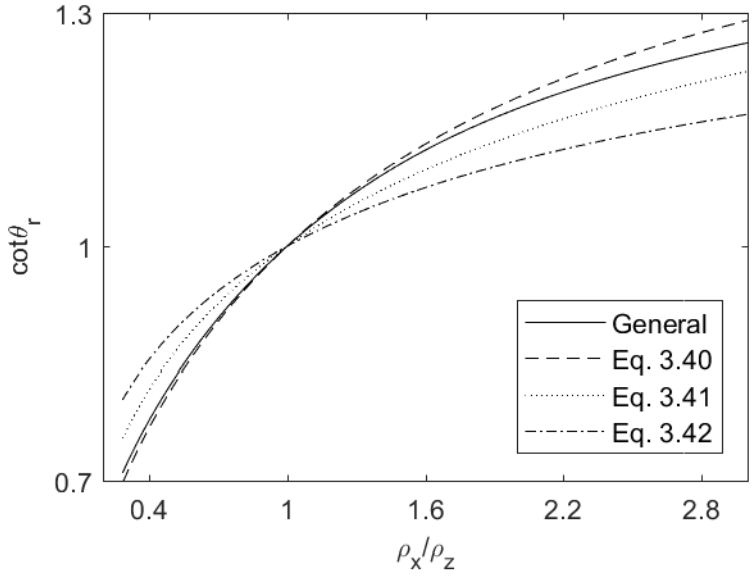

Figure 3.12: Plot of estimated crack angle for varying reinforcement ratios with the different approaches

assumed, we can estimate the tensile concrete strain as follows

$$\varepsilon_1^{(c)} = \frac{\sigma_{c1} - \nu_{13}\sigma_{c3}}{E_c} \tag{3.44}$$

where ν_{13} is the Poisson's ratio. According to Kaufmann (1998), a value of $\nu_{13} \approx 0.15$ gives satisfying results for moderate concrete compressive stresses. Furthermore, Kaufmann (1998) recommends using the values of σ_{c1} and σ_{c3} at the quarter points between the cracks. Note that for stabilized cracking stage, $\sigma_{c1} = \lambda f_{ct}/2$ at the quarter point, while $\sigma_{c3}/E_c = \varepsilon_3$, if concrete stresses are assumed to vary linearly between cracks.

Recalling the compatibility relation of average strains from Eq. (3.22), where ε_x, ε_z and ε_3 are known from the solution of the cracked membrane model, we obtain an estimate for the crack width

$$w_r = S_{rm}(\varepsilon_x + \varepsilon_z - \varepsilon_3 - \varepsilon_1^{(c)}) \tag{3.45}$$

$$= S_{rm}\left(\varepsilon_1 + \nu_{13}\varepsilon_3 - \frac{\lambda f_{ct}}{2E_c}\right) \tag{3.46}$$

As a simple estimate of the crack width, the mean tensile strain can be used instead of the tensile strain at crack in Eq. (3.43).

4 Analysis of Reinforced Concrete Shell Elements

4.1 Introduction

A shell element is defined based on its geometry and the way load is carried. Generally, a shell element is a three-dimensional solid with a small thickness compared to the other two directions. Furthermore, a shell section can be part of both plane and curved structures. A shell section can resist a combination of in-plane forces and bending forces.

Figure 4.1 shows a shell element with corresponding force resultants along the edges. In total, 8 different force resultants are acting on the shell element. These are three membrane forces N_x, N_y and N_{xy}, two bending moments M_x and M_y, torsional moment M_{xy}, and two transverse shear forces V_x and V_y. All forces and moments are given in units per length. It is assumed that N_{xy}=N_{yx} and M_{xy}=M_{yx}.

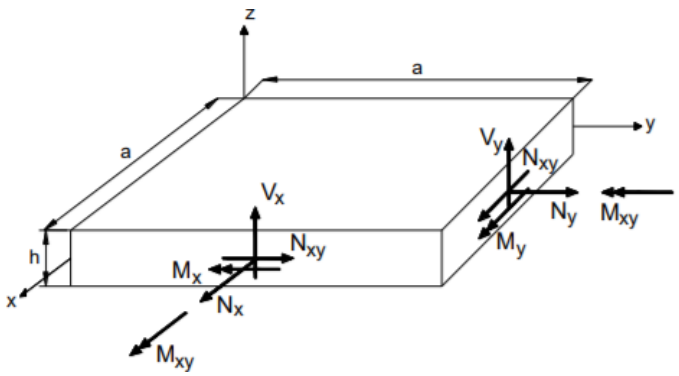

Figure 4.1: Shell element with force resultants (Øverli & Sørensen 2012)

Typically, a structural analysis is carried out with a finite element program to find the distribution of the stress resultants defined above. Based on these resultants, a suitable reinforcement amount is determined by a design procedure, like for instance the sandwich method. The determination of the external forces and reinforcement amounts will not be discussed any further in this thesis, but assumed given.

The iteration method (Øverli & Sørensen 2012) is a tool which can be implemented to obtain the internal response of a reinforced concrete structure, where geometry and reinforcement amounts are given. Equilibrium between external and internal forces is achieved through an iterative process. Transversal shear forces V_x and V_y are not considered in the iteration method, and must be handled separately.

Briefly summarized, the approach of the iteration method is to find the strain distribution of the shell section that ensure equilibrium between external and internal forces. The shell section is divided into layers, where each layer is handled as membranes with in-plane forces only. The internal response of each layer, corresponding to the strain distribution, is found by implementing orthotropic material models in the directions of the principal stresses. By summing the force contributions of each layer, the internal force resultants are found. The material stiffness matrix and the strain distribution are updated at each iteration step until convergence is obtained. The derivation of the model is described below, in accordance with Øverli & Sørensen (2012). Furthermore, the algorithm of the model is given in Appendix D.

4.2 Derivation of the Iteration Method

4.2.1 Constitutive Relations

In order to determine the response in concrete and reinforcement for a given strain, constitutive relations must be formulated.

Concrete has a non-linear behaviour in compression, and will crack for moderate tension stresses. An orthotropic material model in the directions of the principal stresses can be employed to account for these effects. The expression is

$$\boldsymbol{\sigma}_{cp} = \begin{bmatrix} \sigma_1 \\ \sigma_2 \\ \tau_{12} \end{bmatrix} = \boldsymbol{C}_{cp} \cdot \boldsymbol{\varepsilon}_p = \frac{1}{1-\nu^2} \begin{bmatrix} E_{c11} & \nu E_{c12} & 0 \\ \nu E_{c12} & E_{c22} & 0 \\ 0 & 0 & \frac{(1-\nu)E_{c12}}{2} \end{bmatrix} \cdot \begin{bmatrix} \varepsilon_1 \\ \varepsilon_2 \\ \gamma_{12} \end{bmatrix} \tag{4.1}$$

where $\boldsymbol{\sigma}_{cp}$ and $\boldsymbol{\varepsilon}_p$ are the stress and strain vectors in the principal stress direction, and $E_{c12} = (E_{c11} + E_{c22})/2$.

E_{c11} and E_{c22} are secant moduli in the principal stress directions, and may be determined by

$$E_{cii} = \frac{\sigma_{ci}}{\varepsilon_i} \tag{4.2}$$

In order to transfer concrete stresses, strains and stiffness matrices from local principal directions to the global xy-directions, a transformation matrix is needed. The transformation of strains from global axes to principal axes is defined as

$$\boldsymbol{\varepsilon}_p = \boldsymbol{T}(\theta) \cdot \boldsymbol{\varepsilon}_{xy} \tag{4.3}$$

where θ is the angle of the principal strain direction given as

$$\theta = \frac{1}{2} \tan^{-1} \left(\frac{\gamma_{xy}}{\varepsilon_x - \varepsilon_y} \right) \tag{4.4}$$

and the transformation matrix is given as

$$\boldsymbol{T}(\theta) = \begin{bmatrix} \cos^2\theta & \sin^2\theta & \sin\theta\cos\theta \\ \sin^2\theta & \cos^2\theta & -\sin\theta\cos\theta \\ -2\sin\theta\cos\theta & 2\sin\theta\cos\theta & \cos^2\theta - \sin^2\theta \end{bmatrix} \tag{4.5}$$

Assuming that the principal stresses have the same direction as the principal strains, the principal stresses and the material stiffness matrix are transferred to the global axes by

$$\boldsymbol{\sigma}_{cxy} = \boldsymbol{T}^T(\theta) \cdot \boldsymbol{\sigma}_{cp} = \boldsymbol{T}^T(\theta) \cdot \boldsymbol{C}_{cp} \cdot \boldsymbol{\varepsilon}_p = \boldsymbol{T}^T(\theta) \cdot \boldsymbol{C}_{cp} \cdot \boldsymbol{T}(\theta) \cdot \boldsymbol{\varepsilon}_{xy} = \boldsymbol{C}_c \cdot \boldsymbol{\varepsilon}_{xy} \tag{4.6}$$

$$\boldsymbol{C}_c = \boldsymbol{T}^T(\theta) \cdot \boldsymbol{C}_{cp} \cdot \boldsymbol{T}(\theta) \tag{4.7}$$

For reinforcement, it is assumed that the direction of the reinforcement is coincident with the global xy-direction. The constitutive relation for the reinforcement is given as

$$\boldsymbol{\sigma}_{sxy} = \boldsymbol{C}_s \cdot \boldsymbol{\varepsilon}_{xy} = \begin{bmatrix} E_{sx} & 0 & 0 \\ 0 & E_{sy} & 0 \\ 0 & 0 & 0 \end{bmatrix} \cdot \begin{bmatrix} \varepsilon_x \\ \varepsilon_y \\ \gamma_{xy} \end{bmatrix} \tag{4.8}$$

where E_{sx} and E_{sy} are secant moduli for reinforcement in the global xy-directions. Hence, the two reinforcement directions are uncoupled.

4.2.2 Displacement Formulation

The goal of the iteration method is to find the state where the internal forces are equal to the external forces, which means that the correct strain distribution must be determined to provide equilibrium. The following equation must be fulfilled

$$\boldsymbol{R} = \boldsymbol{S}(\boldsymbol{\varepsilon}_{t,r}) \tag{4.9}$$

$$\boldsymbol{R} \begin{bmatrix} N_x \\ N_y \\ N_{xy} \\ M_x \\ M_y \\ M_{xy} \end{bmatrix}, \qquad \boldsymbol{\varepsilon_t} = \begin{bmatrix} \boldsymbol{\varepsilon}_m \\ \boldsymbol{\kappa} \end{bmatrix} = \begin{bmatrix} \varepsilon_{xm} \\ \varepsilon_{ym} \\ \gamma_{xym} \\ \kappa_x \\ \kappa_y \\ \kappa_{xy} \end{bmatrix}$$

where $\mathbf{R}$ is the external load vector, $\mathbf{S}$ is the internal load vector and $\boldsymbol{\varepsilon}_t$ is a vector containing the strains and curvatures at the middle plane of the shell section.

Kirchoff's hypothesis of linear strain distribution over the thickness of the shell is assumed, and gives the situation illustrated in Figure 4.2. The in-plane strains at a distance z from the middle plane of the shell section are now given as

$$\boldsymbol{\varepsilon}_{xy} = \begin{bmatrix} \varepsilon_x \\ \varepsilon_y \\ \gamma_{xz} \end{bmatrix} = \boldsymbol{\varepsilon}_m - z\boldsymbol{\kappa} = \boldsymbol{A} \cdot \boldsymbol{\varepsilon}_t = \begin{bmatrix} 1 & 0 & 0 & -z & 0 & 0 \\ 0 & 1 & 0 & 0 & -z & 0 \\ 0 & 0 & 1 & 0 & 0 & -z \end{bmatrix} \cdot \begin{bmatrix} \varepsilon_x \\ \varepsilon_y \\ \gamma_{xy} \\ \kappa_x \\ \kappa_y \\ \kappa_{xy} \end{bmatrix} \tag{4.10}$$

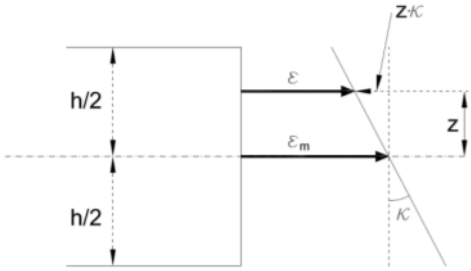

Figure 4.2: Strain distribution over shell thickness (Øverli & Sørensen 2012)

The correlation between strains and stresses of the internal response $\boldsymbol{S}(\boldsymbol{\varepsilon}_{t,r})$ in Eq. (4.9) is non-linear. In serviceability calculations this is due to cracking of concrete in tension and the non-linear behaviour of concrete in compression. The internal force vector must therefore be determined by a displacement formulation as shown below

$$\boldsymbol{S}(\boldsymbol{\varepsilon}_{t,r}) = \boldsymbol{K}(\boldsymbol{\varepsilon}_{t,r}) \cdot \boldsymbol{\varepsilon}_{t,r+1} \tag{4.11}$$

where $\boldsymbol{K}(\boldsymbol{\varepsilon}_{t,r})$ is the stiffness of the section at iteration number r.

4.2.3 Stiffness Matrix

The stiffness matrix may be established by employing the principal of virtual work. The displacement vector **r** is given below, and a is defined in Figure 4.1.

$$\boldsymbol{r} = a \cdot \boldsymbol{\varepsilon}_t = a \begin{bmatrix} \boldsymbol{\varepsilon}_m \\ \boldsymbol{\kappa} \end{bmatrix} = \begin{bmatrix} r_x \\ r_y \\ r_{xy} \\ \theta_x \\ \theta_y \\ \theta_{xy} \end{bmatrix} \tag{4.12}$$

The virtual displacement vector becomes

$$\delta\boldsymbol{r} = a \cdot \delta\boldsymbol{\varepsilon}_t \tag{4.13}$$

External virtual work is given as

$$\delta A_{ext} = \delta \boldsymbol{r}^T \cdot a \cdot \boldsymbol{R} \tag{4.14}$$

where a·$\boldsymbol{R}$ is total force. The internal work is given as

$$\delta A_{int} = \int_V \delta \boldsymbol{\varepsilon}^T \cdot \boldsymbol{\sigma} \cdot dV \tag{4.15}$$

For the derivation, a material model $\mathbf{C}$ is introduced for the combined contribution of concrete and reinforcement. If external and internal virtual work are equated, the following may be shown

$$\boldsymbol{R} = \int_{-h/2}^{h/2} \boldsymbol{A}^T \cdot \boldsymbol{C} \cdot \boldsymbol{A} \cdot dz \cdot \boldsymbol{\varepsilon}_t = \boldsymbol{K} \cdot \boldsymbol{\varepsilon}_t \tag{4.16}$$

The stiffness matrix is therefore given by

$$\boldsymbol{K} = \int_{-h/2}^{h/2} \begin{bmatrix} \boldsymbol{C} & -z\boldsymbol{C} \\ -z\boldsymbol{C} & z^2\boldsymbol{C} \end{bmatrix} \cdot dz \tag{4.17}$$

The stiffness matrix may be solved numerically by dividing the thickness of the shell section into layers, and summing up the contribution of each layer. If the cross section is divided into n layers, each layer has thickness $\Delta h = \frac{h}{n}$. For an increasing number of layers, the numerical integration will approach the exact integral. The stiffness contributions of concrete and steel are handled separately, and the total stiffness is a summation of the two contributions.

The concrete stiffness expression becomes

$$\boldsymbol{K}_C = \Delta h \sum_{i=1}^{n} \begin{bmatrix} \boldsymbol{C}_{ci} & -z_i\boldsymbol{C}_{ci} \\ -z_i\boldsymbol{C}_{ci} & z_i^2\boldsymbol{C}_{ci} \end{bmatrix} \tag{4.18}$$

and the reinforcement stiffness expression becomes

$$\boldsymbol{K}_S = \sum_{j=1}^{m} \left(A_{sxj} \begin{bmatrix} \boldsymbol{C}_{sxj} & -z_j\boldsymbol{C}_{sxj} \\ -z_j\boldsymbol{C}_{sxj} & z_j^2\boldsymbol{C}_{sxj} \end{bmatrix} + A_{syj} \begin{bmatrix} \boldsymbol{C}_{syj} & -z_j\boldsymbol{C}_{syj} \\ -z_j\boldsymbol{C}_{syj} & z_j^2\boldsymbol{C}_{syj} \end{bmatrix} \right) \tag{4.19}$$

where A_{sxj} and A_{syj} are the cross sectional area of the reinforcement in the two

directions at layer j. The total stiffness is

$$\boldsymbol{K} = \boldsymbol{K}_C + \boldsymbol{K}_S \tag{4.20}$$

The strain distribution is now easily determined by

$$\boldsymbol{\varepsilon}_t = \boldsymbol{K}^{-1} \cdot \boldsymbol{R} \tag{4.21}$$

4.2.4 Internal Stress Resultant

With constitutive relations established and the strain distribution determined above, the internal stress resultants may be calculated. The internal stress vector is given as

$$\boldsymbol{S} = \begin{bmatrix} \boldsymbol{S}_N \\ \boldsymbol{S}_M \end{bmatrix} = \begin{bmatrix} N_x \\ N_y \\ N_{xy} \\ M_x \\ M_y \\ M_{xy} \end{bmatrix} \tag{4.22}$$

The vector may be expressed as the integrals shown below

$$\boldsymbol{S}_N = \int_{-h/2}^{h/2} \boldsymbol{\sigma} \cdot dz \tag{4.23}$$

$$\boldsymbol{S}_M = \int_{-h/2}^{h/2} -z \cdot \boldsymbol{\sigma} \cdot dz \tag{4.24}$$

Similar as for the stiffness matrix, these integrals may be solved numerically by a summation of the contributions from the concrete and reinforcement layers. The expressions become

$$\boldsymbol{S}_N = \Delta h \sum_{i=1}^{n} \boldsymbol{\sigma}_{cxyi} + \sum_{j=1}^{m} \begin{bmatrix} A_{sxj} \cdot \sigma_{sxj} \\ A_{syj} \cdot \sigma_{syj} \\ 0 \end{bmatrix} \tag{4.25}$$

$$\boldsymbol{S}_M = -\Delta h \sum_{i=1}^{n} z_i \cdot \boldsymbol{\sigma}_{cxyi} + \sum_{j=1}^{m} \begin{bmatrix} -z_j A_{sxj} \cdot \sigma_{sxj} \\ -z_j A_{syj} \cdot \sigma_{syj} \\ 0 \end{bmatrix} \tag{4.26}$$

where $\boldsymbol{\sigma}_{cxyi}$ are the concrete stresses at layer i, and σ_{sxj} and σ_{syj} are the reinforcement stresses at layer j.

When the internal stress resultants are determined, they are compared with the external force resultants. If the deviation between the internal and external force is smaller than a convergence criteria for all of the six force components, an acceptable equilibrium is reached. If not, the iterations proceed with a new estimate of the stiffness matrix based on the strains found in the previous iteration step.

5 — New Method for Design of Shells in SLS

5.1 General

The goal of this thesis is to develop and propose a new approach for crack width estimation of shell sections in serviceability design. Both the external forces applied to the shell section, and the geometry and reinforcement layout are assumed given. These values are subsequently used as input in a post processing control where this new approach is implemented.

The iteration method and the cracked membrane model presented in chapter 3 and chapter 4, constitute the tools that will be used in the new method. For a given shell section and applied force, the iteration method is used to obtain global equilibrium between external and internal forces. With global equilibrium satisfied, the cracked membrane model is used to determine the response of the cracked face of the shell.

The collaboration between the iteration method and the cracked membrane model forms the new proposed method, referred to as "cracked shell model" throughout the rest of this thesis. In the following, two different approaches for the cracked shell model are proposed.

5.2 Approach

Before the calculations of the method can begin, the designer needs to provide all necessary input values. Therefore, external loading, section geometry and properties, and reinforcement layout must all be determined prior to the implementation

of the method. With input values determined, the iteration method is employed to find the strain distribution that ensure equilibrium between external and internal forces. In the iteration method the height of the cross section is divided into layers, see Figure 5.1. Through the strain distribution, average in-plane strains ε_x, ε_y and γ_{xy} are found for each layer. With known strains and constitutive relations, the steel and concrete stresses in each layer can be determined.

The stresses determined from the iteration method are used as input values for the cracked membrane model, where three values are necessary to solve the system of equations. One possibility is to use the steel stresses in the two reinforcement directions and the concrete shear stress. Another approach is to use the average axial stress in x- and z-direction and the concrete shear stress. The two possible approaches are explained in more detail below.

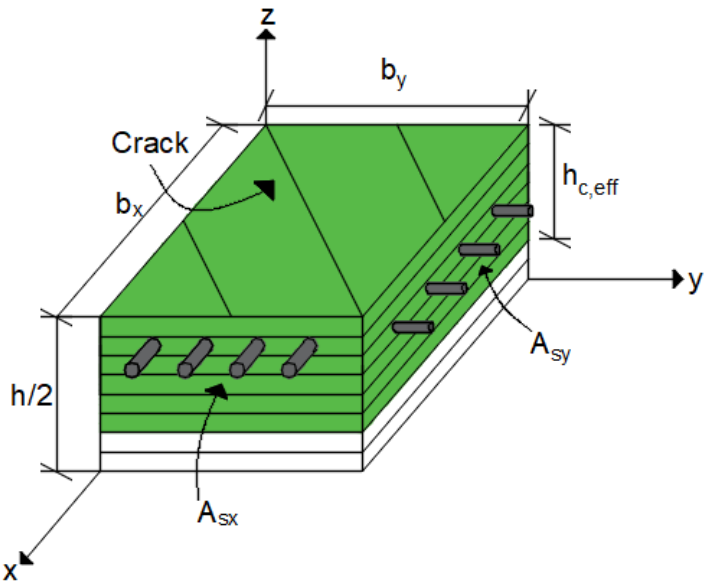

Figure 5.1: Cracked shell section illustrating the effective panel

Approach 1

In the first approach, the stresses in the x- and y-reinforcement, σ_{sx} and σ_{sy}, and the concrete shear stress, τ_{cxy}, are used as input to the cracked membrane model.

The steel stresses obtained from the iteration method are constant in each layer since tension stiffening effects between cracks are neglected. At a cracked surface,

the steel stresses must therefore be equal to the stresses at a crack. This is due to the fact that at a cracked surface, all tensile stresses must be transferred by the reinforcement across the crack. The steel stresses obtained from the iteration method can therefore directly be compared with the reinforcement stresses in the cracked membrane model, $\sigma_{sx} = \sigma_{sxr}$ and $\sigma_{sy} = \sigma_{szr}$.

In the iteration method, all shear stresses are a result of concrete shear stresses since shear contribution from the reinforcement is neglected. The concrete shear loading can therefore be compared with the external shear loading used in the cracked membrane model, $\tau_{cxy} = \tau_{xz}$. However, only the concrete shear stresses from the layers of interest, i.e. the layers within an effective height $h_{c,eff}$ at the cracked surface, must be considered. The situation is illustrated in Figure 5.1

It is not obvious how the effective height should be determined in order to translate the problem to a cracked membrane that is suitable for implementation in the cracked membrane model. The effect of different choices should be studied and compared to experimental results. However, as a first estimate, the effective height will be calculated in accordance with Eurocode 2 (CEN 2004). Thus, it is determined by Eq. (2.4).

Based on the shear stresses from all the layers within the effective height, a mean value for the shear stresses is determined

$$\tau_{cxy} = \frac{1}{h_{c,eff}} \sum_{i=1}^{n_{eff}} h_i \tau_{cxyi} \tag{5.1}$$

where n_{eff} is the number of layers within the effective height, h_i is the height of layer i and τ_{cxyi} is the concrete shear stress at layer i.

The values obtained from the iteration method used as input in the cracked membrane model are therefore:

Alternative 1

Input:

$\sigma_{sx}, \quad \sigma_{sy}, \quad \tau_{cxy}$

Compared to:

$\sigma_{sxr}, \quad \sigma_{syr}, \quad \tau_{xy}$

Approach 2

In the second approach, mean external axial stresses in the x- and y-direction, σ_x and σ_y, are determined from steel and concrete stresses obtained from the iteration method. These values becomes the first two input values in the cracked membrane model. In addition, and similarly as in approach 1, the concrete shear stress, τ_{cxy}, is used as the third input value.

The total internal axial forces of a reinforced concrete shell section originates from a combination of reinforcement and concrete stresses. In order to translate the internal forces into an equivalent external force, mean values of steel and concrete stresses must be determined within the area of interest. The effective height, over which the stresses are averaged, is determined by Eq. (2.4) similarly as for the shear stress. The mean axial stresses in x- and y-direction becomes

$$\sigma_x = \frac{1}{h_{c,eff}} \sum_{i=1}^{n_{eff}} h_i \sigma_{cx} + \frac{1}{b_y h_{c,eff}} \sum_{j=1}^{m_{eff}} A_{sxj} \sigma_{sx} \tag{5.2}$$

$$\sigma_y = \frac{1}{h_{c,eff}} \sum_{i=1}^{n_{eff}} h_i \sigma_{cy} + \frac{1}{b_x h_{c,eff}} \sum_{j=1}^{m_{eff}} A_{syj} \sigma_{sy} \tag{5.3}$$

The mean shear stress over the effective height is calculated the same way as in approach 1.

The values obtained from the iteration method used as input in the cracked membrane model are therefore:

Alternative 2
Input:
$\sigma_x, \quad \sigma_y, \quad \tau_{cxy}$
Compared to:
$\sigma_x, \quad \sigma_y, \quad \tau_{xy}$

The cracked shell model is schematically illustrated by the flowchart in Figure 5.2.

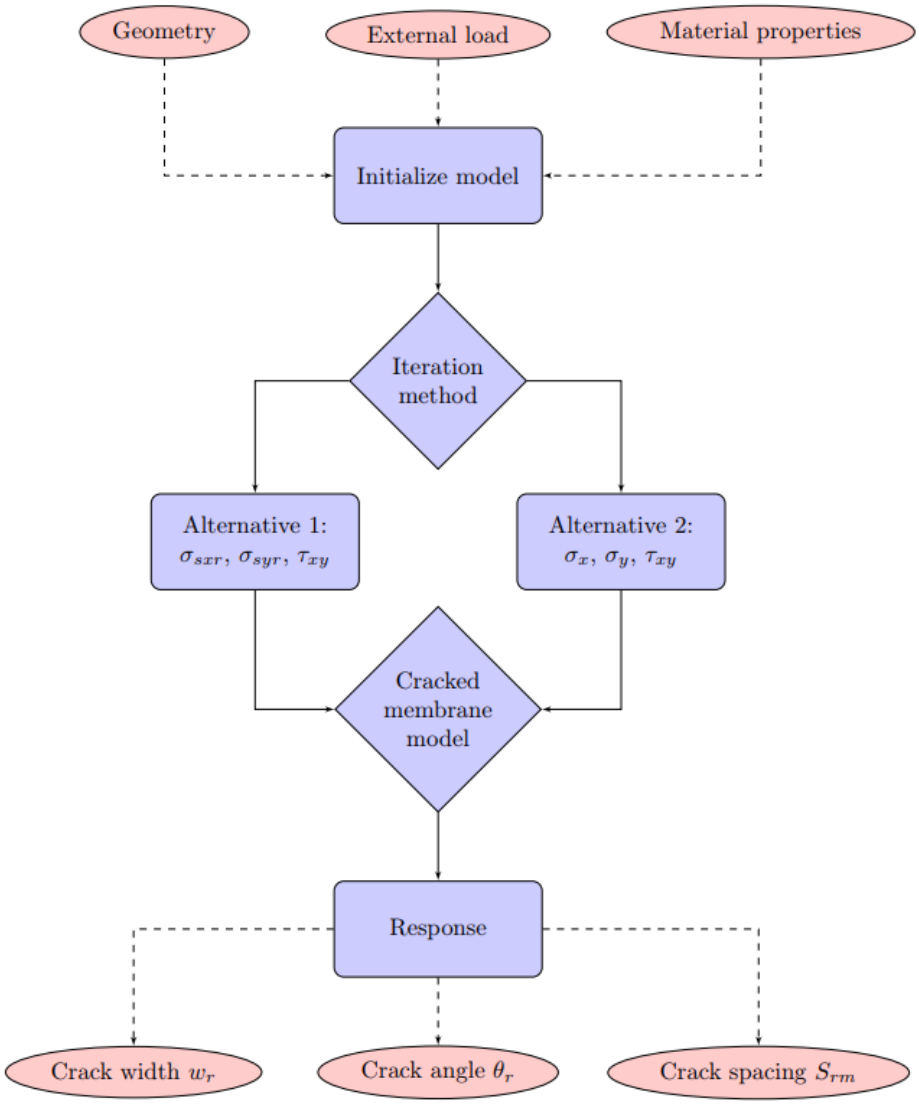

Figure 5.2: Flowchart describing the chain of events in the cracked shell model

6 — Results

6.1 Verification of the Cracked Membrane Model

Based on the algorithm proposed for the cracked membrane model shown in Appendix A, estimates of the response of a reinforced concrete membrane may be obtained. To verify that the algorithm provides reasonable results, it is compared with the results obtained for shear panel PP1 tested by Marti & Meyboom (1992).

Table 6.1 summarizes the main specimen properties for panel PP1. In Figure 6.1, the results predicted by the cracked membrane model are compared with results observed from the experimental tests, and show good agreement between the response predictions of the model and the real behaviour. In addition to demonstrating the ability of CMM to accurately predict the response of a panel, the example also shows that the proposed algorithm works properly. The results of the simplified version of CMM are also included, and show that this approach indeed is capable of predicting the response before yielding in a satisfactory manner. For serviceability considerations with steel stresses below yielding of reinforcement, the simplified method seems to provide reasonable results.

Considering the plot in Figure 6.1 (a), a more or less linear behaviour is observed, before the deformations increase more rapidly for shear stresses above 4 MPa. From plot (d) in the figure it appears that this is due to yielding of the weaker z-reinforcement. The x-reinforcement on the other hand, stays in the elastic domain. After the onset of yielding of the z-reinforcement, it is seen from plot (c) that the crack direction rotates towards the x-axis. The plots show that all these characteristics of the panel behaviour are accurately predicted by CMM.

Kaufmann (1998) employed the cracked membrane model to several other panels as well. In general, very good agreement between experimentally observed and predicted behaviour was obtained. Furthermore, even though not considered in this

Table 6.1: Main properties of panel PP1

Reinforcement:	D_x	[mm]	19.5
	ρ_x	[%]	1.942
	f_{syx}	[MPa]	479
	f_{sux}	[MPa]	667
	ε_{sux}	[10^{-3}]	90
	D_z	[mm]	11.3
	ρ_z	[%]	0.647
	f_{syz}	[MPa]	480
	f_{suz}	[MPa]	640
	ε_{suz}	[10^{-3}]	91
	E_s	[GPa]	200
Concrete:	f'_c	[MPa]	27.0
	f_{ct}	[MPa]	1.71
	ε_{co}	[10^{-3}]	2.12
	E_c	[GPa]	25.98
	G_c	[GPa]	11.13

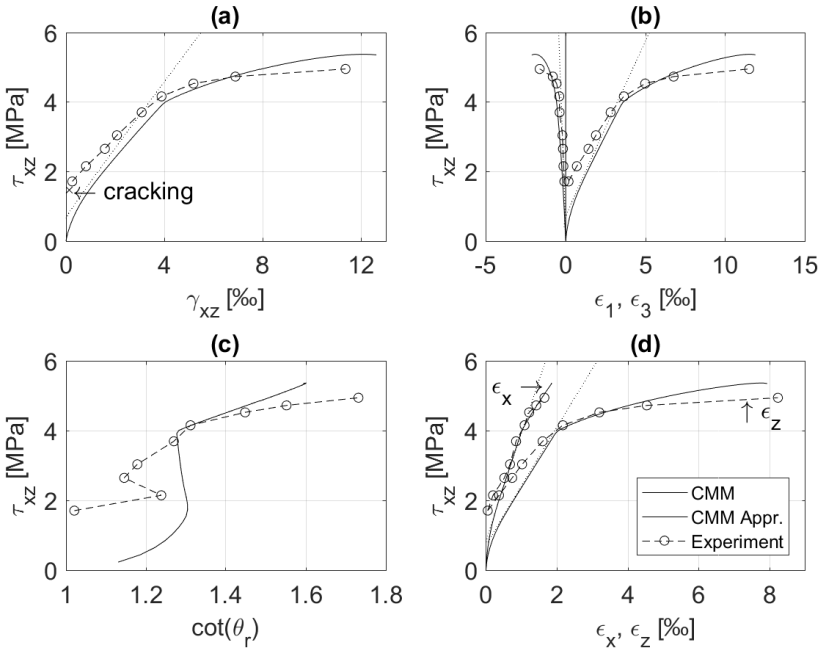

Figure 6.1: Comparison of predicted and observed response for shear panel PP1 tested by Marti & Meyboom (1992)

thesis, the correct failure mode was predicted by CMM for almost all experiments.

Note that in the cracked membrane model it is assumed that cracking has occurred. Thus, CMM is not able to describe the uncracked behaviour of panel PP1, which is seen from the deviation between the predicted and the observed behaviour for low values of τ_{xz} in all four plots in Figure 6.1. The load and strain values (τ_{xz} and γ_{xz}) in the panel when the first crack occurs are calculated below, in accordance with Marti & Meyboom (1992). The cracking point is indicated in Figure 6.1 (a).

For the uncracked stage, the panel is in a state of pure shear. Therefore, it is assumed that all load is carried by concrete ($\varepsilon_x = \varepsilon_z = 0$), and that shear strains are proportional to shear stresses ($\tau_{xz} = G_c\gamma_{xz}$). Furthermore, cracking occurs when the tensile strength of concrete is exceeded. The cracking load becomes

$$\begin{aligned}
\varepsilon_1 &= \frac{f_{ct}}{E_c} \\
\varepsilon_1 &= \frac{\varepsilon_x + \varepsilon_z}{2} + \sqrt{\left(\frac{\varepsilon_x - \varepsilon_z}{2}\right)^2 + \left(\frac{\gamma_{xz}}{2}\right)^2} = \frac{\gamma_{xz}}{2} \\
\tau_{xz} &= G_c\gamma_{xz} = \frac{2G_c f_{ct}}{E_c} \\
\implies &\quad \tau_{xz} = 1.5 \text{ MPa}, \quad \gamma_{xz} = 0.13 \cdot 10^{-3}
\end{aligned}$$

The response of panel VB1 tested by Zhang & Hsu (1998), with high strength concrete $f_c' = 98.2$ MPa, is also predicted by CMM algorithm developed in this thesis. Again, good correspondence between the predictions and the experimental observations is obtained, as shown in Figure 6.2 (a). However, in contrary to panel PP1, panel VB1 is calculated to be in the crack formation stage up to the onset of yielding in the reinforcement, which is indicated in Figure 6.2 (b) and (c). This observation seems to contradict the real physical behaviour, since stabilized cracking stage generally is obtained for steel stress levels considerably below the yield limit. This inconsistency must be attributed to Eq. (3.21) proposed by Seelhofer (2009), which is derived under the assumption of steel stresses above the yield limit. However, the modifications proposed by Seelhofer (2009) seem to be important for the robustness and efficiency of the proposed algorithm.

The original version of CMM (Kaufmann & Marti 1998) assumes that stabilized cracking stage is reached. While Seelhofer (2009) tried to modify the formulation in order to account for the crack formation stage, the elastic domain of the curve still seems to be the biggest weakness in the model. For SLS considerations this is the part of interest, and the possibilities for making changes here should be examined.

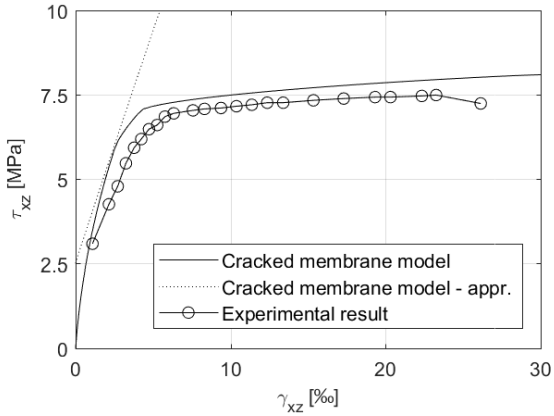

(a) Comparison of predicted and observed response for shear panel VB1 tested by Zhang & Hsu (1998)

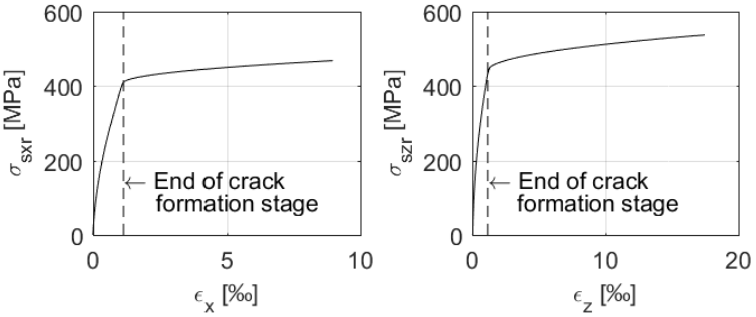

(b) Steel stress distribution with indication of crack formation stage for VB1

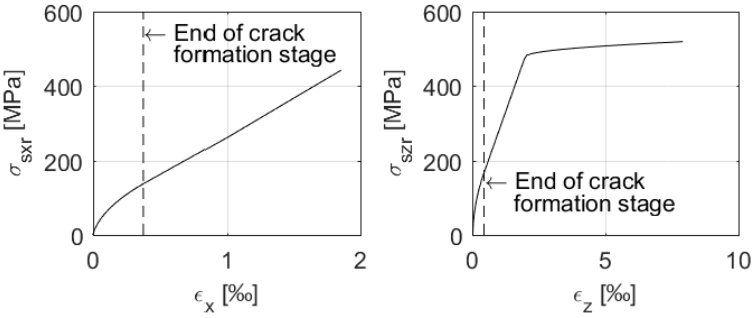

(c) Steel stress distribution with indication of crack formation stage for PP1

Figure 6.2: Response of panel VB1, and comparison of crack formation stage in panel VB1 and PP1.

6.2 Benchmark of Reinforced Concrete Ties

The cracked membrane model is developed for analysis of orthogonally reinforced concrete structures. However, in the special case where the crack angle is perpendicular to one of the reinforcement directions, the situation reduces from a two-directional to a one-directional problem. In this situation, the cracked membrane model is reduced to the uniaxial tension chord model (Sigrist et al. 1998).

In the following, crack width calculations are performed based on the cracked membrane model, Eurocode 2 (CEN 2004) and Model Code 2010 (*fib* 2013) formulations. The results will be compared with the results of virtual experiments conducted by Tan et al. (2018), where four cylindrical reinforced concrete ties were analyzed using non-linear finite element analysis. The ties considered were denoted ϕ20c40, ϕ32c40, ϕ20c90 and ϕ32c90, where ϕ indicates the steel bar diameter and c indicates the cover. For the range of steel stresses considered, the steel is modelled as linear elastic with E-modulus 200 000 MPa. Concrete grade C35 is used for all experiments, with concrete properties in accordance with Model Code 2010.

In Figure 6.3, the crack width development for increasing steel stresses obtained from the virtual experiments of Tan et al. (2018) are compared with the results from EC2, MC10 and CMM. The results show that CMM closely predicts the experimental observations for all four ties. Furthermore, CMM yields significantly better estimates than both EC2 and MC10, independent of bar diameter and concrete cover. However, it is seen that the response predictions are more accurate for $\phi 20c40$ and $\phi 32c40$ compared to $\phi 20c90$ and $\phi 32c90$, which deviates more from the experimental findings. The same effect is observed for EC2 and MC10.

In Table 6.2, the relative strains predicted by CMM, EC2 and MC10 are compared for steel stress equal to 400 MPa. Not surprisingly, EC2 and MC10 obtain the same results, since they are based on the same formula. For $\phi 20c90$, however, the results deviate due to the lower bound given in EC2, which is not included in MC10. The relative strain estimate of CMM is determined based on the formulas for steel stresses at cracks, derived in subsection 3.1.4. The results of CMM closely match the relative strain predictions of EC2 and MC10. This suggests that the deviations in crack width estimations, observed in Figure 6.3, occur due to different crack spacing predictions.

In Table 6.3, the crack distance observed in the virtual experiments is compared with the crack distances estimated by CMM, EC2 and MC10. Again, it is shown that the tension chord model provides much better results than both EC2 and

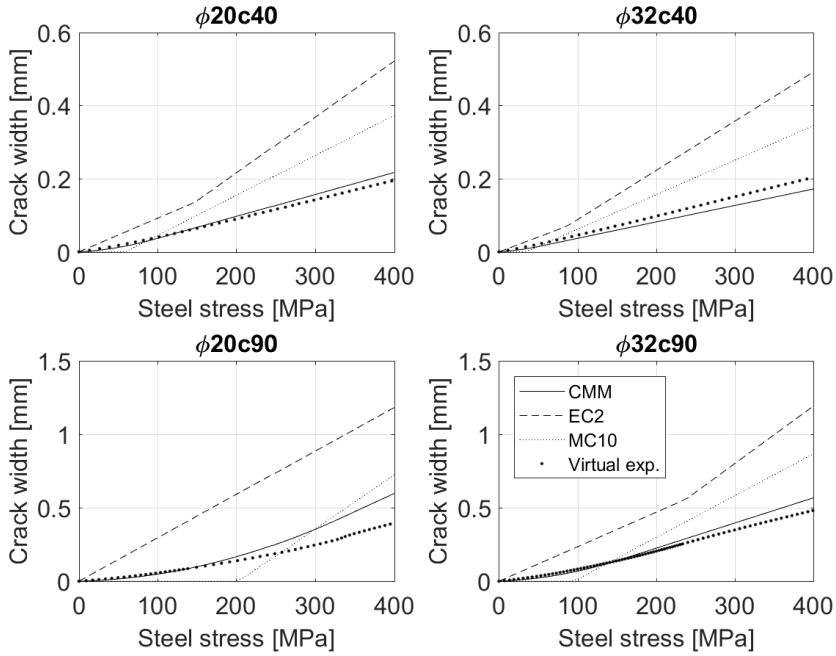

Figure 6.3: Comparison of development of crack widths of virtual experiments ((Tan et al. 2018)), Eurocode 2, Model Code 2010 and the cracked membrane model

Table 6.2: Comparison of relative strains for steel stress equal to 400 MPa

	Relative strain [10^{-3}]		
Tie element	**CMM**	**EC2**	**MC10**
ϕ20c40	1.8	1.7	1.7
ϕ32c40	1.9	1.8	1.8
ϕ20c90	1.2	1.2	0.99
ϕ32c90	1.7	1.5	1.5

MC10. For all three approaches, it is seen that the accuracy decrease for increasing concrete cover, which is particularly the case for the EC2 and MC10 approaches. This suggests that all three are less suitable for large scale concrete structures, and measures should be taken to improve their accuracy in such situations. In addition, it is seen that all three approaches fail at consistently accounting for the dependency of cover size and bar diameter in the predictions of crack spacing. However, the cracked membrane model seems to provide a considerable improvement of crack spacing predictions compared to EC2 and MC10.

Table 6.3: Comparison of crack spacings

	Crack spacing [mm]			
Tie element	**Experiment**	**CMM**	**EC2**	**MC10**
ϕ20c40	105	120	306	219
ϕ32c40	109	90	269	189
ϕ20c90	260	495	986	736
ϕ32c90	272	343	784	570

6.3 Benchmark of Shear Wall

The main purpose of this thesis is to explore the applicability of the cracked membrane model for design of concrete shell structures in the serviceability limit state. Currently, there are no good experimental results available for crack width development in shell sections. However, examining large reinforced concrete structures in the serviceability limit state is a good alternative. In that context, CMM is used for benchmark of a shear-wall examined in the framework of the French national research project CEOS.fr (Rospars & Chauvel 2014).

The shear wall considered, denoted SHW3, was designed to accurately reproduce reinforced thick shear walls used in industrial buildings. A horizontal load was applied to the upper corner of the wall to create a shear force, as shown in Figure 6.4 (a). The dimensions of the wall ensured that diagonal shear cracking is prevailing over cracks as a result of bending. Furthermore, beams with high reinforcement ratio were connected to the upper and bottom part of the wall to allow a better redistribution of shear forces in the wall. The test body was instrumented in order to measure crack widths and crack spacing during loading. The dimensions of the wall were 4200 mm of length, 1050 mm of height and 150 mm of thickness. Class C40 concrete was used, and reinforced with bars of 10 mm diameter and 100 mm spacing in both horizontal and vertical directions on both faces of the wall. For

more information about the test setup and material properties, see Rivillon & Gabs (2011).

A linear finite element (FE) analysis is performed with the FE-program DIANA FEA (2017) in order to estimate the load distribution in the wall. A relatively coarse mesh with element size of approximately 150 mm is used, and the influence of reinforcement is neglected in the analysis. Plots of the stress distribution in the wall are given in Figure 6.4 (b)-(d). It is seen from the plots that the stress distribution is not homogeneous in the wall. Therefore, results of the central part of the wall are considered, where mainly a state of homogeneous shear and horizontal compression are present. The results of an integration point from the FE-analysis in the center of the wall are used for the analytical calculations. The stresses σ_x = -1.155e-6 MPa, σ_y = -2.333e-7 MPa and τ_{xy} = 1.517e-6 MPa are obtained for the load level P = 1 N. Due to the linear elastic model, these stresses can simply be scaled to the load level of interest.

Based on results from the linear analysis, the cracked membrane model is used to estimate the response of the shear wall. In addition, calculations according to Eurocode 2 (CEN 2004) are performed with the MultiCon approach described in subsection 2.2.3. Since the FE-analysis provided the stresses for an integration point, an iterative approach is used to determine σ_{cI} and ε_{II} for the membrane element. This approach is similar to the iteration method, except that it is not necessary to divide the cross-sectional height into layers since there are no bending present.

In Table 6.4 the crack spacing and crack inclinations observed in the experiment are compared with those obtained from the analytical approaches, for an applied force P = 4200 kN. The theoretically predicted crack angles differ quite distinctively from the experimental observations. One possible reason for this may be that both the CMM and the EC2 estimates are based on the results of a rather simple FE-analysis. A more sophisticated analysis, taking into consideration the effect of reinforcement and the stiffness difference between the wall and the upper and lower beam, could yield better results. Additionally, the cracked membrane model is a rotating crack model, and is thus not path dependent. A fixed crack model could possibly provide better crack angle estimates.

Crack spacing results are obtained for both the horizontal and vertical components S_{rmx} and S_{rmy}, as well as the one perpendicular to the crack direction S_{rm}. For crack angles significantly lower than 45°, the crack spacing in the horizontal direction S_{rmx} may be much larger than S_{rm}. The crack spacing in the vertical

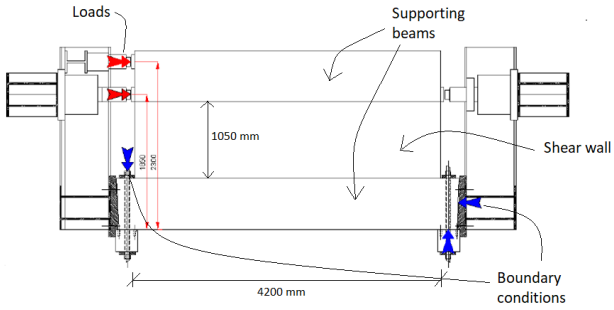

(a) Loads and boundary conditions

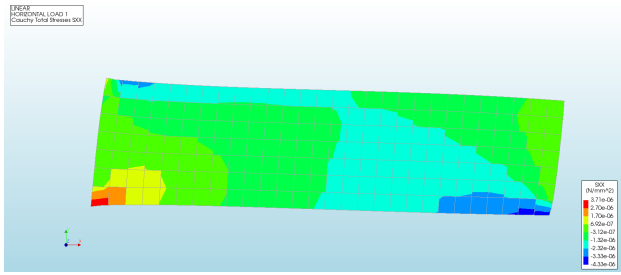

(b) Distribution of horizontal stresses σ_x

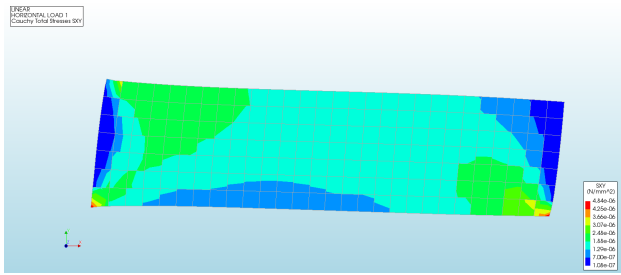

(c) Distribution of vertical stresses σ_y

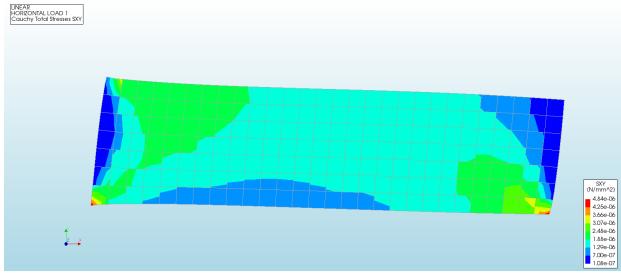

(d) Distribution of shear stresses τ_{xy}

Figure 6.4: Experimental setup and results from FE-analysis

Table 6.4: Crack spacing and direction in shear wall for P = 4200 kN. Note: Experimental values are averaged, while theoretical are characteristic.

		Crack spacing [mm]		
	Angle [°]	$\mathbf{S}_{rmx}$	$\mathbf{S}_{rmy}$	$\mathbf{S}_{rm}$
Experiment	28.4	206.0	111.0	98.0
CMM	39.5	174.6	143.8	111.0
CMM - Simplified	38.6	178.3	142.1	111.1
EC2	40.4	250.6	284.5	190.0

direction S_{rmy} should, however, be more comparable to S_{rm}. These remarks are met by the experimental observations. CMM also achieves this result, although with inaccurate results compared to the experiments. These inaccuracies can be attributed to the overestimation of the crack angle. The results of S_{rmx} and S_{rmy} obtained for EC2, however, give values conflicting the considerations above, and lack a physical interpretation. Finally, the crack spacing S_{rm} is quite accurately determined by both the general and the approximate version of CMM, despite a poor crack angle estimate. EC2 on the other hand overestimates both the crack spacing and its components, and is less accurate than CMM.

In Figure 6.5, the measured crack widths from the experiment are compared with the ones obtained from the analytical methods for increasing applied load. Once again, the central part of the wall is considered and the same integration point is used for the analytical calculations. Both mean and maximum values (the standard deviation) of the experimentally observed crack widths are included in the plot. The analytical results are given as characteristic values, and should therefore be compared to the maximum values from the experiment. During the test, new cracks were observed to keep on forming until P $\approx$ 2700 kN, which is indicated in the figure.

From Figure 6.5, it is seen that the cracked membrane model predicts the observed crack width development quite accurately. The experimental values show that the crack width increases rapidly after the first cracking occurs, while the deformation rate seems to decrease gradually until a linear growth is experienced when stabilized cracking stage is reached. Neither the general nor the approximate version of CMM captures the observed rapid crack width growth rate initially after a crack is formed. However, both estimates approach the linear path observed for the last part of the experimental curve. EC2 on the other hand, considerably overestimates the crack width for the complete load interval, and thus provides very conservative estimates.

A possible reason for the inaccuracies in the predictions of the CMM is that forces

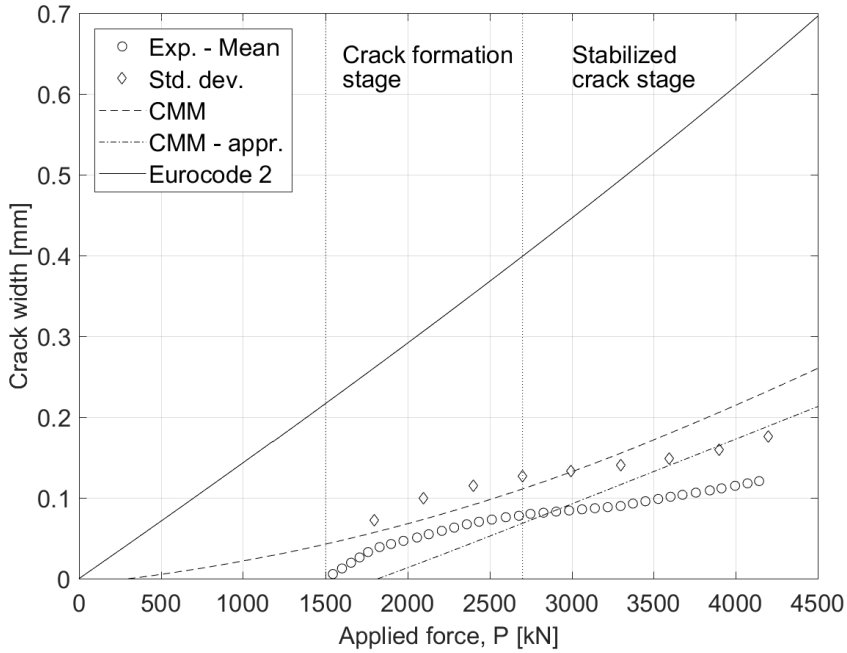

Figure 6.5: Comparison of crack width development. Experimental results obtained from Ruocci et al. (2012)

in the wall are redistributed during the loading. This is particularly the case when cracks are formed. The test setup, with heavily reinforced upper and lower beam and a steel frame, may significantly affect the deformation and crack width development. These effects are not captured by the simple FE-analysis and the cracked membrane model, which may explain the differing results.

Additionally, as discussed in section 6.1, CMM is derived based on the assumption that cracks are developed. Consequently the uncracked behaviour and the crack initiation are therefore not accounted for in the expressions. For loads of higher magnitude than P = 2700 kN, where a stabilized crack pattern is observed, the accuracy of the predictions is improved. This suggests that CMM is quite accurate for the stabilized cracking stage, which it was originally derived for. The crack formation stage, on the other hand, gives more inaccurate results, and it should be investigated whether it is possible to improve this part of the model. However, the FE-analysis combined with the CMM provides much better results than EC2 for the whole loading story.

As a rule of thumb, simplified methods should always produce more conservative results than more sophisticated methods. From Figure 6.5 it is seen that the simplified version of CMM provides less conservative results than the more complex CMM calculation. Thus, the results contradict the principle of simple methods being more conservative. This might reduce the general applicability of the simplified approximate version of CMM.

6.4 Verification of Iteration Method for Shell Section

Based on the algorithm for the iteration method shown in Appendix D, the response of a reinforced concrete shell section may be estimated, excluding the tension stiffening effect. In order to control that the algorithm provides reasonable results, it will in the following be compared with the results of a reliable reference.

Figure 6.6 shows an example of a top slab in a box girder bridge, where properties of the longitudinal reinforcement, geometry and material characteristics are given. The example is taken from Sørensen (2013), where a computer program with the iteration method implemented, was used to analyze the problem. The results from the analysis are presented in Sørensen (2013).

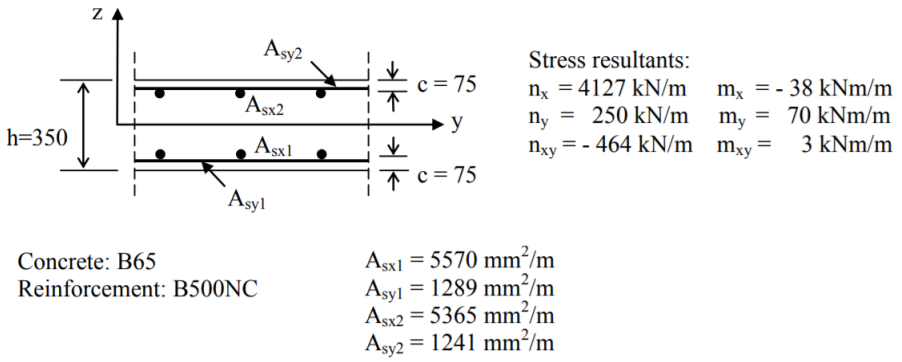

Figure 6.6: Shell section example with loading, geometry and material properties (Sørensen 2013)

The same input values are used in a Matlab-script developed for this thesis in accordance with Appendix D. The results of the reinforcement response predicted by the two different programs are presented in Table 6.5. Both stresses and strains in the reinforcement closely correspond between the two programs. Similarly, results of

the maximum compressive concrete stress and strain are shown in Table 6.6. Also here, the stress and strain values obtained from the two programs closely match. These results show that the program provides correct estimates, and indicate that the program functions properly.

Table 6.5: Stresses and strains in reinforcement

		Results from Sørensen (2013)		**Results from Matlab-script**	
	Reinforcement [mm^2/m]	**Stress** [MPa]	**Strain** [10^{-3}]	**Stress** [MPa]	**Strain** [10^{-3}]
A_{sx1}	5570	401	2.0	401.7	2.01
A_{sy1}	1289	435	3.1	434.8	3.20
A_{sx2}	5365	435	4.1	434.8	4.22
A_{sy2}	1241	262	1.3	262.4	1.31

Table 6.6: Maximum compressive stress and strain in concrete

	Stress [MPa]	**Strain** [10^{-3}]
Sørensen (2013)	12	0.4
Matlab-script "Iteration_method.m"	11.1	0.50

In the derivations of the iteration method in chapter 4, the Poisson's ratio is included to take into account the fact that two principal directions are not independent of each other. However, this is neglected in the calculations, and thus, the results correspond to uncoupled principal directions ($\nu = 0$).

6.5 Calculation Example for Shell Section

In chapter 5, a new approach was proposed for determination of the response of reinforced concrete shell elements. In the following, a demonstration of the calculation process will be performed. Calculations in accordance with Eurocode 2 (CEN 2004) will also be performed, and the results will be compared with the cracked shell model. The same example as in section 6.4 will be considered, with details given in Figure 6.6.

The results of the iteration method are the basis for the calculation of the new method where the cracked membrane model is included. Therefore, the first step of the approach is to employ the iteration method in order to obtain a strain

state over the cross-sectional height that ensures equilibrium between external and internal forces. The iteration method is employed similarly as in section 6.4, with the only exception that safety factors are excluded in the calculations since a SLS problem is considered.

With the results obtained from the iteration method, the cracked membrane model is used to determine the internal response at the cracked face, by consideration of an effective cracked panel. The effective area of the panel is determined by the effective height $h_{c,eff}$, and the panel is assumed to be in a state of plane stress. The two approaches described in chapter 5 are both considered, and the values of the necessary input parameters are given in Table 6.7. For alternative 1, steel and shear stresses (σ_{sxr}, σ_{syr} and τ_{xy}) are used to obtain the internal response, while axial and shear stresses (σ_x, σ_y and τ_{xy}) are used for alternative 2. Note that the diameter of the reinforcement bars is assumed to be 25 mm in x-direction and 16 mm in y-direction.

Table 6.7: Calculated values for input in the cracked membrane model

		Alternative 1
$h_{c,eff}$	[mm]	111.8
σ_{sxr}	[MPa]	443.3
σ_{syr}	[MPa]	195.7
τ_{xy}	[MPa]	-2.1

		Alternative 2
$h_{c,eff}$	[mm]	111.8
σ_x	[MPa]	20.1
σ_y	[MPa]	-1.6
τ_{xy}	[MPa]	-2.1

The EC2 approach follows the description in subsection 2.2.3. First, σ_{cI} is determined in stadium I based on the assumption of linear elastic materials. The iteration method is employed, similarly as in the cracked shell model, to obtain the crack angle at the face, θ_r, and the maximum principal strain at the reinforcement level, ε_{II}. The values underlying the calculations are shown in Table 6.8.

Table 6.8: Calculated values used in EC2 approach

$h_{c,eff}$	[mm]	111.8
$S_{r,max,x}$	[mm]	389.2
$S_{r,max,y}$	[mm]	472.8
ε_{II}	[-]	0.0032
σ_{cI}	[MPa]	12.0
f_{ct}	[MPa]	4.5
β	[-]	0.6

In Table 6.9 the crack angle, crack spacing, relative strain and crack width estimations of the different approaches are compared. The crack angle is given as the angle between the x-axis and the crack direction. In the crack width calculations

based on CMM, the effect of Poisson's ratio is neglected.

Table 6.9: Comparison between values obtained with the cracked shell model and the EC2/MultiCon approach

	Cracked shell model		
	Alternative 1	**Alternative 2**	**Eurocode 2**
Crack angle, θ_r [°]	63.5	62.2	65.1
Crack spacing, S_{rm} **[mm]**	117.8	118.0	310.5
Relative strain [$\mathbf{10^{-3}}$]	2.4	2.5	2.5
Crack width, w_r **[mm]**	0.284	0.291	0.764

The results show that the two alternative versions of the cracked shell model provide practically identical response estimates. This is as expected, since they are based on the same assumptions and the same model. Thus both alternatives are equally applicable to response predictions of shell sections.

The relative strains predicted by the EC2 approach match the cracked shell estimates closely. This result has been observed in the previous examples as well, and suggests that the different approaches for tension stiffening calculations in CMM and EC2 give the same result. However, the crack spacing determined by EC2 differs quite distinctively from the CMM predictions. The crack spacing estimates are therefore the cause of the major deviations in crack width estimates. With almost three times as high crack spacing estimate, the EC2 approach yields very large crack widths compared to the cracked shell model. Since no experimental results are included for comparison, it can not be concluded which of the approaches that produces the best estimate. Based on the previous examples, however, there is much evidence that suggests that cracked shell section provides the best crack width predictions of the two approaches.

The Large Universal Shell Element Tester (Kaufmann et al. 2018), described in subsection 2.1.3, can potentially provide experimental results needed to verify the cracked shell model. If experimental results verify that the cracked shell model produces accurate predictions, it will lead to a huge improvement of crack width estimates in large concrete shell structures. This is illustrated by this example, where the cracked shell model predicts the crack widths to be less than 40 % of the EC2 estimate.

7 — Discussion

7.1 Comparison of Design Codes and the Cracked Membrane Model

In the first part of this thesis, design provisions of Eurocode 2 (CEN 2004) and Model Code 2010 (*fib* 2013) are presented for crack width calculations. Although formulated a bit differently, the formulas include the same parameters and are formulated on the same basis. The crack width formula consists of two factors, the crack spacing and the relative strain. The crack width, crack spacing and relative stain formulas from MC10 are repeated below.

$$w_d = 2l_{s,max}(\varepsilon_{sm} - \varepsilon_{cm})$$

where

$$l_{s,max} = kc + \frac{1}{4}\frac{f_{ctm}}{\tau_{bms}}\frac{\phi}{\rho_{s,eff}}$$

$$\varepsilon_{sm} - \varepsilon_{cm} = \frac{\sigma_s - \beta\sigma_{sr}}{E_s}$$

Crack Spacing

The crack spacing formula consists of two terms, taking into account the effect of concrete cover and bond respectively. This involves the merging of two different theories (Tan et al. 2017), and yields a rather unphysical formulation. Furthermore, the crack spacing formulas of both EC2 and MC10 are empirically adjusted to fit experimental results on beams of relatively small size. This reduces the applicability of the formulas. However, since no other formulas are provided for crack

width calculations, also elements outside the scope of applicability are calculated according to the same formulas.

The tension chord model is developed for reinforced concrete members subjected to axial stress in the reinforcement direction, and is therefore appropriate for comparison with the EC2 and MC10 formulas. The crack spacing formula in the tension chord model Eq. (3.13) looks virtually the same as the last term of $l_{s,max}$ above. The shear bond stress in the MC10 and EC2 formulation is given as an empirically adjusted factor, while in the tension chord model it is based on the proposed shear bond stress - slip relation. However, both are assumed to be proportional to the tensile strength of the concrete, and thus they are practically equal.

The concrete cover term in the EC2 and MC10 formulas is, on the other hand, excluded from the tension chord model formulation. Based on the discussion above, the tension chord model seems to provide a more physically consistent description when it does not include the concrete cover in the crack spacing formula. The results in chapter 6 also show that the tension chord model provides much better crack spacing estimates, and thus a considerable improvement of the current code regulations.

Relative Strains

The relative strain formula in EC2 and MC10 includes the effect of tension stiffening, and is determined from the difference between the mean strains in the reinforcement and the concrete. The factor β is an integration factor that takes into account the distribution of concrete stresses, and it is adjusted for crack formation stage and stabilized cracking stage, respectively. The tension chord model is formulated based on the same ideas. However, the mean strains are determined as a function of crack spacing. Furthermore, the change of concrete stresses is determined based on the idealized shear bond stress-slip relation rather than an integration constant. In total, the tension chord model formulations seem to be more physical with the inclusion of crack distance and the shear bond stress. Based on the findings in chapter 6, however, both approaches seem to provide approximately the same estimates of the relative strain term.

The relative strain formula in EC2 and MC10 is derived based on beams in bending and tension, which makes the formula applicable only for cases where the maximum principle stress direction is coincident with the direction of the reinforcement. Since no provisions are provided for other cases, each designer must make subjec-

tive interpretations of the formula in order to adjust it for other situations. This may result in inconsistent choices and implementations. The MultiCon approach described in this thesis is an example of a interpretation of the formula for shell sections, where simplified assumptions and considerations are performed. Even though the assumptions included in the MultiCon seem reasonable, the approach is still based on an improper formula derived for beams and columns. The effect of the simplifications should therefore be examined in detail. In addition, the MultiCon approach considers a fictive reinforcement bar in direction of the maximum principal strain, which weakens the physical description of the situation.

7.2 Remarks for the Cracked Membrane Model

The cracked membrane model is a development of the modified compression field theory. Both models are based on the basic concepts of the original compression field approaches. However, they differ in the way the tension stiffening is accounted for. CMM implements the tension chord model, where equilibrium is expressed in terms of stresses at the cracks rather than average stresses between the cracks as in MCFT. The cracked membrane model therefore yields a much more physical description of the tension stiffening effect, compared to the MCFT that accounts for the effect through empirical relations between average strains and average stresses.

As a major and significant simplification, stress-free rotating cracks are considered in CMM. Rotating cracks cause the directions of principal stress and strain to be coincident, and the direction of the cracks are perpendicular to the maximum principal direction of average strains. This results in no shear stresses across the crack and greatly simplifies the calculations, since models describing aggregate interlock and dowel action are not needed. The alternative is to consider the crack as fixed, which leads to a path dependent crack direction (Dabbagh & Foster 2006). Although this provides a wider range of applicability, it leads to more complex formulations. Note however, that in the case of reversed cyclic loads, where a multi-directional cracking pattern occurs, the path dependency can provide an important impact on the results (Dabbagh & Foster 2006). As a designer, one must therefore always assess whether the assumptions of a model are appropriate for a given problem.

The tension chord model that is implemented in CMM, uses a stepped rigid plastic bond shear stress-slip relationship to estimate the transfer of bond stresses in between cracks. This gives simple steel stress distributions over the crack distance,

and allows steel stresses at cracks to be obtained from average strains. Furthermore, the crack spacing is determined by a closed form expression. However, actual bond shear stress-slip relationships observed from tests are much more complicated than the proposed method. More sophisticated idealizations are possible, but with the cost of a more complex calculation without closed form solution (Kaufmann 1998). The results in chapter 6 have shown that the crack formation stage formulations are a potential area for improvement, and a more sophisticated bond shear stress-slip relation is certainly of interest in that context.

7.3 Remarks for Shell Calculations

The iteration method is used to determine the strain state that ensures equilibrium between internal and external stresses in a shell section. The method can be adjusted to provide more or less sophisticated predictions of the internal behaviour, based on the material models used in the model. For instance, the most simple estimate is achieved if linear elastic behaviour is assumed for both concrete and reinforcement. This method is used in the MultiCon approach for the determination of σ_{cI}. In that case, equilibrium is obtained without iterations. Models taking into account the non-linear behaviour of concrete and the yield characteristics of reinforcement may provide better results, but with the cost of more complex calculations where iterations are necessary. In the proposed new approach for calculation of shell sections, the constitutive relations follow the recommendations of EC2. CMM could also be included as a material model in the iteration method, and in that way include directly tension stiffening in the layered approach estimates. This would, however, lead to even more complicated calculations and was not found expedient in this introductory examination.

The results of the iteration method provide the necessary results to calculate the response of a shell with the cracked membrane model. However, an effective panel must be chosen over which the response shall be determined. The choice of effective height might influence the final result considerably. In this thesis the effective height is determined according to the effective height used in crack calculations in EC2, since there are no known experimental results to use as a basis for other choices. Further studies should look into how different parameters influence the final result, and formulate an expression that provides the best estimates.

The crack width is generally bigger at the concrete surface than at the reinforcement level, and leads to a discussion about where crack width should be measured. The

relative strain formula specifies the strains of the reinforcement, and thus indicates that material deformations are determined at level with the reinforcement. On the other hand, the concrete cover term (kc) in the crack spacing formulas of EC2 and MC10 can be considered as a measure to include the contribution of the cover deformation to determine the size of the crack width at the surface. In MC10 it is given that the crack width is determined at the concrete surface for pure tension and at level of the reinforcement for bending, while no information is provided in EC2. Note also that for beams and columns the crack width can be physically measured both at level of the reinforcement and at the concrete surface, while results in practice only can be obtained at the surface for plate and shell elements.

8 Recommendations for Future Research

The findings in this thesis are promising, and provide an introductory examination of use of the cracked membrane model in large scale concrete shell structures. Based on the work with this thesis, recommendations for future research are:

- Experimental evidence should be applied in order to verify and, possibly, modify the proposed cracked shell section.
- In order to improve the accuracy of the SLS predictions in the cracked membrane model, a more sophisticated bond shear stress-slip relation may be implemented, which provides a more physically consistent and accurate description of the crack formation stage.
- The approximate simplified version of the cracked membrane model can be further examined in order to develop a simple approach for crack width calculations that is suitable for implementation in code provisions.
- The cracked shell method can be translated into a finite element formulation that is more convenient for practical design analysis, along the same lines as Foster & Marti (2003).

9 — Conclusion

Based on the presentation and discussion of crack width calculations in Eurocode 2 and Model Code 2010, it is clear that the current formulas are unsuitable for large scale and orthogonally reinforced concrete structures. The empirically adjusted factors lead to inaccurate results for large scale structures, and the physical description of the one-dimensional problem can not directly be translated into the two-dimensional case without introducing unphysical assumptions. Therefore, it is necessary to adjust the current formulas or propose new methods, in order to obtain better estimates and an improved physical description of such problems.

In this thesis, the cracked membrane model is proposed as a method to predict the behaviour of shell elements together with the iteration method. The main findings that can be drawn from the investigations and the results are:

- The cracked membrane model has proven its ability to accurately predict the load-deformation response of reinforced concrete panels subjected to plane stress, and is derived on a clear mechanical basis.
- Based on benchmarks conducted for concrete ties with different cover sizes and a large scale shear wall, the cracked membrane model has shown to yield a considerable improvement of crack spacing and crack width estimates compared to Eurocode 2 and Model Code 2010, for both normal size and large scale structures modelled with one- and two-dimensional elements.
- Review of the current design provisions and the theoretical background of the cracked membrane model formulations has demonstrated that the cracked membrane model introduces more physical and consistent formulas when it comes to crack width calculations.
- Although not verified with experimental results, the cracked shell method proposed in this thesis seems to provide better crack width predictions than

Eurocode 2 in terms of the MultiCon approach, which in turn can reduce the current overly conservative estimates

- In sum, the cracked membrane model can be a good basis for development of new crack width formulas in code regulations, and in that context, the approximate simplified version of the cracked membrane model yields an intriguing contribution with its simple, yet accurate response predictions for loads in the serviceability state.

Bibliography

CEN (2004), 'EN 1992-1-1 Eurocode 2: Design of Concrete Structures Part 1-1: General Rules and Rules for buildings', *European Committee for Standardization* .

Collins, M., Vecchio, F. & Mehlhorn, G. (1985), 'An International Competition to Predict the Response of Reinforced Concrete Panels', *Can. J. Civ. Eng.* **12**, 624–644.

Dabbagh, H. & Foster, S. J. (2006), 'A Smeared Fixed Crack Model for FE Analysis of RC Membranes Incorporating Aggregate Interlock', *Advances in Str. Eng.* **9**(1), 91–102.

DIANA FEA (2017), 'DIANA FEM-software release 10.2.'. `https://dianafea.com/manuals/d102/Diana.html` (2018-30-05).

Foster, S. & Marti, P. (2003), 'Cracked Membrane Model: Finite Element Implementation', *Journal of Structural Engineering* **129**(9), 1153–1163.

Karagiannis, D. & Kaufmann, W. (2016), 'Effect of Transverse Bending Moments on the Shear Resistance of Concrete Bridges', Conference paper. 19th IABSE Congress Stockholm, 2016.

Karagiannis, D. & Kaufmann, W. (2018), Capacity Assessment of Concrete Box-Girder Bridge Webs Against the Combined Action of In-plane Shear and Transverse Bending, *in* 'High Tech Concrete: Where Technology and Engineering Meet', Springer, pp. 693–700.

Kaufmann, W. (1998), Strength and Deformations of Structural Concrete Subjected to In-Plane Shear and Normal Forces, PhD thesis, Institute of Structural Engineering Swiss Federal Institute of Technology Zurich.

Kaufmann, W., Beck, A., Karagiannis, D. & Werne, D. (2018), 'Large Universal Shell Element Tester (LUSET)'. https://www.ethz.ch/content/specialinterest/baug/institute-ibk/concrete-and-bridge/en/forschung/LUSET.html (2018-30-05).

Kaufmann, W. & Marti, P. (1998), 'Structural Concrete: Cracked Membrane Model', *J. Struct. Eng.* **124**(12), 1467–1475.

Marti, P. & Meyboom, J. (1992), 'Response of Prestressed Concrete Elements to In-Plane Shear Forces', *ACI Structural Journal* **89**(5), 503–514.

Multiconsult (2016), 'Marine concrete structures', Brochure. https://multiconsult.no/assets/CONCRETE_brochure_ORIG-2016.pdf(2018-15-03).

Nyhus, B. (2014), 'Consistent Practical Design of Concrete Structures', *Structural Concrete* **15**(3), 305–316.

Øverli, J. A. & Sørensen, S. I. (2012), 'TKT4222 Concrete Structures 3'.

Pimentel, M., Brüwhiler, E. & Figueiras, J. (2010), 'Extended cracked membrane model for the analysis of RC panels', *Engineering Structures* **32**(8), 1964–1975.

Rivillon, P. & Gabs, A. (2011), 'M_S_S_003 - Program Shear Wall V3'. https://cheops.necs.fr/fydex/show/Program%20Shear%20Wall%20V3/ (2018-16-05).

Rospars, C. & Chauvel, D. (2014), 'CEOS.fr experimental programme and reference specimen tests results', *European Journal of Environmental and Civil Engineering* **18**(7), 738–753.

Ruocci, G., Rospars, C., Bisch, P., Erlicher, S. & Moreau, G. (2012), 'Cracks Distance and Width in Reinforced Concrete Membranes: Experimental Results from Cyclic Loading Histories', *15 WCEE* . Lisbon, Portugal.

Seelhofer, H. (2009), Ebener Spannungszustand im Betonbau: Grundlagen und Anwendungen, PhD thesis, Institute of Structural Engineering Swiss Federal Institute of Technology Zurich.

Sigrist, V., Marti, P., Alvarez, M. & Kaufmann, W. (1998), 'Tension Chord Model for Structural Concrete', *Structural Engineering International* **8**(4), 287–298.

Sørensen, S. I. (2013), *Betongkonstruksjoner: Beregning og dimensjonering etter Eurocode 2*, Fagbokforlaget, Bergen.

Tan, R., Hendriks, M., Geiker, M. & Kanstad, T. (2018), 'A Analytical Calculation Model for Predicting the Cracking Behaviour of Reinforced Concrete Ties'.

Tan, R., Hendriks, M., Kanstad, T. & Geiker, M. R. (2017), 'Evaluation and Improvement of Crack Width Calculation methods for Large Concrete Structures', Conference Paper.

fib (2013), '*fib* Model Code for Concrete Structures 2010. International Federation for Structural Concrete.', Berlin.

Vecchio, F. & Collins, M. (1986), 'The Modified Compression-Field Theory for Reinforced Concrete Elements Subjected to Shear', *ACI Engineering* **83**(2), 219–231.

Walraven, J. C. (1981), 'Fundamental Analysis of Aggregate Interlock', *ASCE* **107**(11), 2245–2270.

Zhang, L. & Hsu, T. (1998), 'Behavior and Analysis of 100 MPa Concrete Membrane Elements', *Journal of Structural Engineering* **124**(1), 24–34.

A — Algorithm - Cracked Membrane Model

In the following, an algorithm is suggested, that solves the equations of the cracked membrane model in order to determine the response of an orthogonally reinforced concrete membrane. The average total strains ε_x, ε_z and ε_3 are considered as the primary unknowns and are the main output of the program. For a given state of external loading, the equilibrium, compatibility and material models of the cracked membrane model are satisfied to obtain the correct response of a reinforced concrete membrane.

Iterations must be performed to obtain the correct solution. In the suggested algorithm Newton-Raphson iterations are performed.

Step 1 - Decide the external load $\sigma_{x,ext}$, $\sigma_{z,ext}$ and $\tau_{xz,ext}$ (from FEM analysis, iteration method for shell layers etc.). Geometry and material properties given.

Step 2 - Determine if crack angle is positive or negative

$$\theta_{p,1} = \frac{1}{2}\arctan\left(\frac{-2\tau_{xz,ext}}{\sigma_{x,ext} - \sigma_{z,ext}}\right)$$

$$\theta_{r,est} = \begin{cases} \theta_{p,1} - \frac{\pi}{2}, & \text{for } \theta_{p,1} \geq 0 \\ \theta_{p,1} + \frac{\pi}{2}, & \text{for } \theta_{p,1} < 0 \end{cases}$$

Step 3 - Determine max uniaxial crack spacing in x- and z-direction

$$S_{rmx0} = \frac{f_{ct} D_x}{2\tau_{b0}} \frac{(1-\rho_x)}{\rho_x}$$

$$S_{rmz0} = \frac{f_{ct} D_z}{2\tau_{b0}} \frac{(1-\rho_z)}{\rho_z}$$

Step 4 - Prepare for Newton-Raphson iterations: Define max number of iterations, convergence tolerance β and initial guess for ε_x, ε_z and ε_3

Step 5 - Calculate maximum principal strain ε_1

$$\varepsilon_1 = \varepsilon_x + \varepsilon_z - \varepsilon_3$$

Step 6 - Calculate crack angle θ_r

$$|\theta_r| = \arctan\left(\sqrt{\frac{\varepsilon_z - \varepsilon_3}{\varepsilon_x - \varepsilon_3}}\right)$$

$$\theta_r = \begin{cases} |\theta_r|, & \text{for } \theta_{r,est} \geq 0 \\ -|\theta_r|, & \text{for } \theta_{r,est} < 0 \end{cases}$$

Step 7 - Calculate concrete compressive stresses at crack σ_{c3r}

$$f_c = \frac{(f'_c)^{2/3}}{0.4 + 30\varepsilon_1} \leq f'_c$$

$$\sigma_{c3r} = f_c \frac{\varepsilon_3^2 + 2\varepsilon_3\varepsilon_{co}}{\varepsilon_{co}^2}$$

Step 8 - Calculate shear stresses τ_{xz}

$$\tau_{xz} = -\sigma_{c3r} sin\theta_r cos\theta_r$$

Step 9 - Calculate crack spacing S_{rm}

$$\eta = \frac{|\tau_{xz}|}{f_{ct}}$$
$$a = S_{rmx0} \sin|\theta_r| + S_{rmz0} \cos|\theta_r|$$
$$b = S_{rmx0} \cos|\theta_r| + S_{rmz0} \sin|\theta_r|$$
$$c = 2(S_{rmx0}^2 + S_{rmz0}^2) \sin|\theta_r| \cos|\theta_r| - 2S_{rmx0}S_{rmz0}$$
$$d = (S_{rmx0}^2 - S_{rmz0}^2) \sin^2|\theta_r| - 2S_{rmx0}S_{rmz0} \sin|\theta_r| \cos|\theta_r|$$
$$S_{rm0} = \frac{a + \eta b - \sqrt{\eta c + d + S_{rmz0}^2 + \eta^2(S_{rmx0}^2 - d)}}{2}$$

$$S_{rm} = \lambda S_{rm0}$$
$$S_{rmx} = \frac{S_{rm}}{\sin|\theta_r|}$$
$$S_{rmz} = \frac{S_{rm}}{\cos|\theta_r|}$$

Step 10 - Calculate steel stresses at crack σ_{sxr} and σ_{szr}

$$\sigma_{sr} = \begin{cases} E_s\varepsilon_m + \frac{\tau_{b0}S_{rm}}{D} & \text{if } \sigma_{sr} \le f_{sy} \\ f_{sy} + 2\frac{\frac{\tau_{b0}S_{rm}}{D} - \sqrt{(f_{sy} - E_s\varepsilon_m)\frac{\tau_{b1}S_{rm}}{D}(\frac{\tau_{b0}}{\tau_{b1}} - \frac{E_s}{E_{sh}}) + \frac{E_s}{E_{sh}}\tau_{b0}\tau_{b1}\frac{S_{rm}^2}{D^2}}}{\frac{\tau_{b0}}{\tau_{b1}} - \frac{E_s}{E_{sh}}} & \text{elseif } \sigma_{s,min} \le f_{sy} < \sigma_{sr} \\ f_{sy} + (\varepsilon_m - \frac{f_{sy}}{E_s})E_{sh} + \frac{\tau_{b1}S_{rm}}{D} & \text{elseif } \sigma_{s,min} > f_{sy} \end{cases}$$

Must check if slip occurs over whole crack spacing, if not modify expressions (crack formation stage)

$$x_1 = \frac{S_{rm}}{2}\left(\sqrt{n^2\rho^2 + \frac{E_s\varepsilon_m}{\tau_{b0}}\frac{D}{S_{rm}}} - n\rho\right)$$

$$x_2 = \frac{Df_{sy}E_{sh}}{4\tau_{b1}\alpha E_s}\left[\sqrt{1 + 4\alpha\frac{E_s}{E_{sh}}\left[\frac{S_{rm}\tau_{b1}}{Df_{sy}}(\frac{\alpha E_s\varepsilon_m}{f_{sy}} - n\rho) - \frac{\tau_{b1}}{4\alpha\tau_{b0}}\right]} - 1\right]$$

where $n = \frac{E_s}{E_c}$ and $\alpha = 1 + n\rho$.

If $x_1 < 0.5\ S_{rm}$

$$\sigma_{sr} = \begin{cases} x_1\frac{4\tau_{b0}}{D}\alpha & \text{if } x_1\frac{4\tau_{b0}}{D}\alpha \le f_{sy} \\ f_{sy} + x_2\frac{4\tau_{b1}}{D} & \text{else} \end{cases}$$

Note: S_{rm} is the crack spacing in the direction of the reinforcement considered.

Step 11 - Calculate axial stresses in x- and z-direction, σ_x and σ_z

$$\sigma_x = \rho_x \sigma_{sxr} + \sigma_{c3r} cos^2\theta_r$$
$$\sigma_z = \rho_z \sigma_{szr} + \sigma_{c3r} sin^2\theta_r$$

Step 12 - Calculate the function value for current estimates of ε_x, ε_z and ε_3

$$f_1 = \sigma_x - \sigma_{x,ext}$$
$$f_2 = \sigma_z - \sigma_{z,ext}$$
$$f_3 = \tau_{xz} - \tau_{xz,ext}$$

$$\boldsymbol{f} = \begin{bmatrix} f1 \\ f2 \\ f3 \end{bmatrix}$$

Step 13 - Check convergence according to chosen tolerance β

- If max($\boldsymbol{f}$) $\leq$ beta, convergence obtained and calculation can be terminated.
- If max($\boldsymbol{f}$) $>$ beta, no convergence obtained and calculation must proceed

Step 14 - Calculate the Jacobian matrix. The derivatives of function f_1, f_2 and f_3 must be calculated with respect to ε_x, ε_z and ε_3.

$$\boldsymbol{J} = \begin{bmatrix} \frac{\partial f_1}{\partial \varepsilon_x} & \frac{\partial f_1}{\partial \varepsilon_z} & \frac{\partial f_1}{\partial \varepsilon_3} \\ \frac{\partial f_2}{\partial \varepsilon_x} & \frac{\partial f_2}{\partial \varepsilon_z} & \frac{\partial f_2}{\partial \varepsilon_3} \\ \frac{\partial f_3}{\partial \varepsilon_x} & \frac{\partial f_3}{\partial \varepsilon_z} & \frac{\partial f_3}{\partial \varepsilon_3} \end{bmatrix}$$

The elements of the matrix, and details of the derivations are given in Appendix B.

Step 15 - Calculate new estimations of ε_x, ε_z and ε_3 (Newton-Raphson step).

$$\boldsymbol{\varepsilon}_{i+1} = \boldsymbol{\varepsilon}_i - \boldsymbol{J}(\boldsymbol{\varepsilon}_i)^{-1} \boldsymbol{f}(\boldsymbol{\varepsilon}_i)$$

$$\begin{bmatrix} \varepsilon_x \\ \varepsilon_z \\ \varepsilon_3 \end{bmatrix}_{i+1} = \begin{bmatrix} \varepsilon_x \\ \varepsilon_z \\ \varepsilon_3 \end{bmatrix}_i - \begin{bmatrix} \frac{\partial f_1}{\partial \varepsilon_x} & \frac{\partial f_1}{\partial \varepsilon_z} & \frac{\partial f_1}{\partial \varepsilon_3} \\ \frac{\partial f_2}{\partial \varepsilon_x} & \frac{\partial f_2}{\partial \varepsilon_z} & \frac{\partial f_2}{\partial \varepsilon_3} \\ \frac{\partial f_3}{\partial \varepsilon_x} & \frac{\partial f_3}{\partial \varepsilon_z} & \frac{\partial f_3}{\partial \varepsilon_3} \end{bmatrix}_i^{-1} \begin{bmatrix} f_1 \\ f_2 \\ f_3 \end{bmatrix}_i$$

Step 16 - Use new estimates of ε_x, ε_z and ε_3 and return to *Step 5*

B — Derivatives

B.1 Crack Angle

$$\frac{\partial \theta_r}{\partial \varepsilon_x} = \frac{(\varepsilon_z - \varepsilon_3)\sqrt{\frac{\varepsilon_x - \varepsilon_3}{\varepsilon_z - \varepsilon_3}}}{2(\varepsilon_x - \varepsilon_3)(\varepsilon_x + \varepsilon_z - 2\varepsilon_3)}$$

$$\frac{\partial \theta_r}{\partial \varepsilon_z} = -\frac{\sqrt{\frac{\varepsilon_x - \varepsilon_3}{\varepsilon_z - \varepsilon_3}}}{2(\varepsilon_x + \varepsilon_z - 2\varepsilon_3)}$$

$$\frac{\partial \theta_r}{\partial \varepsilon_3} = \frac{(\varepsilon_x - \varepsilon_z)\sqrt{\frac{\varepsilon_x - \varepsilon_3}{\varepsilon_z - \varepsilon_3}}}{2(\varepsilon_x - \varepsilon_3)(\varepsilon_x + \varepsilon_z - 2\varepsilon_3)}$$

B.2 Average Tensile Strains

$$\frac{\partial \varepsilon_1}{\partial \varepsilon_x} = \frac{\partial \varepsilon_1}{\partial \varepsilon_z} = 1$$

$$\frac{\partial \varepsilon_1}{\partial \varepsilon_3} = -1$$

B.3 Concrete Stresses

$$\frac{\partial f_c}{\partial \varepsilon_x} = \frac{\partial f_c}{\partial \varepsilon_z} = -\frac{30(f_c')^{2/3}}{(0.4 + 30\varepsilon_1)^2}$$

$$\frac{\partial \sigma_{c3r}}{\partial \varepsilon_x} = \frac{\partial \sigma_{c3r}}{\partial \varepsilon_z} = \frac{\partial f_c}{\partial \varepsilon_x} \frac{\varepsilon_3^2 + 2\varepsilon_3 \varepsilon_{co}}{\varepsilon_{co}^2}$$

$$\frac{\partial f_c}{\partial \varepsilon_3} = \frac{30(f_c')^{2/3}}{(0.4 + 30\varepsilon_1)^2}$$

$$\frac{\partial \sigma_{c3r}}{\partial \varepsilon_3} = \frac{\partial f_c}{\partial \varepsilon_3} \frac{\varepsilon_3^2 + 2\varepsilon_3 \varepsilon_{co}}{\varepsilon_{co}^2} + 2 f_c \frac{\varepsilon_3 + \varepsilon_{co}}{\varepsilon_{co}^2}$$

B.4 Shear Stress

$$\frac{\partial \tau_{xz}}{\partial \varepsilon_x} = -\frac{\partial \sigma_{c3r}}{\partial \varepsilon_x} \sin\theta_r \cos\theta_r - \sigma_{c3r} \cos^2\theta_r \frac{\partial \theta_r}{\partial \varepsilon_x} + \sigma_{c3r} \sin^2\theta_r \frac{\partial \theta_r}{\partial \varepsilon_x}$$

$$\frac{\partial \tau_{xz}}{\partial \varepsilon_z} = -\frac{\partial \sigma_{c3r}}{\partial \varepsilon_z} \sin\theta_r \cos\theta_r - \sigma_{c3r} \cos^2\theta_r \frac{\partial \theta_r}{\partial \varepsilon_z} + \sigma_{c3r} \sin^2\theta_r \frac{\partial \theta_r}{\partial \varepsilon_z}$$

$$\frac{\partial \tau_{xz}}{\partial \varepsilon_3} = -\frac{\partial \sigma_{c3r}}{\partial \varepsilon_3} \sin\theta_r \cos\theta_r - \sigma_{c3r} \cos^2\theta_r \frac{\partial \theta_r}{\partial \varepsilon_3} + \sigma_{c3r} \sin^2\theta_r \frac{\partial \theta_r}{\partial \varepsilon_3}$$

B.5 Crack Spacing

$$\frac{\partial a}{\partial \varepsilon_x} = -S_{rmx0} \sin\theta_r \frac{\partial \theta_r}{\partial \varepsilon_x} + S_{rmz0} \cos\theta_r \frac{\partial \theta_r}{\partial \varepsilon_x}$$

$$\frac{\partial b}{\partial \varepsilon_x} = S_{rmx0} \cos\theta_r \frac{\partial \theta_r}{\partial \varepsilon_x} - S_{rmz0} \sin\theta_r \frac{\partial \theta_r}{\partial \varepsilon_x}$$

$$\frac{\partial c}{\partial \varepsilon_x} = 2(S_{rmx0}^2 + S_{rmz0}^2)(\cos^2\theta_r - \sin^2\theta_r) \frac{\partial \theta_r}{\partial \varepsilon_x}$$

$$\begin{aligned} \frac{\partial d}{\partial \varepsilon_x} = {} & (S_{rmx0}^2 - S_{rmz0}^2) 2 \sin\theta_r \cos\theta_r \frac{\partial \theta_r}{\partial \varepsilon_x} \\ & + 2 S_{rmx0} S_{rmz0} (\cos^2\theta_r - \sin^2\theta_r) \frac{\partial \theta_r}{\partial \varepsilon_x} \end{aligned}$$

$$\frac{\partial \eta}{\partial \varepsilon_x} = \frac{1}{f_{ct}} \frac{\partial \tau_{xz}}{\partial \varepsilon_x}$$

$$\frac{\partial S_{rm}}{\partial \varepsilon_x} = \frac{1}{2}\left[\frac{\partial a}{\partial \varepsilon_x} + \frac{\partial \eta}{\partial \varepsilon_x} b + \eta \frac{\partial b}{\partial \varepsilon_x} - \frac{1}{2}\left(\eta c - d + S_{rmx0}^2 + \eta^2 (d + S_{rmz0}^2)\right)^{-\frac{1}{2}} \cdot \left(\frac{\partial \eta}{\partial \varepsilon_x} c + \eta \frac{\partial c}{\partial \varepsilon_x} - \frac{\partial d}{\partial \varepsilon_x} + 2\eta \frac{\partial \eta}{\partial \varepsilon_x}(d + S_{rmz0}^2) + \eta^2 \frac{\partial d}{\partial \varepsilon_x}\right)\right]$$

$$\frac{\partial a}{\partial \varepsilon_x} = S_{rmx0} \cos\theta_r \frac{\partial \theta_r}{\partial \varepsilon_x} - S_{rmz0} \sin\theta_r \frac{\partial \theta_r}{\partial \varepsilon_x}$$

$$\frac{\partial b}{\partial \varepsilon_x} = -S_{rmx0} \sin\theta_r \frac{\partial \theta_r}{\partial \varepsilon_x} + S_{rmz0} \cos\theta_r \frac{\partial \theta_r}{\partial \varepsilon_x}$$

$$\frac{\partial c}{\partial \varepsilon_x} = 2(S_{rmx0}^2 + S_{rmz0}^2)(\cos^2\theta_r - \sin^2\theta_r) \frac{\partial \theta_r}{\partial \varepsilon_x}$$

$$\frac{\partial d}{\partial \varepsilon_x} = (S_{rmx0}^2 - S_{rmz0}^2) 2 \sin\theta_r \cos\theta_r \frac{\partial \theta_r}{\partial \varepsilon_x} - 2 S_{rmx0} S_{rmz0} (\cos^2\theta_r - \sin^2\theta_r) \frac{\partial \theta_r}{\partial \varepsilon_x}$$

$$\frac{\partial \eta}{\partial \varepsilon_x} = \frac{1}{f_{ct}} \frac{\partial \tau_{xz}}{\partial \varepsilon_x}$$

$$\frac{\partial S_{rm}}{\partial \varepsilon_x} = \frac{1}{2}\Bigg[\frac{\partial a}{\partial \varepsilon_x} + \frac{\partial \eta}{\partial \varepsilon_x} b + \eta \frac{\partial b}{\partial \varepsilon_x} - \frac{1}{2}\Big(\eta c + d + S_{rmz0}^2 + \eta^2 (S_{rmx0}^2 - d)\Big)^{-\frac{1}{2}} \cdot \Big(\frac{\partial \eta}{\partial \varepsilon_x} c + \eta \frac{\partial c}{\partial \varepsilon_x} + \frac{\partial d}{\partial \varepsilon_x} + 2\eta \frac{\partial \eta}{\partial \varepsilon_x}(S_{rmx0}^2 - d) - \eta^2 \frac{\partial d}{\partial \varepsilon_x}\Big)\Bigg]$$

$$\frac{\partial S_{rmx}}{\partial \varepsilon_x} = \frac{\frac{\partial S_{rm}}{\partial \varepsilon_x} \sin\theta_r - S_{rm} \cos\theta_r \frac{\partial \theta_r}{\partial \varepsilon_x}}{\sin^2 \theta_r}$$

$$\frac{\partial S_{rmz}}{\partial \varepsilon_x} = \frac{\frac{\partial S_{rm}}{\partial \varepsilon_x} \cos\theta_r + S_{rm} \sin\theta_r \frac{\partial \theta_r}{\partial \varepsilon_x}}{\cos^2 \theta_r}$$

The derivatives of the crack spacing wrt ε_z and ε_3 are obtained similiarly.

B.6 Reinforcement Stresses

Derivative of reinforcement stresses in x-direction wrt to ε_x:

If $\sigma_{sxr} \leq f_{syx}$ (Regime 1)

$$\frac{\partial \sigma_{sxr}}{\partial \varepsilon_x} = \begin{cases} E_{sx} + \frac{\tau_{b0}}{D_x} \frac{\partial S_{rmx}}{\partial \varepsilon_x}, & \text{if } E_{sx}\varepsilon_x + \frac{\tau_{b0} S_{rmx}}{D_x} < 2E_{sx}\varepsilon_x \\ 2E_{sx}, & \text{otherwise} \end{cases}$$

Elseif $\sigma_{sx,min} \leq f_{syx} < \sigma_{sxr}$ (Regime 2)

$$\begin{aligned} \frac{\partial \sigma_{sxr}}{\partial \varepsilon_x} =& \frac{2}{\frac{\tau_{b0}}{\tau_{b1}} - \frac{E_{sx}}{E_{shx}}} \Bigg[\frac{\tau_{b0}}{D_x} \frac{\partial S_{rmx}}{\partial \varepsilon_x} \\ & - \frac{1}{2}\Bigg\{(f_{syx} - E_{sx}\varepsilon_x)\frac{\tau_{b1} S_{rmx}}{D_x}\Big(\frac{\tau_{b0}}{\tau_{b1}} - \frac{E_{sx}}{E_{shx}}\Big) + \frac{E_{sx}}{E_{shx}} \tau_{b0}\tau_{b1} \frac{S_{rmx}^2}{D_x^2}\Bigg\}^{-\frac{1}{2}} \\ & \cdot \Bigg\{\Big(-E_{sx}\frac{\tau_{b1} S_{rmx}}{D_x} + (f_{syx} - E_{sx}\varepsilon_x)\frac{\tau_{b1}}{D_x}\frac{\partial S_{rmx}}{\partial \varepsilon_x}\Big)\Big(\frac{\tau_{b0}}{\tau_{b1}} - \frac{E_{sx}}{E_{shx}}\Big) \\ & + \frac{E_{sx}}{E_{shx}} \tau_{b0}\tau_{b1} \frac{2S_{rmx}}{D_x^2} \frac{\partial S_{rmx}}{\partial \varepsilon_x}\Bigg\}\Bigg] \end{aligned}$$

Elseif $f_{syx} < \sigma_{sx,min}$ (Regime 3)

$$\frac{\partial \sigma_{sxr}}{\partial \varepsilon_x} = E_{shx} + \frac{\tau_{b1}}{D_x}\frac{\partial S_{rmx}}{\partial \varepsilon_x}$$

Must check if slip is not occuring over the whole element (crack formation stage), and in that case use other equations.

If $x_1 < \frac{1}{2}S_{rmx}$ (crack formation stage)

If $x_1 \frac{4\tau_{b0}}{D_x}(1 + n_x\rho_x) < f_{syx}$

$$\begin{aligned}
\frac{\partial x_1}{\partial \varepsilon_x} &= \frac{1}{2}\frac{\partial S_{rmx}}{\partial \varepsilon_x}\left(\sqrt{n_x^2\rho_x^2 + \frac{E_{sx}\varepsilon_x}{\tau_{b0}}\frac{D_x}{S_{rmx}}} - n_x\rho_x\right) \\
&\quad + \frac{S_{rmx}E_{sx}D_x}{4\tau_{b0}}\left(n_x^2\rho_x^2 + \frac{E_{sx}\varepsilon_x}{\tau_{b0}}\frac{D_x}{S_{rmx}}\right)^{-\frac{1}{2}}\left(\frac{S_{rmx} - \varepsilon_x\frac{\partial S_{rmx}}{\partial \varepsilon_x}}{S_{rmx}^2}\right) \\
\frac{\partial \sigma_{sxr}}{\partial \varepsilon_x} &= \frac{\partial x_1}{\partial \varepsilon_x}\frac{4\tau_{b0}}{D_x}(1 + n_x\rho_x)
\end{aligned}$$

Else

$$\begin{aligned}
\frac{\partial x_2}{\partial \varepsilon_x} &= \frac{1}{2}\left[1 + 4\frac{\alpha_x E_{sx}}{E_{shx}}\left\{\frac{S_{rmx}\tau_{b1}}{D_x f_{syx}}\left(\frac{\alpha_x E_{sx}\varepsilon_x}{f_{syx}} - n_x\rho_x\right) - \frac{\tau_{b1}}{4\alpha_x\tau_{b0}}\right\}\right]^{-\frac{1}{2}} \\
&\quad \left[\frac{\partial S_{rmx}}{\partial \varepsilon_x}\left(\frac{\alpha_x E_{sx}\varepsilon_x}{f_{syx}} - n_x\rho_x\right) + S_{rmx}\frac{\alpha_x E_{sx}}{f_{syx}}\right] \\
\frac{\partial \sigma_{sxr}}{\partial \varepsilon_x} &= \frac{\partial x_2}{\partial \varepsilon_x}\frac{4\tau_{b1}}{D_x}
\end{aligned}$$

Derivative of reinforcement stresses in x-direction wrt to ε_z:

If $\sigma_{sxr} \leq f_{syx}$ (Regime 1)

$$\frac{\partial \sigma_{sxr}}{\partial \varepsilon_z} = \begin{cases} \frac{\tau_{b0}}{D_x}\frac{\partial S_{rmx}}{\partial \varepsilon_z}, & \text{if } E_{sx}\varepsilon_x + \frac{\tau_{b0}S_{rmx}}{D_x} < 2E_{sx}\varepsilon_x \\ 0, & \text{otherwise} \end{cases}$$

Elseif $\sigma_{sx,min} \leq f_{syx} < \sigma_{sxr}$ (Regime 2)

$$\begin{aligned}\frac{\partial \sigma_{sxr}}{\partial \varepsilon_z} =& \frac{2}{\frac{\tau_{b0}}{\tau_{b1}} - \frac{E_{sx}}{E_{shx}}} \Bigg[\frac{\tau_{b0}}{D_x} \frac{\partial S_{rmx}}{\partial \varepsilon_z} \\ & - \frac{1}{2} \Bigg\{ (f_{syx} - E_{sx}\varepsilon_x) \frac{\tau_{b1} S_{rmx}}{D_x} \Big(\frac{\tau_{b0}}{\tau_{b1}} - \frac{E_{sx}}{E_{shx}} \Big) + \frac{E_{sx}}{E_{shx}} \tau_{b0} \tau_{b1} \frac{S_{rmx}^2}{D_x^2} \Bigg\}^{-\frac{1}{2}} \\ & \cdot \Bigg\{ (f_{syx} - E_{sx}\varepsilon_x) \frac{\tau_{b1}}{D_x} \frac{\partial S_{rmx}}{\partial \varepsilon_z} \Big(\frac{\tau_{b0}}{\tau_{b1}} - \frac{E_{sx}}{E_{shx}} \Big) + \frac{E_{sx}}{E_{shx}} \tau_{b0} \tau_{b1} \frac{2 S_{rmx}}{D_x^2} \frac{\partial S_{rmx}}{\partial \varepsilon_z} \Bigg\} \Bigg]\end{aligned}$$

Elseif $f_{syx} < \sigma_{sx,min}$ (Regime 3)

$$\frac{\partial \sigma_{sxr}}{\partial \varepsilon_z} = \frac{\tau_{b1}}{D_x} \frac{\partial S_{rmx}}{\partial \varepsilon_z}$$

Must check if slip is not occuring over the whole element (crack formation stage), and in that case use other equations.

If $x_1 < \frac{1}{2} S_{rmx}$ (crack formation stage)

If $x_1 \frac{4\tau_{b0}}{D_x}(1 + n_x \rho_x) < f_{syx}$

$$\begin{aligned}\frac{\partial x_1}{\partial \varepsilon_z} =& \frac{1}{2} \frac{\partial S_{rmx}}{\partial \varepsilon_z} \Bigg(\sqrt{n_x^2 \rho_x^2 + \frac{E_{sx}\varepsilon_x}{\tau_{b0}} \frac{D_x}{S_{rmx}}} - n_x \rho_x \Bigg) \\ & - \frac{S_{rmx} E_{sx} D_x}{4\tau_{b0}} \Bigg(n_x^2 \rho_x^2 + \frac{E_{sx}\varepsilon_x}{\tau_{b0}} \frac{D_x}{S_{rmx}} \Bigg)^{-\frac{1}{2}} \frac{\varepsilon_x}{S_{rmx}^2} \frac{\partial S_{rmx}}{\partial \varepsilon_z} \\ \frac{\partial \sigma_{sxr}}{\partial \varepsilon_z} =& \frac{\partial x_1}{\partial \varepsilon_z} \frac{4\tau_{b0}}{D_x} (1 + n_x \rho_x)\end{aligned}$$

Else

$$\begin{aligned}\frac{\partial x_2}{\partial \varepsilon_z} =& \frac{1}{2} \Bigg[1 + 4 \frac{\alpha_x E_{sx}}{E_{shx}} \Bigg\{ \frac{S_{rmx} \tau_{b1}}{D_x f_{syx}} \Big(\frac{\alpha_x E_{sx} \varepsilon_x}{f_{syx}} - n_x \rho_x \Big) - \frac{\tau_{b1}}{4\alpha_x \tau_{b0}} \Bigg\} \Bigg]^{-\frac{1}{2}} \\ & \frac{\partial S_{rmx}}{\partial \varepsilon_z} \Big(\frac{\alpha_x E_{sx} \varepsilon_x}{f_{syx}} - n_x \rho_x \Big) \\ \frac{\partial \sigma_{sxr}}{\partial \varepsilon_z} =& \frac{\partial x_2}{\partial \varepsilon_z} \frac{4\tau_{b1}}{D_x}\end{aligned}$$

The expression for $\frac{\partial \sigma_{szr}}{\partial \varepsilon_z}$ look similar to $\frac{\partial \sigma_{sxr}}{\partial \varepsilon_x}$, and the expressions for $\frac{\partial \sigma_{sxr}}{\partial \varepsilon_3}$, $\frac{\partial \sigma_{szr}}{\partial \varepsilon_x}$, $\frac{\partial \sigma_{szr}}{\partial \varepsilon_3}$ look similar to $\frac{\partial \sigma_{sxr}}{\partial \varepsilon_z}$.

B.7 Axial Stresses

$$\frac{\partial \sigma_x}{\partial \varepsilon_x} = \rho_x \frac{\partial \sigma_{sxr}}{\partial \varepsilon_x} + \frac{\partial \sigma_{c3r}}{\partial \varepsilon_x} \cos^2 \theta_r - 2\sigma_{c3r} \sin \theta_r \cos \theta_r \frac{\partial \theta_r}{\partial \varepsilon_x}$$

The expressions for $\frac{\partial \sigma_x}{\partial \varepsilon_z}$ and $\frac{\partial \sigma_x}{\partial \varepsilon_3}$, are similar to $\frac{\partial \sigma_x}{\partial \varepsilon_x}$.

$$\frac{\partial \sigma_z}{\partial \varepsilon_x} = \rho_z \frac{\partial \sigma_{szr}}{\partial \varepsilon_x} + \frac{\partial \sigma_{c3r}}{\partial \varepsilon_x} \sin^2 \theta_r + 2\sigma_{c3r} \sin \theta_r \cos \theta_r \frac{\partial \theta_r}{\partial \varepsilon_x}$$

The expressions for $\frac{\partial \sigma_z}{\partial \varepsilon_z}$ and $\frac{\partial \sigma_z}{\partial \varepsilon_3}$, are similar to $\frac{\partial \sigma_z}{\partial \varepsilon_x}$.

B.8 Jacobian Matrix

$$\boldsymbol{J} = \begin{bmatrix} \frac{\partial f_1}{\partial \varepsilon_x} & \frac{\partial f_1}{\partial \varepsilon_z} & \frac{\partial f_1}{\partial \varepsilon_3} \\ \frac{\partial f_2}{\partial \varepsilon_x} & \frac{\partial f_2}{\partial \varepsilon_z} & \frac{\partial f_2}{\partial \varepsilon_3} \\ \frac{\partial f_3}{\partial \varepsilon_x} & \frac{\partial f_3}{\partial \varepsilon_z} & \frac{\partial f_3}{\partial \varepsilon_3} \end{bmatrix}$$

where

$$\begin{aligned} \frac{\partial f_1}{\partial \varepsilon_x} &= \frac{\partial \sigma_x}{\partial \varepsilon_x}, & \frac{\partial f_1}{\partial \varepsilon_z} &= \frac{\partial \sigma_x}{\partial \varepsilon_z}, & \frac{\partial f_1}{\partial \varepsilon_3} &= \frac{\partial \sigma_x}{\partial \varepsilon_3} \\ \frac{\partial f_2}{\partial \varepsilon_x} &= \frac{\partial \sigma_z}{\partial \varepsilon_x}, & \frac{\partial f_2}{\partial \varepsilon_z} &= \frac{\partial \sigma_z}{\partial \varepsilon_z}, & \frac{\partial f_2}{\partial \varepsilon_3} &= \frac{\partial \sigma_x}{\partial \varepsilon_3} \\ \frac{\partial f_3}{\partial \varepsilon_x} &= \frac{\partial \tau_{xz}}{\partial \varepsilon_x}, & \frac{\partial f_3}{\partial \varepsilon_z} &= \frac{\partial \tau_{xz}}{\partial \varepsilon_z}, & \frac{\partial f_3}{\partial \varepsilon_3} &= \frac{\partial \tau_{xz}}{\partial \varepsilon_3} \end{aligned}$$

C — Derivation of Crack Spacing Formula

In the following the derivation of the crack spacing formula (3.32) is shown. The formula is similar to the one shown in (Dabbagh & Foster 2006).

The derivation is based on (3.31)

$$\frac{f_{ct}}{2}(\lambda_x + \lambda_z) - \frac{\tau_{xz}}{2}(cot\theta_r + tan\theta_r) + \sqrt{\left[\frac{\tau_{xz}}{2}(cot\theta_r - tan\theta_r) - \frac{f_{ct}}{2}(\lambda_x - \lambda_z)\right]^2 + \tau_{xz}^2} \leq f_{ct} \quad \text{(C.1)}$$

At the limit, Eq. (C.1) can be solved on closed form. The equality may be written as

$$\frac{S_{rm0}}{2}\left(\frac{1}{S_{rmx0}\sin\theta_r} + \frac{1}{S_{rmz0}\cos\theta_r}\right) - \frac{\eta}{2}\left(\cot\theta_r + \tan\theta_r\right) + \sqrt{\left[\frac{\eta}{2}\left(\cot\theta_r - \tan\theta_r\right) - \frac{S_{rm0}}{2}\left(\frac{1}{S_{rmx0}\sin\theta_r} - \frac{1}{S_{rmz0}\cos\theta_r}\right)\right]^2 + \eta^2} = 1 \quad \text{(C.2)}$$

where the following relations are used

$$\lambda_x = \frac{S_{rm0}}{S_{rmx0}\sin\theta_r}$$
$$\lambda_x = \frac{S_{rm0}}{S_{rmz0}\cos\theta_r}$$
$$\eta = \frac{|\tau_{xz}|}{f_{ct}}$$

Now, the square root is left on one side and the other terms on the other side of the equal sign. Furthermore, the squared expression inside the square root is calculated

$$\begin{aligned}
&\left\{\frac{\eta^2}{4}\left(\cot^2\theta_r + \tan^2\theta_r - 2\right)\right. \\
&+ \frac{S_{rm0}^2}{4}\left(\frac{1}{S_{rmx0}^2\sin^2\theta_r} + \frac{1}{S_{rmz0}^2\cos^2\theta_r} - \frac{2}{S_{rmx0}S_{rmz0}\sin\theta_r\cos\theta_r}\right) \\
&\left. - \frac{\eta S_{rm0}}{2}\left(\frac{\cos\theta_r}{S_{rmx0}\sin^2\theta_r} - \frac{1}{S_{rmz0}\sin\theta_r} - \frac{1}{S_{rmx0}\cos\theta_r} + \frac{\sin\theta_r}{S_{rmz0}\cos^2\theta_r}\right) + \eta^2\right\}^{1/2} \\
&= 1 - \frac{S_{rm0}}{2}\left(\frac{1}{S_{rmx0}\sin\theta_r} + \frac{1}{S_{rmz0}\cos\theta_r}\right) + \frac{\eta}{2}\left(\cot\theta_r + \tan\theta_r\right)
\end{aligned} \tag{C.3}$$

If both sides of the equality are squared, and all the terms organized, the following is obtained

$$\begin{aligned}
&S_{rm0}^2\left[\frac{1}{S_{rmx0}S_{rmz0}\sin\theta_r\cos\theta_r}\right] - S_{rm0}\left[\frac{1}{S_{rmx0}\sin\theta_r} + \frac{1}{S_{rmz0}\cos\theta_r}\right] \\
&+ \eta\left(\frac{1}{S_{rmx0}\cos\theta_r} + \frac{1}{S_{rmz0}\sin\theta_r}\right)\Bigg] + \left[1 + \eta\left(\cot\theta_r + \tan\theta_r\right)\right] = 0
\end{aligned} \tag{C.4}$$

To simplify the expression, multiply with $S_{rmx0}S_{rmz0}\sin\theta_r\cos\theta_r$, which gives

$$S_{rm0}^2 - S_{rm0}\Big[S_{rmx0}\sin\theta_r + S_{rmz0}\cos\theta_r + n\Big(S_{rmx0}\cos\theta_r + S_{rmz0}\sin\theta_r\Big)\Big] + \Big[S_{rmx0}S_{rmz0}\sin\theta_r\cos\theta_r + nS_{rmx0}S_{rmz0}\Big] = 0 \tag{C.5}$$

Now, a quadratic equation with respect to S_{rm0} is obtained, and it can be solved with the quadratic formula

$$S_{rm0}^2 A + S_{rm0}B + S_{rm0}C = 0$$
$$S_{rm0} = \frac{-B \pm \sqrt{B^2 - 4AC}}{2A}$$

$$\begin{aligned} S_{rm0} = {} & \frac{S_{rmx0}\sin\theta_r + S_{rmz0}\cos\theta_r}{2} + \frac{n(S_{rmx0}\cos\theta_r + S_{rmz0}\sin\theta_r)}{2} \\ & \pm \frac{1}{2}\Bigg\{ S_{rmx0}^2\sin^2\theta_r + S_{rmz0}^2\cos^2\theta_r + 2S_{rmx0}S_{rmz0}\sin\theta_r\cos\theta_r \\ & + \eta^2\Big(S_{rmx0}^2\cos^2\theta_r + S_{rmz0}^2\sin^2\theta_r + 2S_{rmx0}S_{rmz0}\sin\theta_r\cos\theta_r\Big) \\ & + 2\eta\Big(S_{rmx0}^2\sin\theta_r\cos\theta_r + S_{rmz0}^2\sin\theta_r\cos\theta_r - S_{rmx0}S_{rmz0}\Big)\Bigg\}^{1/2} \end{aligned} \tag{C.6}$$

To make the expression easier to read, and reduce the risk of errors, the following parameters is introduced

$$\begin{aligned} a =& S_{rmx0}\sin\theta_r + S_{rmz0}\cos\theta_r \\ b =& S_{rmx0}\cos\theta_r + S_{rmz0}\sin\theta_r \\ c =& 2(S_{rmx0}^2 + S_{rmz0}^2)\sin\theta_r\cos\theta_r - 2S_{rmx0}S_{rmz0} \\ d =& (S_{rmx0}^2 - S_{rmz0}^2)\sin^2\theta_r - 2S_{rmx0}S_{rmz0}\sin\theta_r\cos\theta_r \end{aligned}$$

The expression for the maximum crack spacing becomes

$$S_{rm0} = \frac{a + \eta b - \sqrt{\eta c + d + S_{rmz0}^2 + \eta^2 (S_{rmx0}^2 - d)}}{2} \tag{C.7}$$

This expression and the parameters a,b,c and d look almost similar to the expression given in Dabbagh & Foster (2006), but with a few small modifications. The differences occur because of the choice of crack angle basis, where there is 90 degree shift between the basis here and in the article of Dabbagh & Foster (2006). However, the same approach may be applied for the other crack angle basis, to obtain the result presented in Dabbagh & Foster (2006).

D — Algorithm - The Iteration Method

In the following a step by step algorithm is shown for the iteration method. It is based on the derivations shown in section 4.2, and in accordance with Øverli & Sørensen (2012). The algorithm is implemented in a Matlab program developed for this thesis, called "Iteration_method.m".

Step 1 - Decide the external load **R** (from FEM analysis). Also determine geometry and necessary reinforcement amounts.

Step 2 - Calcuate the stiffness matrix **K**. For the initial iteration step assume isotropic, linear elastic behaviour for concrete and linear elastic behaviour for reinforcement.

$$\boldsymbol{K}_C = \Delta h \sum_{i=1}^{n} \begin{bmatrix} \boldsymbol{C}_{ci} & -z_i \boldsymbol{C}_{ci} \\ -z_i \boldsymbol{C}_{ci} & z_i^2 \boldsymbol{C}_{ci} \end{bmatrix}$$

$$\boldsymbol{K}_S = \sum_{j=1}^{m} \left(A_{sxj} \begin{bmatrix} \boldsymbol{C}_{sxj} & -z_j \boldsymbol{C}_{sxj} \\ -z_j \boldsymbol{C}_{sxj} & z_j^2 \boldsymbol{C}_{sxj} \end{bmatrix} + A_{syj} \begin{bmatrix} \boldsymbol{C}_{syj} & -z_j \boldsymbol{C}_{syj} \\ -z_j \boldsymbol{C}_{syj} & z_j^2 \boldsymbol{C}_{syj} \end{bmatrix} \right)$$

$$\boldsymbol{K} = \boldsymbol{K}_C + \boldsymbol{K}_S$$

Step 3 - Determine strains and curvatures at the middle plane of the shell

$$\boldsymbol{\varepsilon}_t = \boldsymbol{K}^{-1} \boldsymbol{R}$$

Step 4 - Determine the in-plane strains of each concrete and reinforcement layer in the global xy-axes

$$\boldsymbol{\varepsilon}_{xyi} = \boldsymbol{A}_i \cdot \boldsymbol{\varepsilon}_t$$

Step 5 - Determine the principal strains and principal directions in each concrete layer

$$\boldsymbol{\varepsilon}_{pi} = \boldsymbol{T}(\theta_i) \cdot \boldsymbol{\varepsilon}_{xyi}$$

$$\theta_i = \frac{1}{2} \tan^{-1} \left(\frac{\gamma_{xy,i}}{\varepsilon_{x,i} - \varepsilon_{y,i}} \right)$$

Step 6 - Calculate the principal concrete stresses in each concrete layer

$$\boldsymbol{\sigma}_{cpi} = \boldsymbol{C}_{cpi} \cdot \boldsymbol{\varepsilon}_{pi}$$

Step 7 - Transform the principal concrete stresses in each concrete layer to the global xy-system

$$\boldsymbol{\sigma}_{cxyi} = \boldsymbol{T}^T(\theta_i) \cdot \boldsymbol{\sigma}_{cpi}$$

Step 8 - Calculate reinforcement stresses in each reinforcement layer

$$\boldsymbol{\sigma}_{sxyj} = \boldsymbol{C}_{sj} \cdot \boldsymbol{\varepsilon}_{xyj}$$

Step 9 - Calculate the internal force vector

$$\boldsymbol{S} = \Delta h \sum_{i=1}^{n} \begin{bmatrix} \boldsymbol{\sigma}_{cxyi} \\ -z_i \cdot \boldsymbol{\sigma}_{cxyi} \end{bmatrix} + \sum_{j=1}^{m} \begin{bmatrix} A_{sxj} \cdot \sigma_{sxj} \\ A_{syj} \cdot \sigma_{syj} \\ 0 \\ -z_j A_{sxj} \sigma_{sxj} \\ -z_j A_{syj} \sigma_{syj} \\ 0 \end{bmatrix}$$

Step 10 - Determine maximum relative deviation between components of internal and external force resultants

$$Maxdiff = max\left(\frac{R_k - S_k}{R_k}\right); \quad k = 1, 2, .., n$$

Step 11 - Check convergence according to tolerance β

- If Maxdiff $\leq \beta$ equilibrium obtained, iterations may be terminated
- If Maxdiff $> \beta$ equilibrium not obtained, calculations proceed

Step 12 - Find new secant moduli for all concrete and reinforcement layers

$$E_{cii} = \frac{\sigma_{ci}}{\varepsilon_i}, \qquad E_{c12} = \frac{(E_{c11} + E_{c22})}{2}$$
$$E_{sxj} = \frac{\sigma_{sxj}}{\varepsilon_{sxj}}, \qquad E_{syj} = \frac{\sigma_{syj}}{\varepsilon_{syj}}$$

Step 13 - Calculate new material matrix for concrete

$$\boldsymbol{C}_{cpi} = \frac{1}{1-\nu^2}\begin{bmatrix} E_{c11} & \nu E_{c12} & 0 \\ \nu E_{c12} & E_{c22} & 0 \\ 0 & 0 & \frac{(1-\nu)E_{c12}}{2} \end{bmatrix}$$

Step 14 - Transform local stiffness matrix to global xy-system for each concrete layer

$$\boldsymbol{C}_{ci} = \boldsymbol{T}^T(\theta_i) \cdot \boldsymbol{C}_{cpi} \cdot \boldsymbol{T}(\theta_i)$$

Step 15 - Return to step 2